

University of Montana

ScholarWorks at University of Montana

Graduate Student Theses, Dissertations, &
Professional Papers

Graduate School

2022

LiDAR-Landsat Covariance for Predicting Canopy Fuels

Margaret D. Epstein

Follow this and additional works at: <https://scholarworks.umt.edu/etd>



Part of the [Environmental Monitoring Commons](#), and the [Other Forestry and Forest Sciences Commons](#)

Let us know how access to this document benefits you.

Recommended Citation

Epstein, Margaret D., "LiDAR-Landsat Covariance for Predicting Canopy Fuels" (2022). *Graduate Student Theses, Dissertations, & Professional Papers*. 11996.

<https://scholarworks.umt.edu/etd/11996>

This Thesis is brought to you for free and open access by the Graduate School at ScholarWorks at University of Montana. It has been accepted for inclusion in Graduate Student Theses, Dissertations, & Professional Papers by an authorized administrator of ScholarWorks at University of Montana. For more information, please contact scholarworks@mso.umt.edu.

LIDAR-LANDSAT COVARIANCE FOR PREDICTING CANOPY FUELS

By

MARGARET DORSEY EPSTEIN

Bachelor of Science, Montana State University, Bozeman, Montana 2020

Thesis

Presented in partial fulfillment of the requirements

For the degree of:

Master of Science

In Forestry

The University of Montana

Missoula, Montana

September 2022

Approved by:

Scott Whittenburg, Dean of The Graduate School

Graduate School

Carl Seielstad

Department of Forestry

Lloyd Queen

Department of Forestry

Anna Klene

Department of Geography

ABSTRACT

Epstein, Margaret, M.S., Summer 2022

Forestry

LiDAR-LANDSAT COVARIANCE FOR PREDICTING CANOPY FUELS

Managing wildfires in the western United States is becoming increasingly complex. Visualizing and quantifying canopy structures allows fire managers to both plan for fire and track recovery. Light detecting and ranging, or LiDAR can measure forests in three dimensions, but has limited spatial and temporal coverage. LiDAR-Landsat covariance uses machine learning to fill in the spatial and temporal gaps of LiDAR coverage with supplemental Landsat imagery. However, in order to capture real forest dynamics, a model needs to be stable enough to detect long term trends, sensitive to episodic disturbance, and general enough to work on multiple landcovers. The purpose of this research is to refine the methodology behind LiDAR-Landsat covariance and assess if these predictions can yield stable and ecologically sensible time series to track forest fire recovery over time. Gradient boosted machine models (GBMs) were built to predict canopy cover, height, and base height. Then, they were tested on a series of validation sites in order to quantify the spatial and temporal sources of error associated with these models. Finally, the models were used to predict the trajectories of canopy cover, height, and base height on 164 fire scars in Montana, Idaho and Wyoming over the course of 36 years. The models were sensitive to moderate and high severity disturbance, both on an incident wide and pixel by pixel basis. Overall model R^2 values were 0.89 for canopy cover, 0.84 for height, and 0.88 for base height. Year to year variability in canopy cover on validation sites was 2.3%. Height had more variability due to a sensor artifact from the transition from Landsat 5 to Landsat 8. On the Lost Fire the model found high severity fire corresponded with greater canopy fuel losses on a pixel-wise basis. The models also detected canopy recovery, and found four distinct trajectories in which burned sites recover from disturbance. Seventy-seven percent of sites fully recovered canopy cover to pre-fire conditions within the 36-year time series. Further refinement of GBM-based LiDAR-Landsat covariance can increase the sensitivity to smaller disturbances and reduce the impact of model error on performance.

TABLE OF CONTENTS

ABSTRACT.....	ii
ACKNOWLEDGEMENTS.....	vi
INTRODUCTION.....	1
METHODS.....	5
MACHINE LEARNING FRAMEWORK.....	6
LIDAR.....	7
LANDSAT.....	10
SAMPLING AND VALIDATION.....	13
FIRE ANALYSIS.....	14
RESULTS:.....	19
MODEL PERFORMANCE (OBJECTIVE 1):.....	19
VARIABLE IMPORTANCE.....	19
RANDOMLY SELECTED VALIDATION PIXELS:.....	20
VALIDATION OF INDEPENDENT LANDSCAPES (OBJECTIVE 2):.....	27
POWELL:.....	27
POWELL THROUGH TIME:.....	32
LUBRECHT:.....	36
LUBRECHT THROUGH TIME:.....	44
CANOPY FUELS ON BURNED LANDSCAPES (OBJECTIVE 3):.....	47
SHAPESELECTFOREST SPLINE CLASSIFICATION:.....	49
CUSTOM CLASSIFICATION FOR GBM TIME SERIES:.....	53
FIRE RECOVERY:.....	57
CASE STUDY: INTRA-FIRE HETEROGENEITY:.....	60
DISCUSSION.....	70
VARIABLE IMPORTANCE AND SENSOR EFFECT.....	70
STABILITY THROUGH TIME.....	72
SENSITIVITY TO DISTURBANCE.....	73
BURNED AREA CLASSIFICATION FRAMEWORK.....	76
CONCLUSION.....	78
BIBLIOGRAPHY.....	80

Figures

Figure 1: Workflow by objective.....	5
Figure 2: Map of training sites with year of LiDAR acquisition	8
Figure 3: Example of a flat fire.....	17
Figure 4: Example of a V-shaped fire.....	17
Figure 5: Example of a U-Shaped fire	18
Figure 6: Example of a Wave Fire	18
Figure 7: Variable importance by model	20
Figure 8: Predicted versus observed canopy cover on a sample of random pixels.....	24
Figure 9: Predicted versus observed height for a selection of random validation pixels.....	25
Figure 10: Predicted versus observed base height for a selection of random validation pixels.....	26
Figure 11: Observed canopy cover, predicted canopy cover, and residual canopy cover at North Powell	29
Figure 12: Observed, predicted and residual tree height at North Powell.	30
Figure 13: Observed, predicted, and residual base height at North Powell.	31
Figure 14: predicted versus observed canopy cover, height, and base height at North Powell	32
Figure 15: Predicted canopy cover from 1985 to 2021 at North Powell.....	33
Figure 16: Predicted height from 1985 to 2021 at North Powell.....	34
Figure 17: Predicted base height from 1985 to 2021 at North Powell.....	34
Figure 18: Observed and predicted canopy cover at Lubrecht Experimental Forest in 2005 and 2015	37
Figure 19: Residual canopy cover at Lubrecht Experimental Forest.....	38
Figure 20: Observed and predicted tree height at Lubrecht in 2005 and 2015	39
Figure 21: Residual tree height at Lubrecht Experimental Forest.	40
Figure 22: Observed and predicted base height at Lubrecht Experimental Forest in 2005 and 2015.....	41
Figure 23: Residual base height at Lubrecht Experimental Forest in 2005 and 2015	42
Figure 24: Predicted and observed canopy cover, height and base height in 2005 and 2015.....	43
Figure 25: Predicted canopy cover from 1985 to 2021 at Lubrecht.....	44
Figure 26: Predicted tree height from 1985 to 2021 at Lubrecht.....	45
Figure 27: Predicted base height from 1985 to 2021 at Lubrecht.....	45
Figure 28: Canopy cover trajectory by severity.....	48
Figure 29: Height trajectory by severity.	48
Figure 30: Base height trajectory by severity.	49
Figure 31: ShapeSelectForest splines from Moisen et. Al 2016 and the fire trajectories that resemble each spline.....	50
Figure 32: ShapeSelectForest classification by severity.....	51
Figure 33: Canopy cover trajectories of burned sites over time.	54
Figure 34: Height trajectories of burned sites over time.....	55
Figure 35: Base height trajectories of burned sites over time.....	55
Figure 36: Time to recover canopy cover as a function of pre-fire mean canopy cover, trajectory shape, and severity.....	58
Figure 37: Time to recover height as a function of pre-fire mean canopy cover, trajectory shape, and severity.....	59
Figure 38: Time to recover base height as a function of pre-fire mean canopy cover, trajectory shape, and severity.....	60
Figure 39: Imagery of the Lost Fire in 2022.....	61
Figure 40: Monitoring Trends in Burn Severity (MTBS) severity classification for the Lost Fire	62
Figure 41: Canopy cover through time on the Lost Fire.....	63

Figure 42: tree height through time on the Lost Fire	64
Figure 43: Base height through time on the Lost Fire	65
Figure 44: Proportion of pre-fire canopy cover on the Lost Fire 2 years post fire, 12 years post fire, 22 years post fire, and 32 years post fire.....	66
Figure 45: Proportion of pre-fire height on the Lost Fire 2 years post fire, 12 years post fire, 22 years post fire, and 32 years post fire.....	67
Figure 46: Proportion of pre-fire base height on the Lost Fire 2 years post fire, 12 years post fire, 22 years post fire, and 32 years post fire.....	68
Figure 47: Canopy cover, height, and base height trajectory by severity.	69

Tables

Table 1: LiDAR acquisitions used for model training	9
Table 2: Hyperparameters by model.....	19
Table 3: Performance metrics of each model.....	21
Table 4: Model performance by site	23
Table 5: Comparison of performance metrics on North and South Powell	28
Table 6: Year to year change in predicted canopy cover, height, and base height at North Powell	35
Table 7: Year to year change in canopy cover, height, and base height at Lubrecht.....	46
Table 8: Canopy cover characteristics of fires in each ShapeSelectForest bin.	52
Table 10: Characteristics of flat fires, U fires, V fires, and Wave Fires.	56
Table 11: Contingency Table of canopy cover and height classifications.....	56
Table 12: Contingency Table of canopy cover and base height classifications.....	56
Table 13: Contingency Table of base height and height classifications.	57

ACKNOWLEDGEMENTS

I am incredibly grateful to the many scientists and fire professionals who have supported and mentored me through my graduate experience. In particular, thank you to my advisor, Carl Seielstad, for your patience, mentorship, and trust in my ability to work through the obstacles. Anthony Marcozzi and Dr. Chris Moran both put hours of their own time into technical support for this project as well. I would not be doing this work without my mother, a pioneer who has defined my own environmental ethic. Thank you for modeling excellence.

INTRODUCTION

Fire is a natural and necessary force on western United States landscapes. However, anthropogenic climate change and altered forest structures are creating unprecedented fire conditions (Abatzoglou et al., 2021; Hagsmann et al., 2021a; Hanan et al., 2021). Fire management requires increasingly powerful decision-making tools to match the complexity of the natural and human factors in the fire environment (Noonan-Wright et al., 2011). Tools that improve the ability to quickly and accurately predict fuel type and distribution are especially relevant for forecasting fire behavior, planning fuel treatments, and better understanding landscape change.

Fuel, weather, and topography are the drivers of fire behavior at the scale of individual fires (McGranahan and Wonkka, 2018). Fuel is the flammable material in a wildland environment, and is the only element of fire behavior that can be directly manipulated through forest management. Fuel models depict the quantity and arrangement of flammable material on the landscape. They are also the substrate on which fire behavior modeling is performed (Reeves et al., 2006) which then informs operational decision making (Noonan-Wright et al., 2011). The horizontal distribution of fuels controls canopy connectivity and thus fire's ability to spread between trees or stands. The vertical distribution of fuels controls the ease at which a fire can move from the ground to the canopy. Increased fuel loading and ladder fuel components are associated with high severity fire (Hagsmann et al., 2021b; Skowronski et al., 2020) and subsequent slower vegetation recovery time (Bright et al., 2019).

Over the past few years, technological and computational improvements have allowed for more spatially and temporally detailed canopy fuel models. Light detecting and ranging (LiDAR)

is an active remote sensing technique that is increasingly being used for detailed forest observations (Coops et al., 2021; Guo et al., 2021). A laser is mounted and fired from a drone, airplane, or fixed stand. Then, the LiDAR sensor measures the time it takes for the emitted energy to bounce off the surrounding environment and return to the sensor. This method yields a detailed three-dimensional point cloud that can then be summarized into two dimensional rasters representing canopy fuel characteristics such as cover, height, or base height. In this thesis, canopy fuels refers to canopy cover, height, and base height together.

These LiDAR-derived canopy fuel metrics are important both ecologically and in fire behavior modeling. Canopy cover is the proportion of ground covered by the projection of tree canopies. Closed canopies create cooler, moister micro-climates that are somewhat buffered from fluctuations in air temperature (Davis et al., 2019). Closed canopies are associated with higher fuel loads (D'Este et al., 2021) and subsequently more severe fire (Hagmann et al., 2021b). Height is the distance from the ground to the top of the tree crown. Base height is the distance between the ground and the base of the canopy. Together, height and base height describe the vertical distribution of fuels in the canopy. Base height drives crown fire initiation because lower base heights require less energy and subsequently shorter flame lengths to move from the ground into tree crowns (Wagner, 1977).

LiDAR is particularly powerful for these metrics because it has high spatial resolution and is the best available sensor for measuring in the vertical plane (Hyde et al., 2006). However, LiDAR data is expensive and time consuming to acquire. These data acquisitions tend to have small spatial footprints because they are limited by the amount of ground the sensor can cover. Additionally, LiDAR datasets are static and only reflect the landscape at the time of acquisition. They become less relevant for vegetation assessment if they are not updated as the landscape

changes through time or succession. In contrast, traditional optical remote sensors provide global coverage and updates on a predictable cycle (16 days for Landsat). Landsat images are free and publicly available. But, Landsat does not measure directly in the vertical domain. Machine learning can draw upon both kinds of sensors to create fuel predictions with the spatial and temporal coverage of Landsat and three-dimensional measurements of LiDAR.

LiDAR-Landsat covariance is the process of identifying exploitable relationships between Landsat and LiDAR observations on the same pixels. This method can be used to extrapolate LiDAR-derived metrics beyond their original geographic footprints (Hudak et al., 2002; Matasci et al., 2018; Wilkes et al., 2015) or to update older LiDAR data without collecting another acquisition (Matasci et al., 2018). It has been successfully used to predict canopy cover (Matasci et al., 2018), height (Hudak et al., 2002; Pascual et al., 2010), and biomass (Pflugmacher et al., 2014).

Using LiDAR-Landsat covariance for fuels mapping has several advantages over existing methodologies such as the one used by LANDFIRE. LANDFIRE is an interagency data clearinghouse designed to create and provide raster datasets for wildland fire suppression and fuels planning. It includes national fuel predictions and is ubiquitous on wildfires across the United States. LiDAR-Landsat covariance has significantly outperformed LANDFIRE fuel models for predicting cover, height and base height (Moran et al., 2020), is faster to update after a disturbance, and is adept at predicting forward and backward in time. So, there is strong potential to outperform the current fuel products in use on wildland fires through LiDAR-Landsat covariance, both in accuracy of predictions and updating speed.

However, successful forest time series of forest attributes need to be stable enough to detect subtle, long term trends, yet also sensitive to episodic disturbance. This combination of

constraints is a challenging barrier to integrating machine learning into ecological applications. Despite the promise of the LiDAR-Landsat covariance method, all machine learning techniques have inherent error associated with them. Understanding the nature of these errors is critical to applying LiDAR-Landsat covariance to natural systems. Additionally, LiDAR-Landsat covariance tends to perform best on sites that are ecologically or spectrally similar to the sites the model was trained upon. So, the inherent variability within the predictions is often greater than the year to year change on the landscape, potentially leading to noisy or uninterpretable time series. The relative contributions of these spatial and temporal sources of error have not been explicitly explored.

The purpose of this thesis is to build upon previous work in LiDAR-Landsat covariance to quantify spatial and temporal errors and to determine the viability of this method for predicting canopy structures through time.

OBJECTIVES

- 1) To refine the methodology of Moran et al. (2020) to model canopy fuel using Landsat-LiDAR covariance and produce fuel metrics within Montana, Idaho, and Wyoming across a 36-year time period.
- 2) To assess the quality of predicted canopy fuel attributes, including the contributions of space and time in model prediction variability.
- 3) To evaluate changes in forest canopy fuels on burned landscapes from 1985 to 2021 as sites recover from wildfire.

METHODS

There are three phases to this project (Figure 1). Each phase corresponds to one of the above objectives. The first is to develop machine learning models to predict canopy cover, height, and base height from a series of Landsat and topographical indices. The second is to validate these models. The third phase is to apply the model predictions to a series of burned sites to track how canopy fuels recover over time.

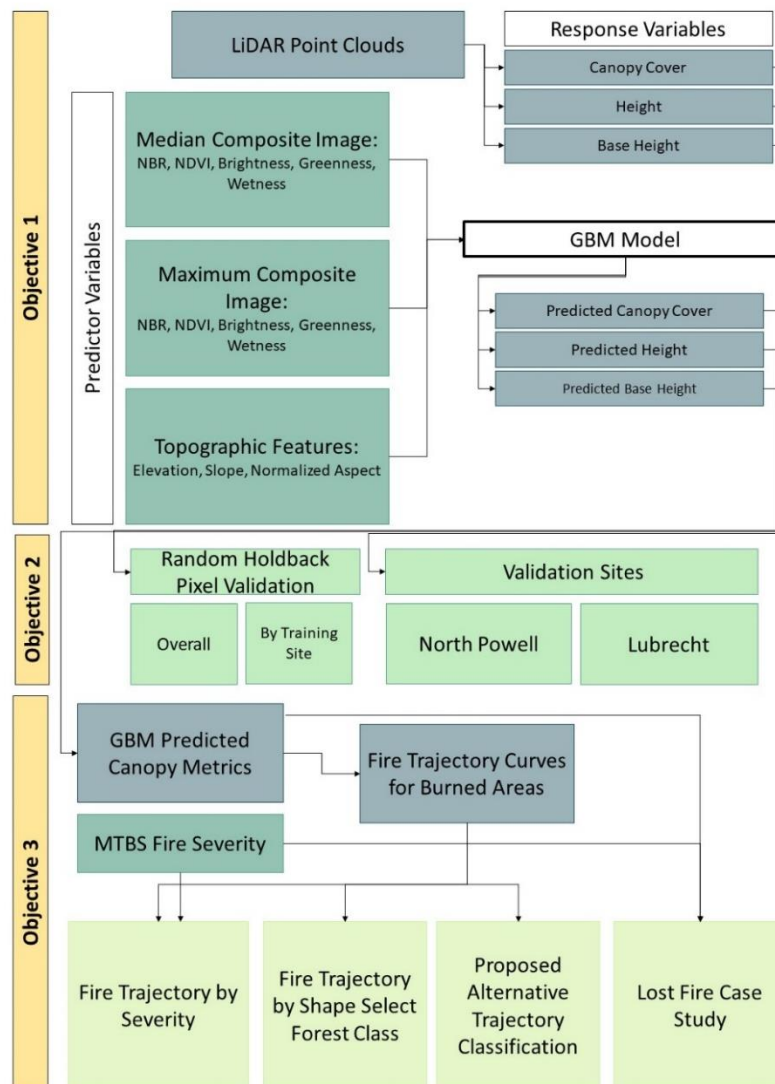


Figure 1: Workflow by objective.

MACHINE LEARNING FRAMEWORK

This project utilizes gradient boosted machine learning (GBM) to predict canopy fuel characteristics. Three separate GBM models were built to predict canopy cover, height, and base height respectively. The goal of the machine learning process was to teach the model to predict LiDAR-derived canopy metrics in areas where LiDAR does not exist.

GBM is a supervised machine learning (ML) method that iterates through a series of regression or classification trees and improves as it builds more trees. At each node in a tree, data is partitioned into groups based on some threshold value in the features. Eventually the data is sorted into smaller and smaller groups as the tree branches further. In this case, the regression trees are used to predict canopy cover, height, and base height based on Landsat-derived characteristics of the sites.

GBM is an ensemble method where final predictions are drawn from a composite of multiple regression trees. Trees are boosted by combining multiple weak learners into a single, better performing tree. However, unlike traditional decision-tree methods such as random forest, the trees are built sequentially, and the model improves relative to a loss function between each tree (Malohlava and Candel, 2021). The model gradient refers to progress along the loss function. The model is only allowed to move in a positive direction along the gradient. This is powerful because over several iterations the model will learn to create more effective ensembles of trees for the machine learning task, as measured by the loss function. The canopy cover, height, and base height gradients were calculated in respect to root mean square error (RMSE).

Parameters are metrics that are innate to the data, while hyperparameters are controls on the machine learning process that can be adjusted by the user. The objective of model tuning in

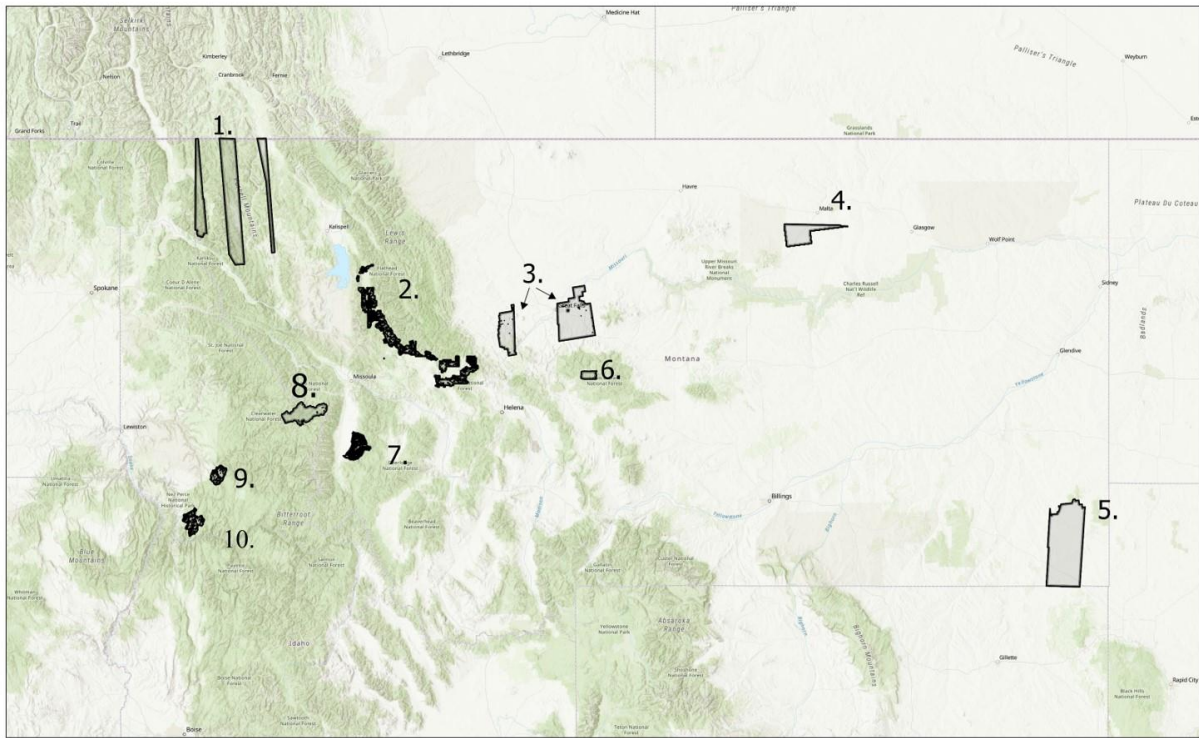
this instance, is to create a model that is sensitive to change in canopy conditions without overfitting to specific ecosystems or forest structures. Several hyperparameters were manipulated over the course of model tuning for this objective. Tree depth controls how many nodes are allowed in each decision tree, and is the single biggest control on model performance. Tree depth and number of trees together dictate the degree of nuance the model can detect. Overfit trees perform worse on novel data that they were not exposed to in training (Garcia Leiva et al., 2019) and decision tree-based systems can be prone to overfitting. Small ensembles of deep trees are more closely fit to the training data than big ensembles of shallow trees. Avoiding overfitting is important in this application because overfit trees will perform worse on new landscapes or landscapes that have been altered by disturbance or succession.

Cartesian grid searches are the process of testing all possible combinations from a list of hyperparameters. Two grid searches were used for model tuning. First, a preliminary grid tested several tree depths while holding all other hyperparameters constant. This grid search was performed first because tree depth has the single biggest impact on model performance of any user-defined control. The number of trees in the ensemble was not limited to encourage the machine to build a shallow forest of many trees. Then, once the optimal tree depth was defined, a second grid search was performed across learn rate, sample rate, and column sample rate to find the best performing overall model. The two-step approach is a systematic way of choosing every hyperparameter and parameter in the model with the least possible number of grid searches.

LIDAR

LiDAR-derived canopy cover, height, and base height observations served as the response variable in the model training process. The models were trained on a collection of ten

LiDAR acquisitions from across Montana and Northern Idaho. The LiDAR acquisitions were chosen to represent a wide variety of biomes across the Northern Rockies (Table 1). Training on a variety of ecosystems and forest types prevents the model from becoming overfit to a specific type of forest. Each LiDAR acquisition met the requirements for the US Geological Survey’s Quality Level 1, which includes 8 returns or more per square meter.



Training Sites:

- | | | | |
|--------------------------|----------------------|-----------------------|------------------------|
| 1. Lincoln (2020) | 4. Phillips (2020) | 7. Daly Gold (2010) | 10. Slate Creek (2009) |
| 2. Blackfoot-Swan (2015) | 5. Carter (2020) | 8. Powell (2011) | |
| 3. Cascade (2020) | 6. Tenderfoot (2005) | 9. Clear Creek (2011) | |

Figure 2: Map of training sites with year of LiDAR acquisition

Site	Acquisition Year	Hectares	Site Description:
Blackfoot-Swan	2014-2015	73055	Multi-piece LiDAR acquisition collected over two years. 110 miles north to south, covering most of the Blackfoot-Swan valley and into the Helena National Forest.
Carter	2018	14184	40 miles east of Broadus, Montana in Carter County. Originally collected in a survey of sage grouse habitat.
Cascade	2020	29426	Two-piece LiDAR acquisition covering Cascade County, Montana. Includes Great Falls and the surrounding foothills.
Clear Creek	2011	1983	Nez Perce-Clearwater National Forest. 15 miles southeast of Kooskia, Idaho.
Daly Gold	2010	4374	10 miles east of Hamilton, Montana. Bounded by the Bitterroot River to the North and Daly Creek to the South.
Lincoln	2020	36299	Three swaths of LiDAR acquired in Lincoln County, Montana. The north acquisition boundary is the Canadian border and the west edge is the Idaho border. Over 90% of the acquisition falls on the Salish-Kootenai National Forest.
Phillips	2018	4681	11 miles south of Malta, Montana.
Powell	2011	13404	Nez Perce-Clearwater National Forest. Bounded on the east by the Montana/Idaho state line. Partially bounded on the South by the Lochsa River.
Slate	2009	33396	Nez Perce-Clearwater National Forest. 24 miles south of Grangeville, ID. Transected east/west by Slate Creek.
Tenderfoot	2005	11604	Helena-Lewis and Clark National Forest. 3 miles west of Neihart, Montana.

Table 1: LiDAR acquisitions used for model training

Each LiDAR dataset was initially represented in a three-dimensional point cloud of XYZ values. Each cloud was then indexed using LasTools. The indexed point clouds were processed to 30-meter resolution using the R package LidR. The processing resolution was chosen to match the Landsat satellite imagery. The following definitions of height, cover, and base height were used to process all 10 acquisitions.

- Height is the 99th percentile of Z values greater than 2 meters within a pixel
- Cover is the sum of all Z values greater than 2 meters divided by the total number of returns*100
- Base height is the mean of all Z values greater than two meters minus the standard deviation of all Z values greater than two meters. There are multiple methods for calculating base height from LiDAR point clouds, including 1st percentile, ½ of height, and 25th percentile, and the value of the lowest non-ground point. Mean-SD was chosen for this application because it has previously outperformed other metrics in similar forests (Peterson et al., 2015).

Nonsensical values were removed from the LiDAR sets prior to training. Any value less than zero was set to zero. Canopy cover values greater than 100% were set to 100. Height and base height values greater than 70 meters were removed from the set. Base height values greater than 90% of the of the height in the same pixel were removed from the set.

LANDSAT

Landsat is the predictor variable in model training, and also the model input when predicting beyond the spatial or temporal footprint of an existing LiDAR acquisition. The study period stretches over 36 years and three iterations of Landsat sensors. The time period was determined based on the availability of Landsat 5, 7, and 8 imageries. Landsat 8 was used from

2013 to 2020, Landsat 5-7 composites were used in 2012, and Landsat 5 alone was used from 1985 to 2012. Landsat 5-7 composites were used in 2012 rather than Landsat 7 alone to avoid the effects of the scan line corrector failure on the Landsat 7 satellite, which causes striping in the imagery.

Landsat 8 has higher radiometric resolution and spectrally narrower bands than previous Landsat iterations (Flood 2014; Roy et al. 2016). This initially caused disjointed time series, as the model tended to underpredict forest characteristics in the years collected by Landsat 8. Two separate methods were used to address this issue. First, linear regression was used to transform Landsat 8 raw channel data to match Landsat 7 and 5. Landsat 8 was transformed to Landsat 7 instead of vice versa because most of the training data comes from Landsat 5 and 7. The transformation methodology and linear regression coefficients came from Roy et. al (2016). Because the Landsat 8 bands are spectrally narrower, the linear transformations presented by Roy are imperfect. So, the GBM was allowed to know which sensor a given pixel was acquired from so it could adjust for sensor differences internally.

All Landsat pre-processing and compositing was done in Google Earth Engine (GEE). The Landsat 5 and Landsat 7 Level 2 Collection 2 Tier 1 surface reflectance image collections were used from 1985 to 2012. The Landsat 8 Level 2 Collection 2 Tier 1 was used from 2013 to 2021. Each image collection was first filtered to only include images from May 1st to October 1st of the given year, in order to capture the full scope of vegetation growth while minimizing the impacts of snow and ice on the imagery. The QA_PIXEL band was used to identify pixels with clouds, cloud shadows, snow, ice and terrain occlusion, and the confidence that those unfavorable conditions exist. This band was used to select and mask pixels that were unfit for analysis. Any pixel with terrain occlusion was removed. Any pixel with a medium or high

confidence of clouds, shadow, or snow and ice was removed. Since the Landsat series covers the earth on a 16-day cycle, most places had multiple Landsat images within the growing season. Compositing is the process of summarizing multiple Landsat images into a single final image on a pixel by pixel basis. Two composite images were created for each year. One depicts the median pixel value of all images in the composite, and one depicts the maximum. Each image has 5 bands: normalized difference vegetation index (NDVI), normalized burn ratio (NBR), and Tassled Cap brightness, greenness, and wetness. NDVI and NBR are both normalized ratios of specific bands. NDVI includes near infrared and red bands, whereas NBR includes the near infrared and shortwave infrared bands. Tassled-Cap indices are derived from a principal component analysis (PCA) process, where many dimensions of spectral information are summarized along three axes of brightness, greenness, and wetness.

These five indices are useful because they are well understood in remote sensing and more intuitive to visualize than raw spectral information. However, some nuance is lost when raw spectral information is summarized into indices prior to machine learning. Ultimately, machine learning was performed on indices rather than raw spectral data for a few reasons. Decision trees are built around thresholds within the data. They essentially sort the input data into finer and finer bins. A strong interaction between two bands is harder to detect with a tree-based system. So, NBR and NDVI might add helpful information to the analysis because they better describe the distribution of burned land and vegetation than their component bands individually. Additionally, all five Landsat indices are well established and meaningful in natural resource applications. So, it is easier to visually check the model and determine that the outputs are sensible relative to the input indices. It is also more meaningful to fire managers since the model operates with familiar metrics such as NBR.

In addition to Landsat-derived indices, the models were trained on elevation, slope, and normalized aspect. These factors were included to capture the range of geophysical site characteristics that may control the distribution of canopy fuels on the landscape. Elevation and slope came from LANDFIRE (U.S. Department of Interior & U.S. Department of Agriculture, 2022). Aspect was normalized so the machine learning process would treat 0 and 360 degrees as adjacent slopes rather than opposites.

The LANDFIRE Existing Vegetation Cover dataset (US Geological Survey and US Department of Agriculture 2016) was used to query out training pixels with bare ground, urban development, or irrigated cropland. This was done so the model was only trained on pixels containing wildland fuels. Pixels with missing values for any Landsat or topographic feature were removed from the set. Following model development, predictions were made on entire landscapes, including bare ground, urban, and water pixels.

SAMPLING AND VALIDATION

The LiDAR acquisition sites ranged in size from 1783 to 73054 ha (Table 1). Model gradients in this project were calculated relative to root mean square error, and because unbalanced datasets are difficult to evaluate using this metric (Branco et al., 2019), each site was up-sampled or down-sampled to the mean number of pixels across all sites. Then, the sites were combined and shuffled, and 5% of the combined data was held back for validation. After all quality control and sampling holdbacks, each model was ultimately trained on 4,005,816 pixels.

There were two steps to model validation. The first step predicts on the random 5% holdback and compares the predictions to the respective LiDAR observations. Since these pixels

were selected randomly, they are spatially independent from each other, even within the same site. In addition, two ‘holdback validation’ sites were examined, which were not included in model development.

The first ‘hold back’ site is North Powell. Prior to model training, the Powell landscape was split into two equal parts. The south half of Powell was included in training, while the North half was reserved for validation. The North and South halves of Powell are ecologically and structurally similar. Both sites have experienced logging and have a distinct checkerboard pattern delineating these timber projects. The purpose of the Powell holdback is to evaluate variability through time while controlling for space, since the model was trained on a landscape that is functionally identical to North Powell. The second holdback landscape is Lubrecht Experimental Forest. Lubrecht has two separate LiDAR acquisitions covering the same area, flown ten years apart (2005, 2015). The purpose of the Lubrecht holdback is primarily to assess how well the model predict canopy trends between the two acquisitions.

FIRE ANALYSIS

The third objective and phase of this thesis is to evaluate how sites recover from wildfire. First, wildfire perimeters were gathered from the Monitoring Trends in Burn Severity (MTBS) database (USDA Forest Service & US Geological Survey, 2017). The minimum fire size in this dataset is 1000 acres. Fires were filtered to Montana, Idaho, and Wyoming and the years 1988 through 1994. This date range was chosen because it includes several large fire years, ensures 3-9 years of pre-fire data, and also has many years of Landsat available post-fire in which to detect a recovery signal. Fires were not included if any part returned after the original disturbance.

The MTBS dataset includes a pixel by pixel severity estimate. The possible pixel values are unburned to low severity, low severity, moderate severity, and high severity. These classes are calculated on a fire by fire basis based on the difference normalized burn ratio (dNBR), which is the difference in NBR pre and post-fire. These values are then manually sorted into severity classes by an analyst. A reference dataset is used to maintain consistency between different analysts (Eidenshink et al., 2007).

Each fire was assigned an overall severity classification. The classification is the mode of the severity classification of the pixels within the fire. Fires are rarely homogenous in severity but summarizing the fires into overall severity classes can capture the general fire effects of a site and allows for fires to be more easily compared to each other. Landsat data for each fire and each year from 1985 to 2021 was acquired through Google Earth Engine. Then, the GBM models were used to predict canopy cover, height, and base height for each pixel in the time series.

Each fire was summarized into a time-series curve based on the median observation for each year. In this thesis, recovery trajectory refers to these median curves. Fire and recovery present in many different ways on the landscape and classifying these recovery trajectories can help speak to the nature of the fire that causes specific recovery shapes. Classifying these curves is also necessary for comparing fires to one another.

The ShapeSelectForest (SSF) classification is a method of describing temporal patterns in Landsat time series (Moisen et al., 2016). It was developed to identify and classify forest disturbance regimes on broad geographic areas over time. The possible shapes are flat, decreasing, jump, a single jump, inverted vee, vee, linear increase, and double jump. Each shape is an archetype of a particular way in which disturbance presents spectrally on Landsat imagery. Some shapes include multiple kinds of disturbance. For example, the inverted vee shape is

associated with fire, harvest, stress, and conversion (Moisen et al., 2016). Fire is most commonly associated with a single jump or inverted vee shaped trajectory (Moisen et al., 2016). The R package ShapeSelectForest was used to classify fire trajectories into these pre-defined shapes. Canopy cover, height, and base height curves were classified separately. So, one fire could potentially have three different shapes associated with it if the cover, height, and base height curves are dissimilar from each other.

The ShapeSelectForest classification was then used as a guide for a new proposed classification specific to GBM-derived recovery trajectories. There are four shapes in the new proposed classification system based on the location of the local minimum in the trajectory following a disturbance. The local minimum is the inflection point where a forest begins to recover and regain canopy after disturbance. The goal of this classification system was to create a method for sorting curves by recovery trajectory without sorting by underlying forest type by default. These new classes are: V shaped fires, U shaped fires, Wavy fires, and Flat fires.

Flat fires have no distinct minimums or maximums (Figure 3). They have consistent values throughout the time series and are identical to the flat spline in the ShapeSelectForest system (Moisen et al., 2016).

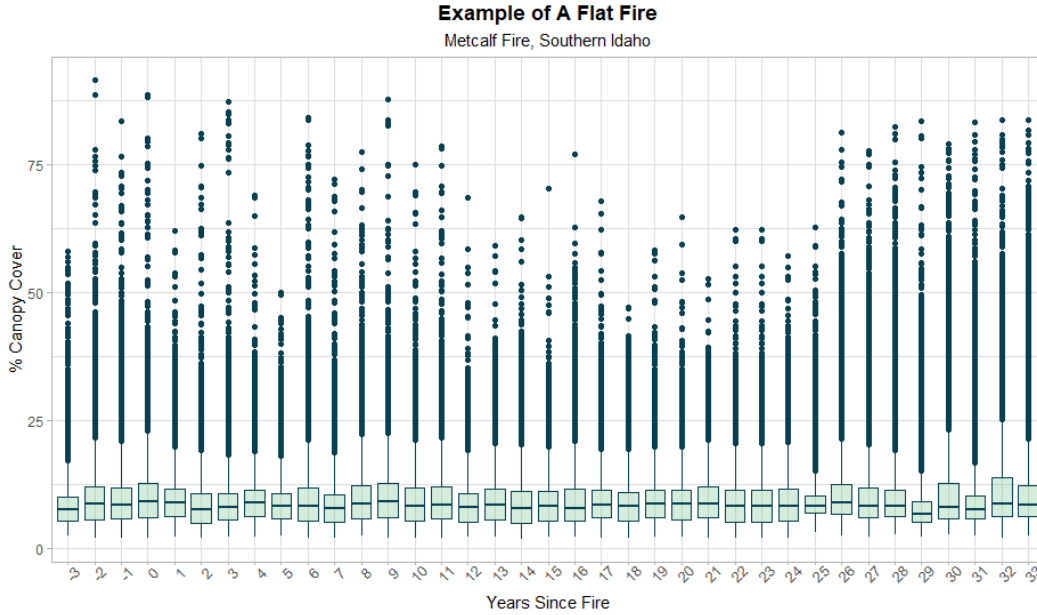


Figure 3: Example of a flat fire. The Metcalf Fire started on 8/10/1988 and burned 11,946 acres west of Malad City, Idaho. The plot is a traditional box and whisker in which the green box is defined by the 25th and 75th percentiles. The horizontal bar is the median, and the dots are outliers.

V fires decrease dramatically and reach their local minimum within two years of the fire event. Then, they gradually climb (Figure 4).

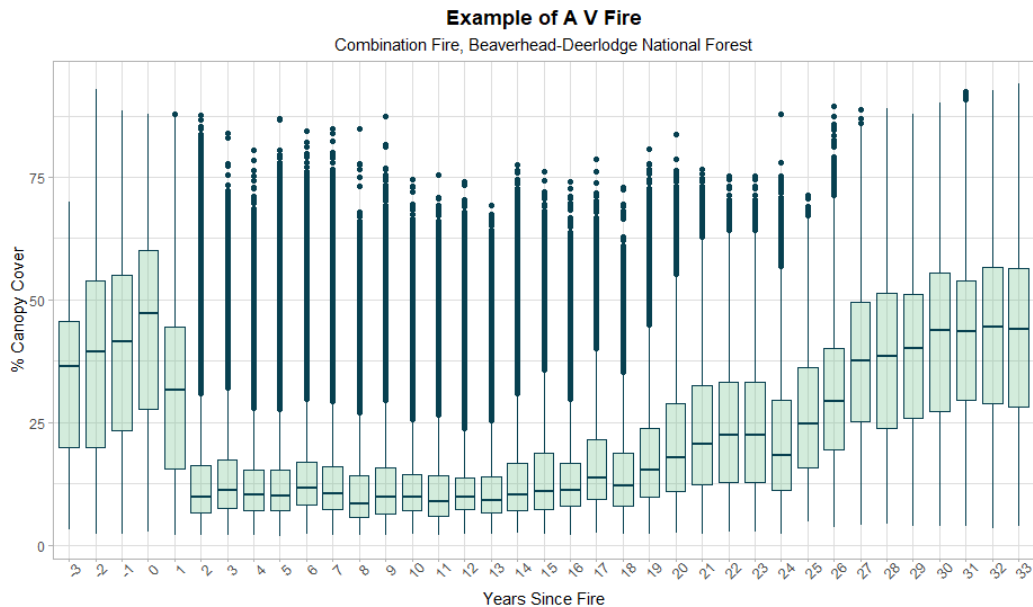


Figure 4: Example of a V-shaped fire trajectory. The Combination Fire began on 8/25/1988 and burned 8,588 acres 30 miles west of Deer Lodge, Montana on the Beaverhead-Deerlodge National Forest. This fire reached it's minimum on year 2.

U fires also have a single minimum in the time series but take more than two years to bottom out (Figure 5).

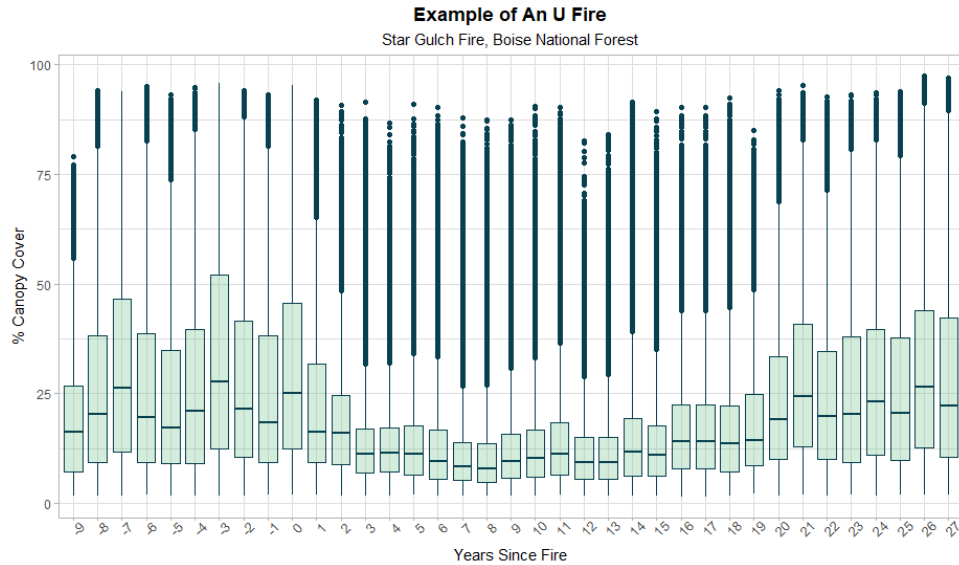


Figure 5: Example of a U-Shaped fire. The Star Gulch Fire burned 28,570 acres outside on the Boise National Forest, 17 miles east of Boise, Idaho. It began on 8/19/1994 and was part of the Idaho City Complex. The local minimum is at year 8, after which this fire began recovering canopy.

Wave fires have multiple peaks and valleys within the time series (Figure 6).

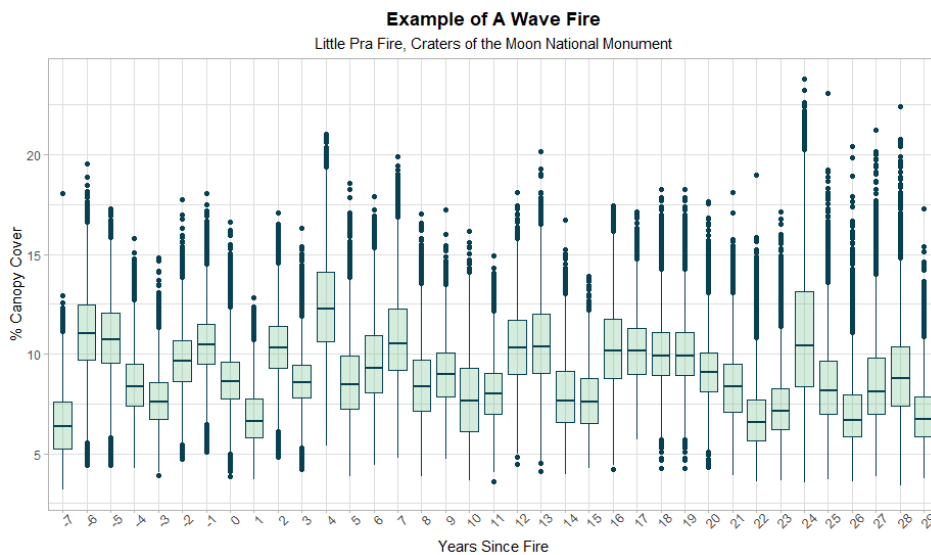


Figure 6: Example of a Wave Fire. The Little Pra Fire started on 8/3/1992 and burned 2,326 acres on the Craters of the Moon National Monument.

RESULTS:

The best performing models for canopy cover, height, and base height used the following hyperparameters (Table 2).

Model	N trees	Max Depth	Learn Rate	Sample Rate	Column Sample Rate
Canopy Cover	178	22	0.05	0.7	0.6
Height	119	26	0.05	0.7	0.6
Base Height	118	23	0.05	0.9	0.7

Table 2: Hyperparameters by model.

MODEL PERFORMANCE (OBJECTIVE 1):

VARIABLE IMPORTANCE:

Variable importance represents the relative influence of each training variable in the model. Greater variable importance is associated with variables that were frequently selected to split upon during tree building, and caused the tree to make bigger improvements relative to the loss function. The relative weight of each variable at each location in the tree and its contribution to improvement along the loss function was calculated with the Gedeon method (Gedeon, 1997) then normalized between 0 and 1.

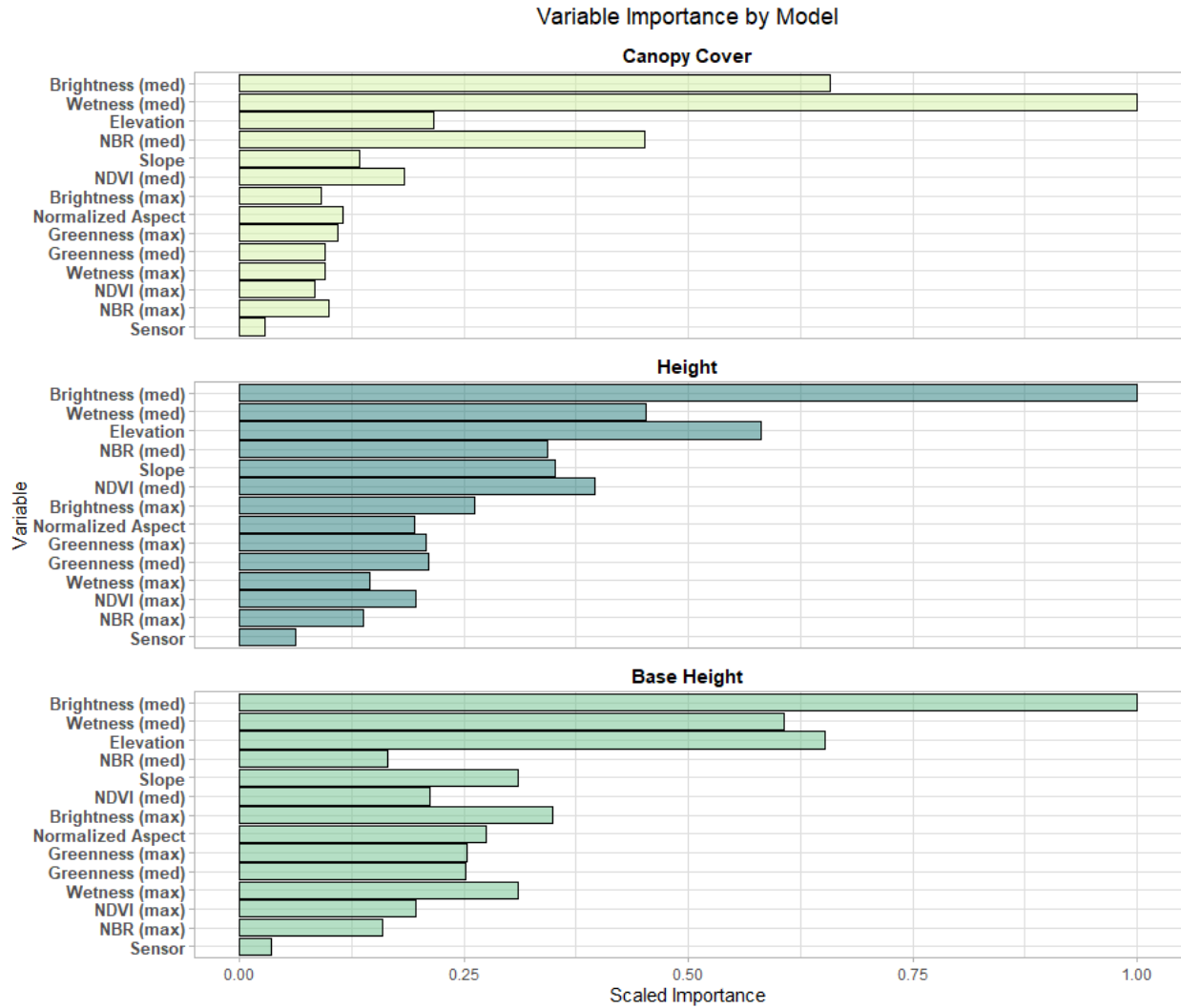


Figure 7: Variable importance by model

The most important training variables for predicting canopy cover were median wetness, median brightness, and median NBR. The most important variables for both base height and height were median brightness, elevation, and median wetness (Figure 7).

RANDOMLY SELECTED VALIDATION PIXELS:

Validation was performed by comparing the model-predicted canopy metrics with the directly measured LiDAR observations for randomly selected pixels (Table 3). The holdback pixels were not included in model training.

Metric	RMSE	MAE	R²	Bias	Observed Mean	Predicted Mean	Observed Kurtosis	Predicted Kurtosis	Observed skew	Predicted Skew
Canopy										
Cover (%)	9.46	6.41	0.89	2.00	49.59	47.59	1.90	1.91	-0.06	-0.05
Height (m)	5.96	3.34	0.84	0.82	24.84	24.02	3.68	3.36	0.93	0.73
Base										
Height (m)	1.65	1.01	0.88	0.30	5.92	5.61	6.23	5.63	1.39	1.16

Table 3: Performance metrics of each model. The validation was performed on a group of pixels randomly selected from within all 10 training sites. Root mean squared error (RMSE) and mean absolute error (MAE) describe the agreement between the model outputs and LiDAR observations.

Within individual LiDAR acquisition areas, model performance also was largely good, with differences among and between canopy metrics and sites (Table 5). Phillips and Tenderfoot were the best performing sites across all metrics. Lincoln was the worst performing site for both canopy cover and base height. South Powell also consistently underperformed the other sites. Otherwise, the best and worst ranking sites varied metric to metric. Site performance does not appear to depend on geography, forest type, or sensor. For example, Carter and Phillips are in eastern Montana. Phillips is primarily grassland with low density mixed conifer forest and Carter is primarily mixed grassland and sagebrush with isolated stands of juniper and ponderosa (Comer et al., 2003). The rangeland sites performed similarly to the forested western sites. The Idaho sites performed similarly to the sites east of the Continental Divide. Data for Clear Creek, Daly-Gold, South Powell, Slate, and Tenderfoot were collected by Landsat 5. Data for Blackfoot-Swan, Carter, Cascade, Lincoln, and Phillips were collected by Landsat 8. There does not appear to be a correlation between sensor and site performance at the sitewide level. The relationship between predicted and observed canopy cover and height are linear with residuals distributed mostly evenly between over and under estimation though, most under estimation at the highest canopy covers (Figures 8, 9). LiDAR-derived height values greater than 70 meters were removed prior to training, creating a ceiling in the possible observed values (Figure 9).

Base height had a linear relationship between predicted and observed values up to about 20 meters, then the model tends to under-predict high base heights (Figure 10).

Canopy Cover										
Site	RMSE	MAE	R ²	Bias	Observed Mean	Predicted Mean	Observed Kurtosis	Predicted Kurtosis	Observed Skew	Predicted skew
Phillips	1.49	0.66	0.99	0.30	9.79	9.49	12.44	13.26	2.79	2.88
Tenderfoot	3.71	2.59	0.93	0.46	33.14	32.67	2.95	3.07	-0.13	-0.31
Carter	8.43	4.39	0.87	2.83	22.52	19.70	4.57	4.83	1.45	1.52
Clear Creek	7.35	5.55	0.86	1.92	75.79	73.87	3.92	4.10	-1.18	-1.23
Slate	8.27	5.83	0.85	2.33	63.53	61.20	2.96	2.84	-0.68	-0.61
Daly Gold	8.47	6.15	0.83	2.15	47.45	45.30	2.28	2.30	-0.24	-0.28
South Powell	11.74	8.83	0.80	0.96	50.03	49.06	1.98	2.08	-0.06	-0.10
Lincoln	12.72	9.08	0.78	3.30	65.75	62.45	2.39	2.19	-0.68	-0.62
Blackfoot-Swan	10.39	7.79	0.75	1.76	54.98	53.22	2.67	2.76	-0.56	-0.65
Cascade	11.86	8.44	0.75	2.93	29.07	26.14	2.39	2.64	0.66	0.83
Height										
Site	RMSE	MAE	R ²	Bias	Observed Mean	Predicted Mean	Observed Kurtosis	Predicted Kurtosis	Observed Skew	Predicted skew
Phillips	1.34	0.72	0.99	0.08	13.27	13.19	5.48	5.29	1.66	1.60
Tenderfoot	1.31	0.84	0.95	0.07	17.38	17.31	3.21	3.43	-0.89	-1.06
Clear Creek	2.71	1.92	0.94	0.72	31.33	30.62	2.21	2.19	-0.29	-0.37
Carter	1.42	0.89	0.90	0.14	8.72	8.86	17.19	16.32	2.21	2.31
Slate	2.84	2.03	0.88	0.79	30.11	29.32	3.48	3.36	-0.42	-0.54
Daly Gold	2.56	1.82	0.83	0.42	22.52	22.10	3.00	3.20	0.09	0.00
Cascade	3.07	2.17	0.74	0.12	13.31	13.43	2.64	2.97	0.16	0.26
Blackfoot-Swan	5.01	3.60	0.48	0.57	21.32	21.90	3.02	4.29	0.33	0.58
South Powell	8.57	6.82	0.33	0.63	24.68	25.31	2.04	2.24	0.05	0.22
Lincoln	13.30	9.53	0.26	6.43	49.58	43.14	3.12	2.66	-0.87	-0.62

Base Height										
Site	RMSE	MAE	R ²	Bias	Observed Mean	Predicted Mean	Observed Kurtosis	Predicted Kurtosis	Observed Skew	Predicted skew
Phillips	2.23	1.52	0.97	0.22	5.46	5.24	5.14	3.52	2.08	2.01
Tenderfoot	1.31	0.84	0.97	0.07	17.38	17.31	3.21	3.43	0.58	0.46
Slate	0.52	0.30	0.88	0.04	3.64	3.60	2.58	2.36	0.47	0.19
Clear Creek	2.08	1.32	0.87	0.58	8.22	7.65	3.35	2.40	0.81	0.36
Carter	0.93	0.44	0.85	0.08	3.38	3.30	148.04	222.53	8.24	10.71
Daly Gold	1.30	0.91	0.83	0.30	6.36	6.06	3.20	3.26	0.41	0.11
South Powell	1.98	1.36	0.78	0.63	9.21	8.57	3.28	2.90	1.38	1.01
Cascade	1.38	0.89	0.70	0.16	3.99	3.83	17.07	14.95	2.28	2.15
Blackfoot-Swan	1.87	1.32	0.57	0.35	6.03	5.68	3.92	3.07	0.85	0.42
Lincoln	0.76	0.31	0.13	0.14	5.54	5.40	6.79	6.45	-0.86	0.71

Table 4: Model performance by site

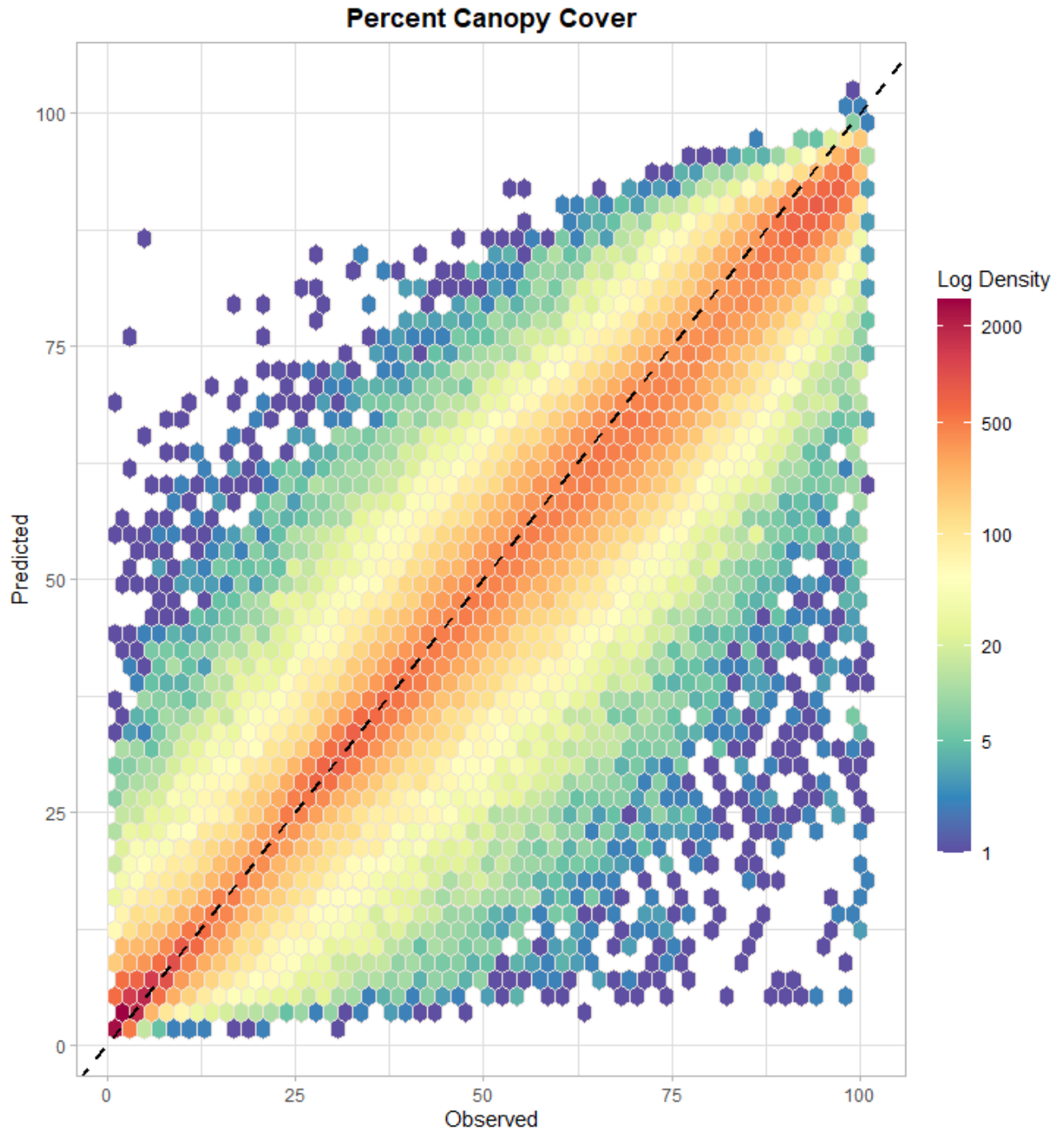


Figure 8: Predicted versus LiDAR observed canopy cover on a sample of random pixels. Density is displayed on a logarithmic scale.

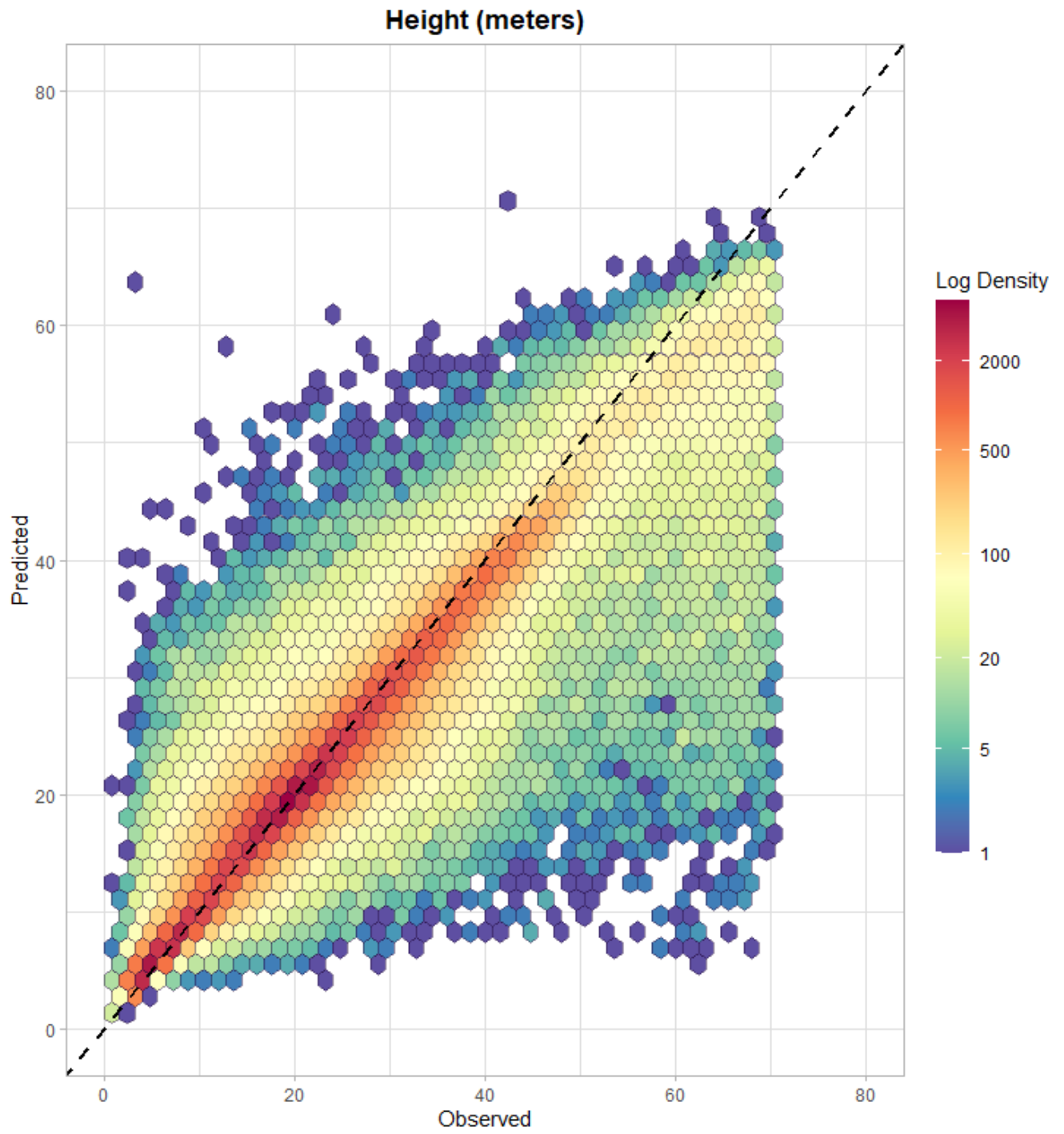


Figure 9: Predicted versus LiDAR observed height for a selection of random validation pixels. Density is displayed on a logarithmic scale.

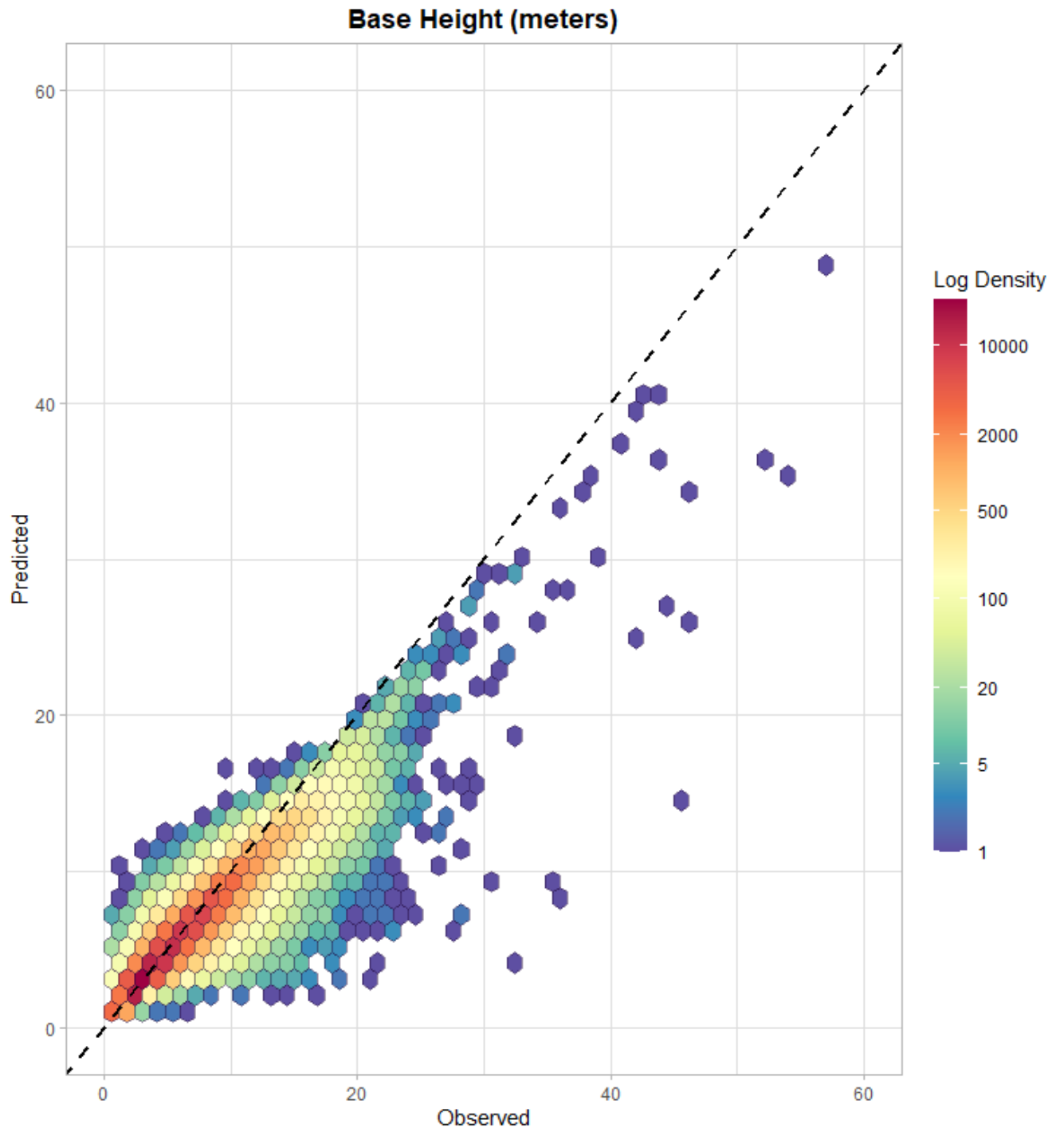


Figure 10: Predicted versus LiDAR observed base height for a selection of random validation pixels. Density is displayed on a logarithmic scale.

VALIDATION OF INDEPENDENT LANDSCAPES (OBJECTIVE 2):

POWELL:

North Powell and Lubrecht Experimental Forest were reserved from model training to examine if predictions on independent landscapes make coherent spatial sense. At Powell, there has been continuous timber harvest throughout the study period with the earliest recorded timber harvest on the site in 1954 (US Department of Agriculture, 2021). Powell is powerful for validation because the timber projects occurred on private land inholdings delineated by the Public Land Survey System (PLSS) grid, resulting in a checkerboard effect in the forest (Figure 11). Each pixel is spatially independent in the machine learning process, meaning the ML does not know which pixels neighbor each other. So, a strong visual test would be to examine the straight lines along the PLSS grid, to see if the ML correctly predicts the values (at least in a relative sense) of each pixel along the section boundaries (Figure 11, 12, 13).

Table 5 shows the statistics for North Powell and South Powell. They perform similarly, but North Powell has consistently higher error and lower R^2 , particularly for the Base Height metric. Variability contributing to error can be observed in the observed versus predicted plots (Figure 14). A zippering effect occurred in the canopy-cover predictions in North Powell (Figure 11), which could explain some of the difference in performance. This occurs because Powell straddles the border between two swaths of Landsat scenes. The zippering effect is a function of how the scenes are knitted together within Google Earth Engine. All three metrics

were calculated on the same Landsat imagery, but the zippering is less evident in height and base height predictions.

Additionally, predicted minus observed plots (Figures 11, 12, 13, bottom panel) show coherent spatial patterns to model over- and under-prediction. These patterns appear to occur on a topographic template, but on closer inspection, landcover seems to play a role too. However, they do not occur on the obvious harvest checkerboard pattern.

	Observed Mean	Predicted Mean	RMSE	R ²	MAE
	North Powell				
Canopy Cover (%)	40.61	41.15	13.65	0.65	10.45
Height (meters)	22.6	23.79	11.6	0.23	9.3
Base Height	4.95	3.28	3.26	0.17	2.54
	South Powell (random holdback pixels)				
Canopy Cover (%)	50	49.06	11.74	0.8	8.82
Height (meters)	24.68	25.31	8.6	0.33	6.8
Base Height	9.2	8.57	1.98	0.78	1.26

Table 5: Comparison of performance metrics on North and South Powell

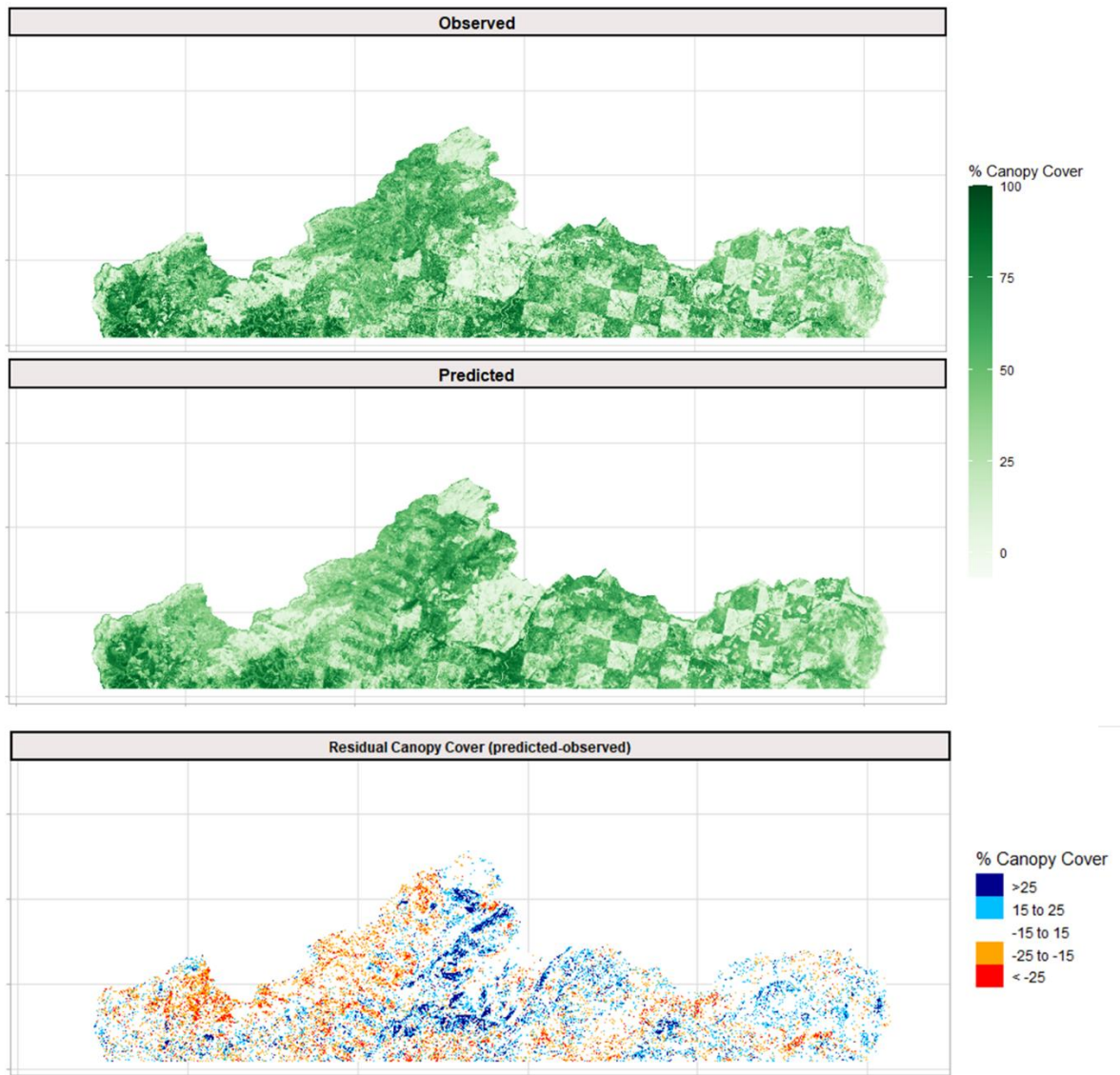


Figure 11: Lidar observed canopy cover (top), predicted canopy cover (middle), and residual canopy cover (bottom) at North Powell. Residual canopy cover is predicted canopy cover minus observed canopy cover

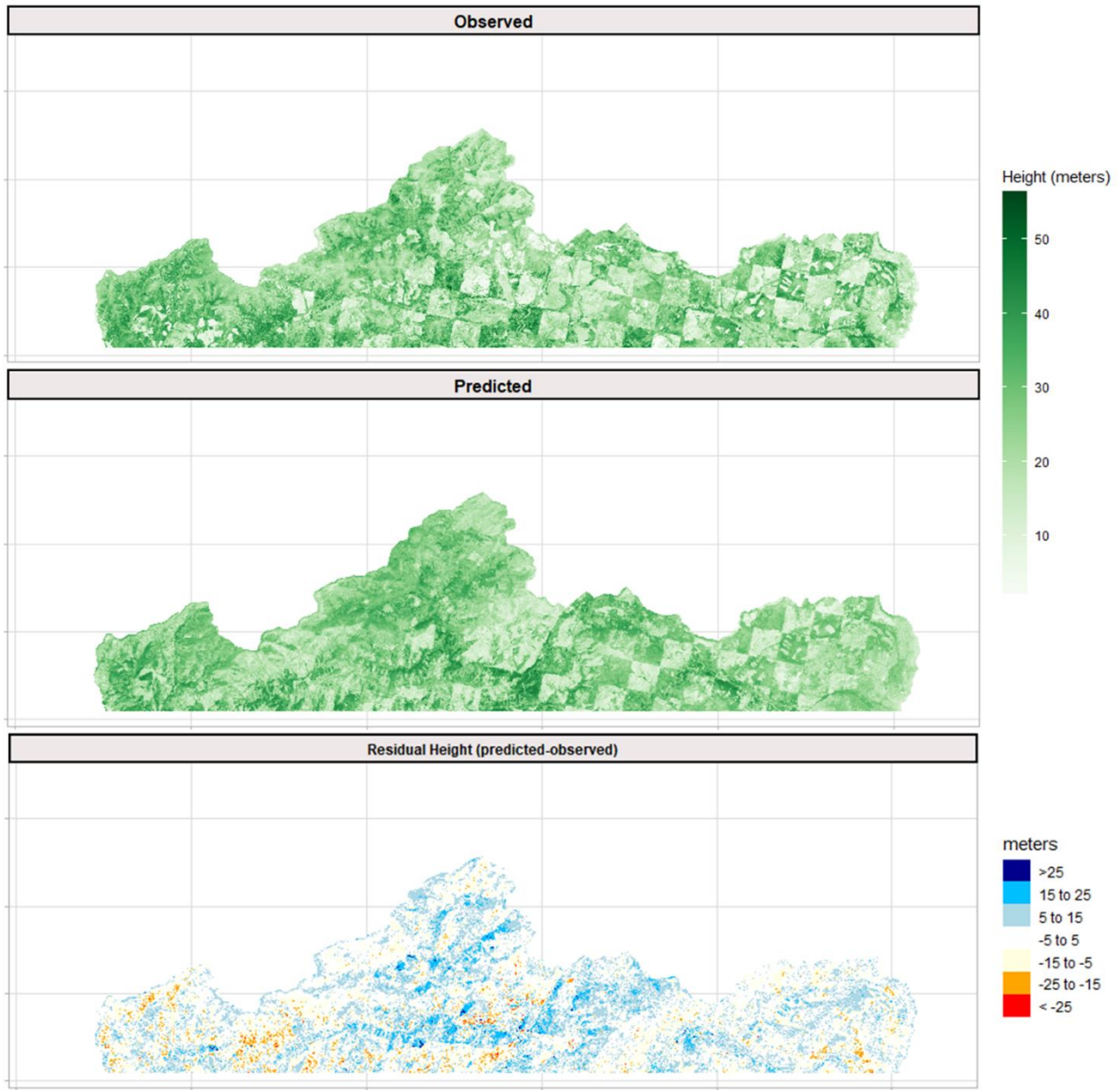


Figure 12: Observed (top), predicted (middle) and residual (bottom) tree height at North Powell.

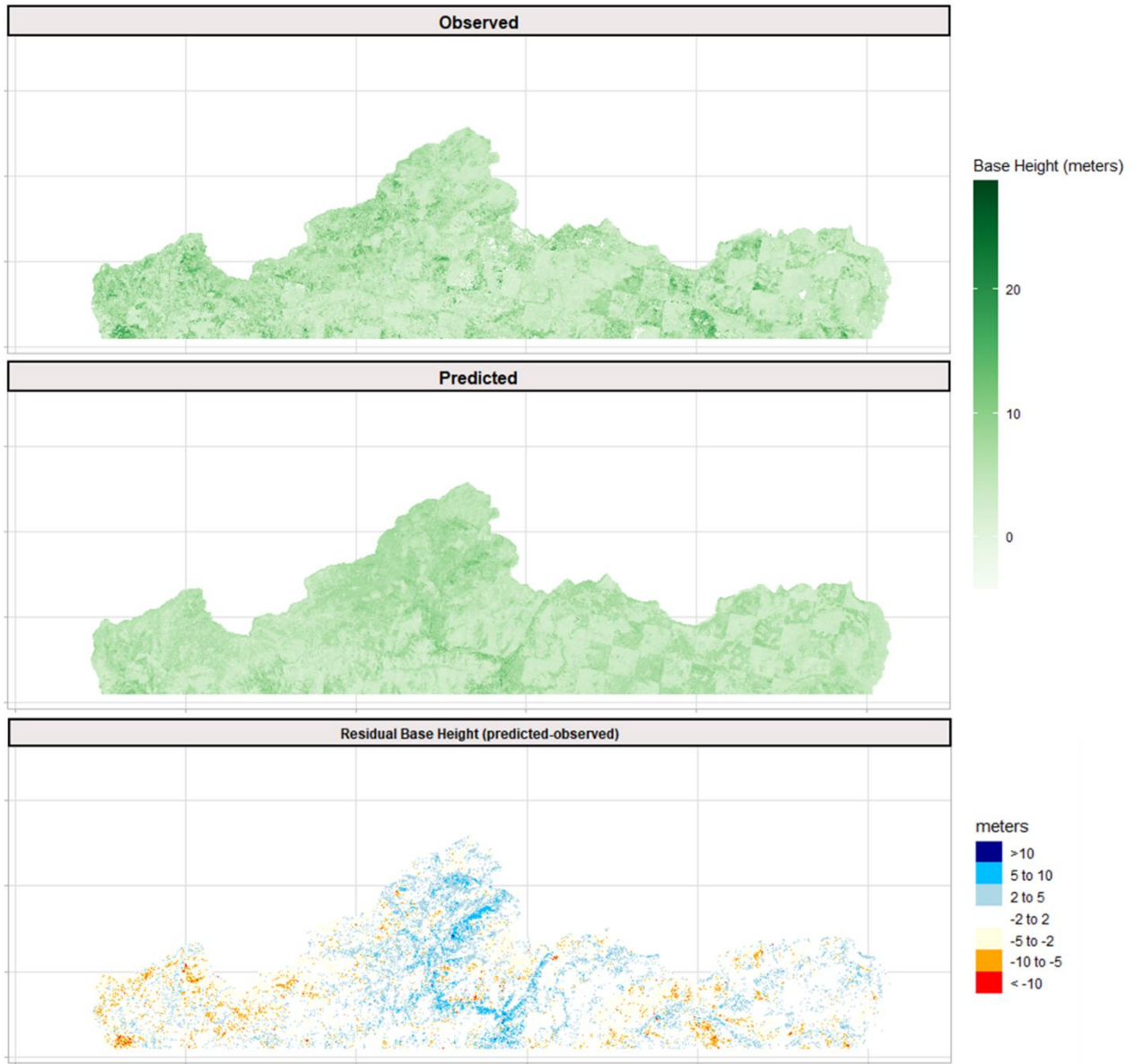


Figure 13: Observed (top), predicted (middle) and residual (bottom) base height at North Powell.

The predicted versus observed values for canopy cover and height are linear with even distribution of over and underestimating residuals. The GBM tended to slightly underpredict base height, which was also true of the randomly sampled validation pixels (Figure 14).

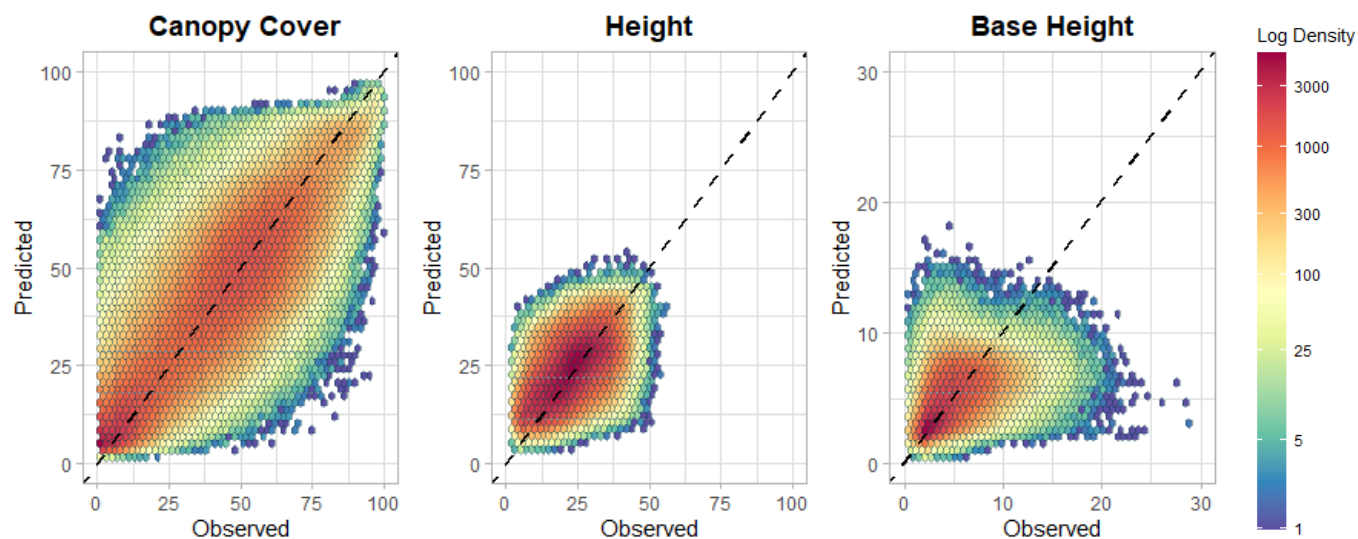


Figure 14: From left to right: predicted versus observed canopy cover, height, and base height at North Powell

POWELL THROUGH TIME:

North Powell experienced small fuel treatments and logging operations on various parts of the landscape throughout the time series, so the occasional year to year decreases are sensible as trees are harvested. However, large annual increases in canopy cover, height, and base height are of more concern because these are less likely to reflect actual change on the ground.

Overall, North Powell experienced stable median canopy cover from 1985-1994 at which point it declined systematically to a minimum in 2009, and began recovering (Figure 15).

Median canopy height showed a similar pattern with less variability (Figure 16). Base height

declined slowly from roughly 1992 to 2006 and then leveled off (Figure 17). The average year to year change in median canopy cover is 2.3% (Table 6). The greatest increase in canopy cover in any given year was 7.93%. The average absolute change in height and base height were 0.745 meters and 0.208 meters respectively. The greatest single year in increase in height was 2.9 meters and the single greatest increase in base height was 0.95 meters. Interannual increases and decreases tended to track across all three metrics, indicating that they are more likely a function of an underlying signal in the spectral data and not noise produced by the GBM. These trends are also consistent across the entire range of prediction values for a given year, not just the means. All three sets of predictions are fairly stable through time (Figures 15, 16, 17) and changes in canopy cover, height, and base height tend to track together.

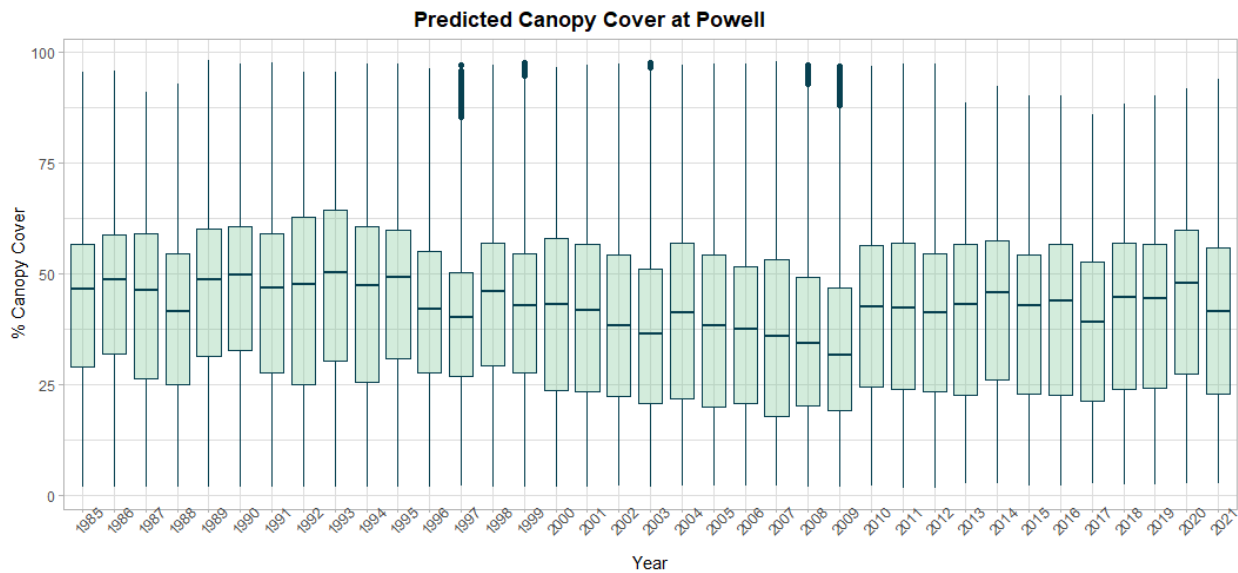


Figure 15: Predicted canopy cover from 1985 to 2021 at North Powell

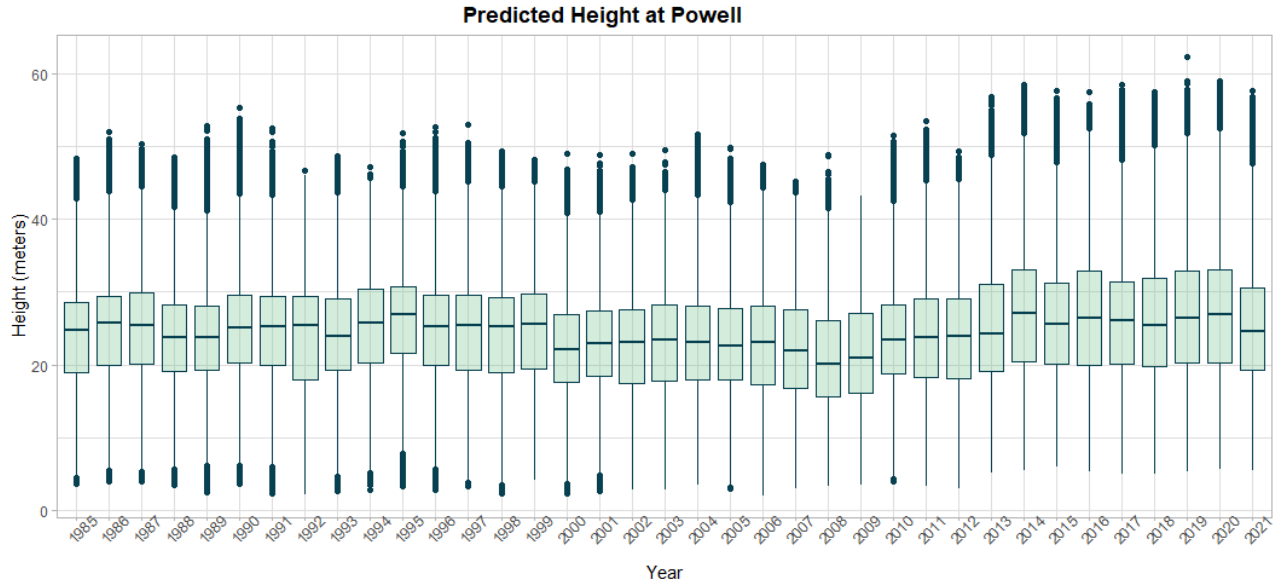


Figure 16: Predicted height from 1985 to 2021 at North Powell

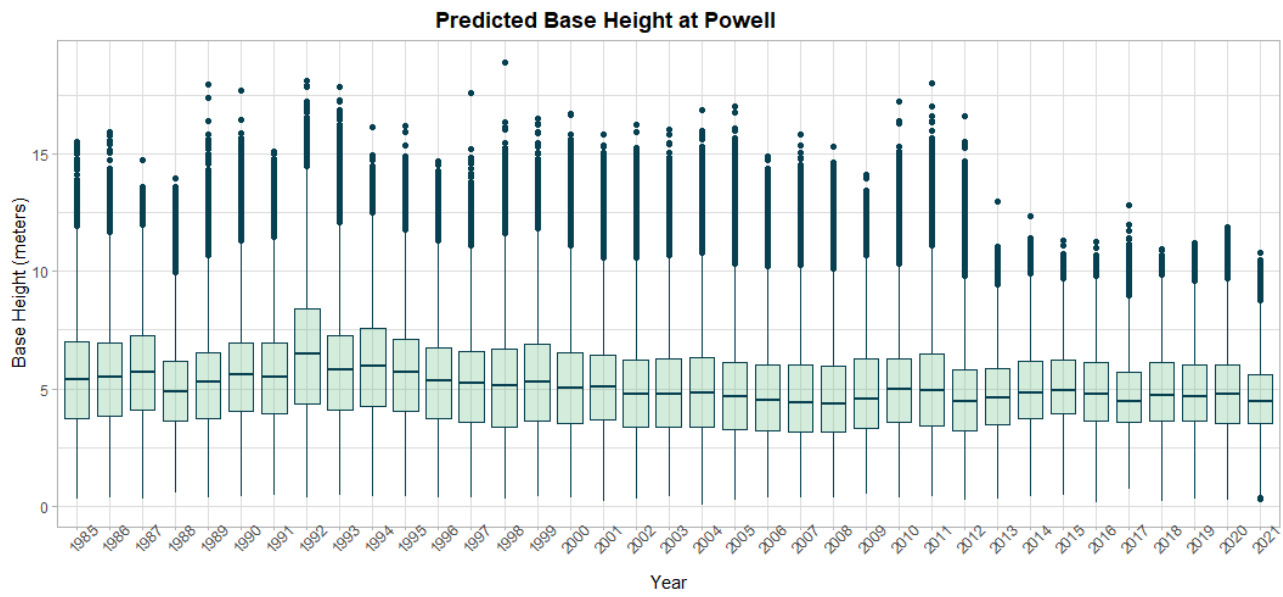


Figure 17: Predicted base height from 1985 to 2021 at North Powell

Year	Canopy Cover (%)				Height (m)				Base Height (m)			
	Median	Mean	Standard Dev.	Annual Change	Median	Mean	Standard Dev.	Annual Change	Median	Mean	Standard Dev	Annual Change
2021	42.29	40.48	19.35	-4.02	24.91	25.26	7.15	-1.62	4.42	4.58	1.44	-0.21
2020	48.27	44.50	19.41	2.86	27.13	26.88	7.89	0.21	4.70	4.78	1.62	-0.03
2019	44.88	41.63	19.45	0.02	26.60	26.67	8.01	0.74	4.62	4.81	1.57	-0.05
2018	45.20	41.62	19.53	3.78	25.63	25.92	7.63	-0.02	4.69	4.86	1.63	0.20
2017	39.61	37.83	18.62	-3.25	26.09	25.95	7.53	-0.58	4.41	4.66	1.48	-0.24
2016	44.41	41.09	19.91	1.53	26.58	26.53	7.87	0.65	4.78	4.90	1.61	-0.14
2015	42.64	39.56	19.10	-3.00	25.60	25.88	7.29	-1.08	4.86	5.04	1.50	0.11
2014	45.82	42.55	19.40	2.16	27.06	26.96	7.87	2.11	4.77	4.94	1.59	0.28
2013	43.00	40.39	19.86	0.43	24.12	24.86	7.42	1.18	4.55	4.66	1.58	0.14
2012	41.40	39.97	20.42	-1.19	23.77	23.68	7.39	-0.11	4.36	4.52	1.71	-0.46
2011	42.14	41.15	21.07	0.21	23.74	23.79	7.55	0.01	4.81	4.98	1.95	0.00
2010	42.32	40.94	20.23	7.93	23.42	23.78	7.34	2.50	4.92	4.98	1.77	0.19
2009	31.30	33.01	17.44	-2.03	20.68	21.28	6.66	0.57	4.43	4.79	1.84	0.16
2008	34.15	35.04	18.60	-1.16	20.01	20.71	6.68	-1.38	4.27	4.63	1.85	-0.04
2007	35.38	36.20	20.92	-0.72	21.82	22.09	7.22	-0.60	4.31	4.67	1.90	0.06
2006	37.10	36.92	19.80	-0.90	22.84	22.69	7.26	-0.22	4.41	4.61	1.77	-0.15
2005	37.87	37.83	20.75	-2.25	22.52	22.91	7.25	-0.29	4.58	4.77	1.85	-0.15
2004	40.68	40.07	21.29	4.02	22.88	23.19	7.39	0.36	4.76	4.91	1.93	0.06
2003	35.40	36.06	19.77	-2.51	23.06	22.84	7.21	0.24	4.67	4.85	1.85	-0.06
2002	37.87	38.57	20.91	-1.03	22.84	22.60	7.18	-0.36	4.68	4.92	1.95	-0.21
2001	40.60	39.60	20.85	-1.18	22.94	22.95	7.05	0.67	5.00	5.12	1.85	-0.05
2000	41.99	40.78	21.41	-0.16	22.09	22.28	7.01	-2.12	4.94	5.18	2.07	-0.11
1999	42.10	40.94	18.58	-1.70	25.29	24.40	7.15	0.28	5.17	5.28	1.99	0.21
1998	45.49	42.64	19.22	3.84	25.17	24.12	7.52	-0.17	5.00	5.07	1.99	-0.03
1997	39.96	38.80	17.09	-2.58	25.13	24.29	7.10	-0.25	5.13	5.10	1.84	-0.16
1996	42.07	41.38	19.31	-3.39	25.08	24.54	7.14	-1.56	5.23	5.26	1.93	-0.31
1995	48.82	44.77	19.78	1.46	26.93	26.10	7.26	0.90	5.61	5.57	1.97	-0.36
1994	46.72	43.31	21.65	-3.50	25.89	25.20	7.13	0.93	5.86	5.93	2.13	0.13
1993	49.54	46.80	22.31	2.40	24.07	24.26	7.49	0.47	5.71	5.80	2.23	-0.60
1992	47.50	44.41	22.30	1.61	25.22	23.79	7.27	-0.91	6.39	6.41	2.48	0.95
1991	46.36	42.80	20.12	-3.01	25.37	24.70	7.07	-0.29	5.43	5.46	1.94	-0.04
1990	49.33	45.81	19.52	0.71	25.06	24.99	7.20	1.07	5.55	5.49	1.91	0.32
1989	48.50	45.10	19.85	5.67	23.76	23.92	7.02	0.22	5.21	5.18	1.82	0.24
1988	40.97	39.43	19.28	-3.04	23.81	23.70	6.75	-1.11	4.82	4.93	1.70	-0.76
1987	46.10	42.46	20.09	-2.18	25.43	24.81	6.81	0.07	5.63	5.69	2.00	0.28
1986	48.32	44.64	18.68	2.25	25.67	24.74	7.11	0.98	5.43	5.41	1.97	0.04
1985	46.31	42.39	18.62	-	24.74	23.76	6.74	-	5.35	5.38	2.02	-

Table 6: Year to year change in predicted canopy cover, height, and base height at North Powell Cell color corresponds with the magnitude of year to year change, with green cells decreasing in value between the previous and current year, and red cells increasing in value.

The landscape of North Powell is adjacent to and similar to South Powell, providing a baseline for inferring the inherent error associated with GBM predictions prior to diverging geographically and ecologically from the training data. The results suggest that GBM predictions yield stable time series and reveal spatial patterns that are consistent with what is expected on the ground. They indicate that GBM canopy cover models yield about 14% (based on RMSE) uncertainty intrinsic to the modeling process before any spatial or temporal error is introduced. These intrinsic error estimates are about 12 meters and 3 meters for height and base height respectively.

LUBRECHT:

Lubrecht Experimental Forest has two separate LiDAR acquisitions for validation. The first was flown in 2005, and the second in 2015. The purpose of the Lubrecht validation is to evaluate the model's ability to detect the direction and magnitude of forest change between two points in time. It is worth acknowledging that the 2005 LiDAR acquisition did not meet USGS Quality Level 1 standards due to low return density (1.5 returns/m²) and large scan angles (± 30 degrees), and some of the differences in model performance are likely related to these differences.

The mean LiDAR-observed canopy cover at Lubrecht in 2005 was 51.55%. The predicted canopy cover was 43.03%. The mean LiDAR-observed canopy cover in 2015 was 43.76% and the predicted canopy cover was 44.44%. The RMSE between predicted and observed canopy cover was 16.41 in 2005 and 12.14 in 2015. The R^2 was 0.57 in 2005 and 0.69

in 2015. The model mostly under predicted canopy cover in 2005, while 2015 errors were more evenly divided between over and under-prediction (Figure 19). As with North Powell, error was not spatially random, with similar patterns observed that may be associated with a complex interaction between terrain and landcover.

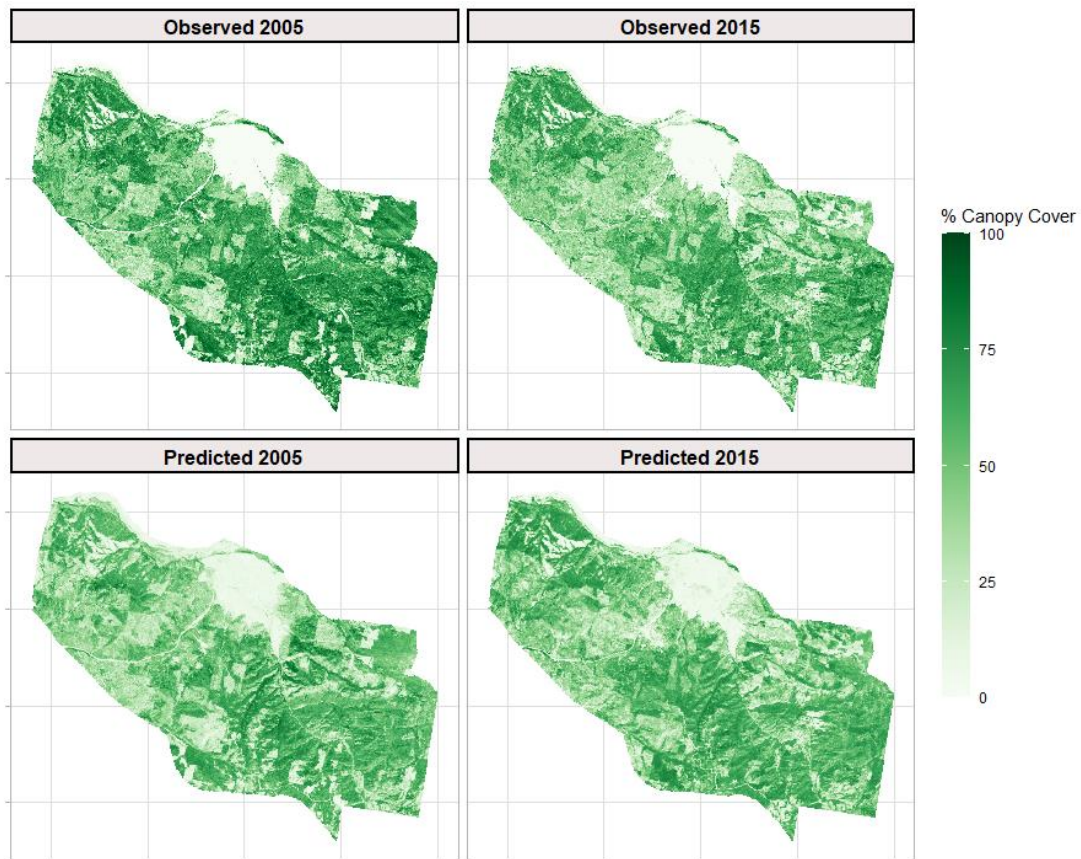


Figure 18: Observed (top) and predicted (bottom) canopy cover at Lubrecht Experimental Forest in 2005 (left) and 2015 (right).

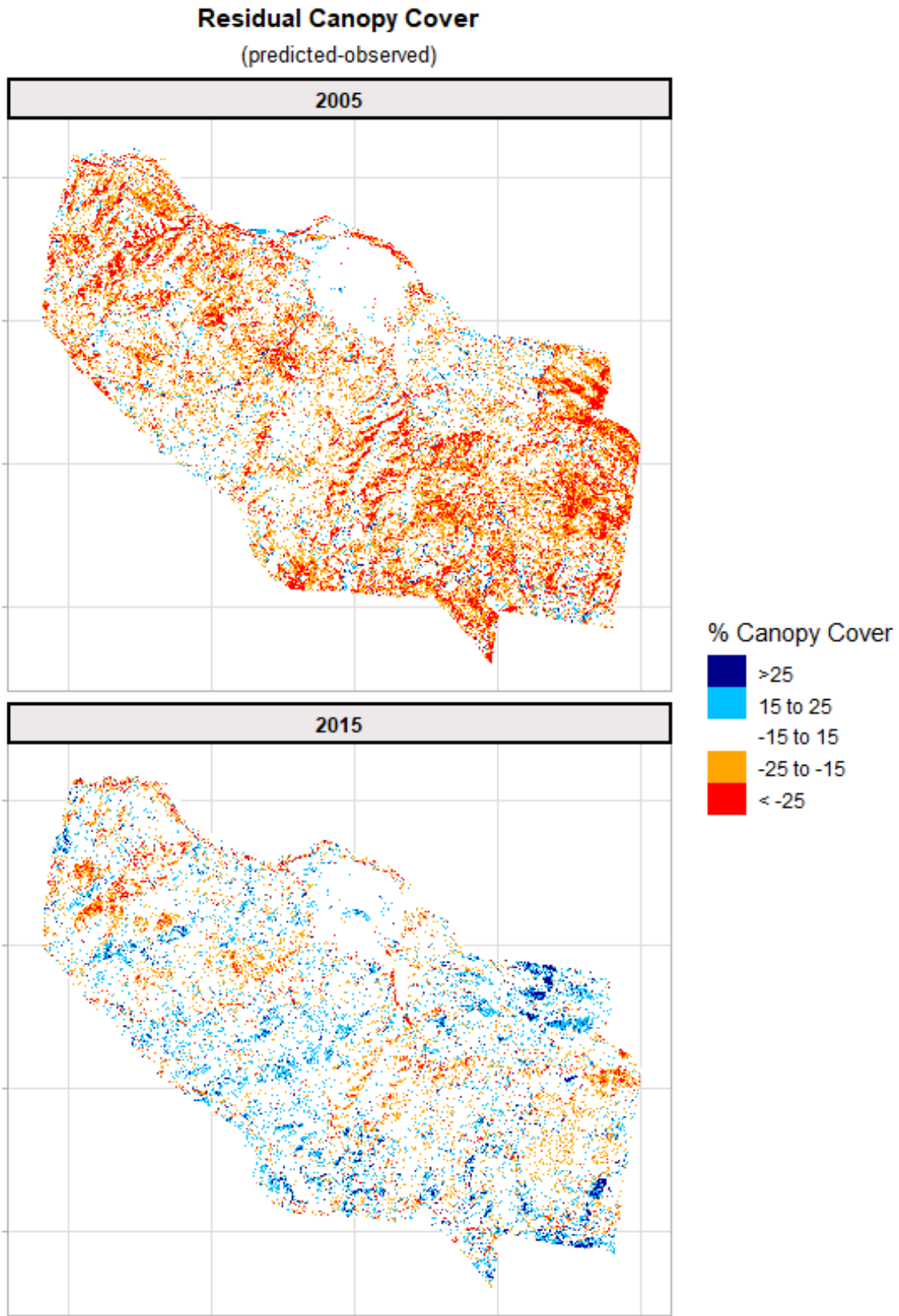


Figure 19: Residual (predicted-observed) canopy cover at Lubrecht Experimental Forest

Mean observed height in 2005 was 20.90 meters and predicted height was 25.26 meters, compare with a 2015 observed mean height of 19.32 meters and predicted height of 22.87 meters. The RMSE between predicted and observed height was 9.35 in 2005 and 7.92 in 2015. The R^2 was 0.97 in both 2005 and 2015. The model tended to over predict height in the large meadow in the north central part of the acquisition, while underpredicting height in riparian corridors and mountainous terrain (Figure 21), and the spatial patterns in predicted minus observed are similar between the two years.

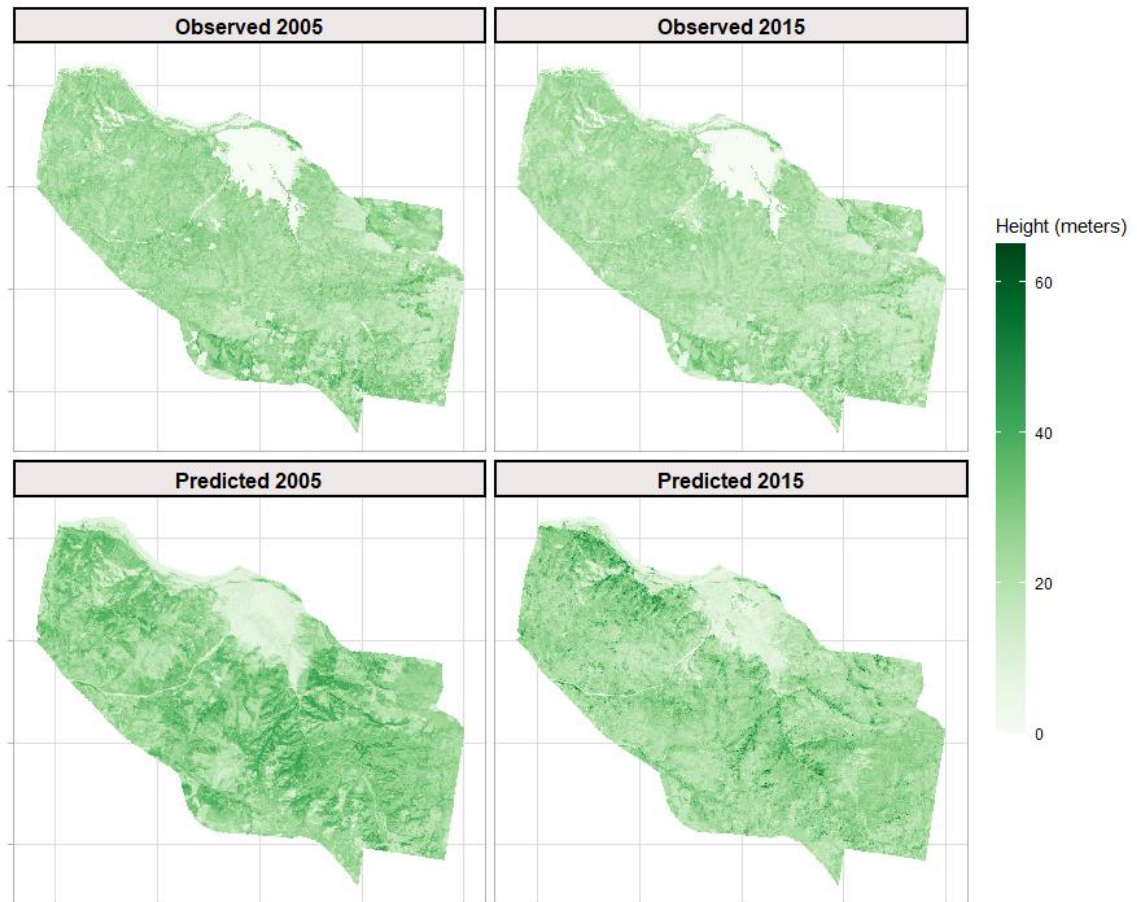


Figure 20: Observed (top) and predicted (bottom) tree height at Lubrecht in 2005 (left) and 2015 (right)

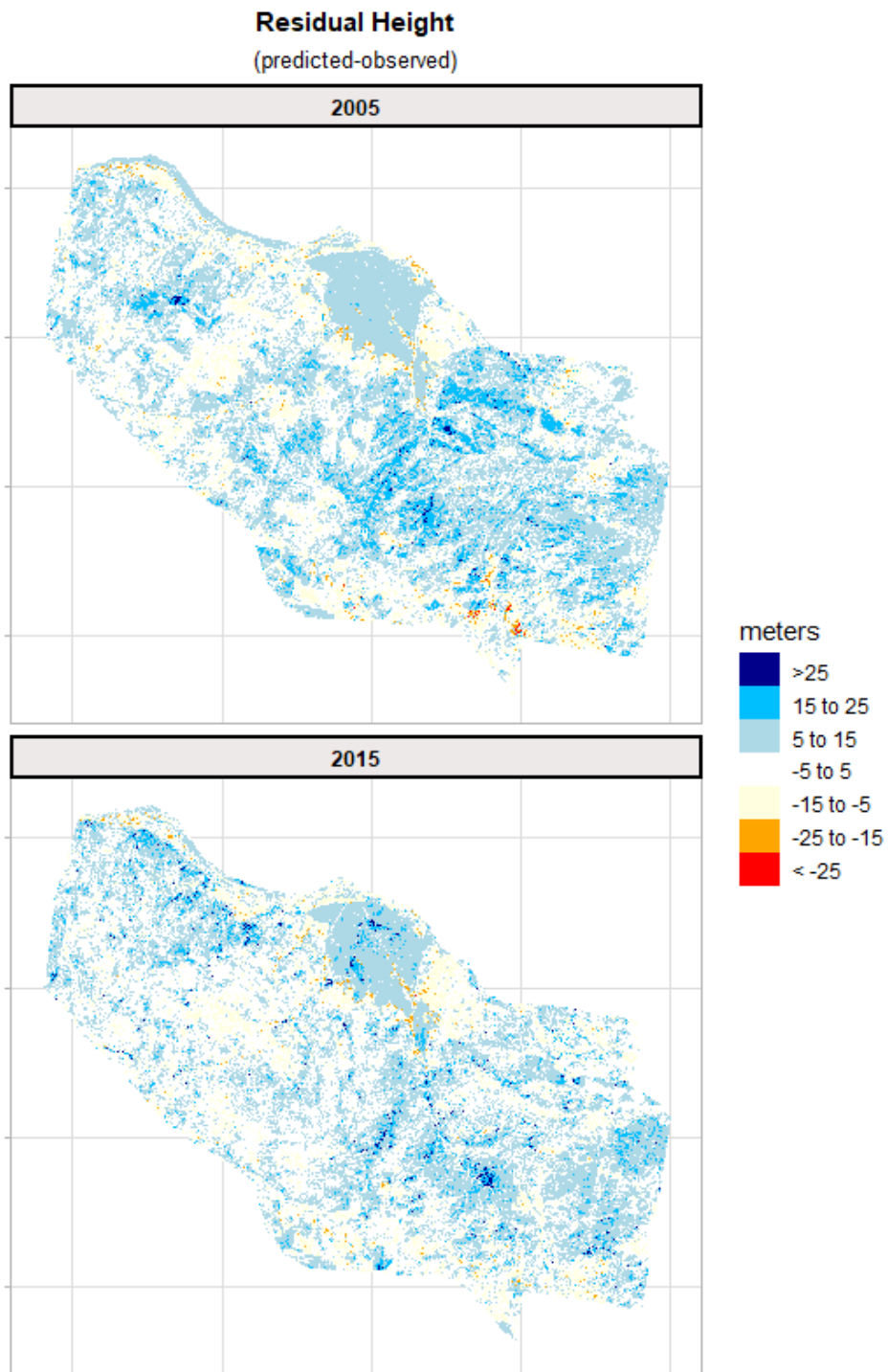


Figure 21: Residual (predicted-observed) tree height at Lubrecht Experimental Forest. The blue pixels represent overpredicted height, and the yellow and red pixels are underpredicted height.

Finally, the observed mean base height in 2005 was 5.67 meters, compared to a predicted 6.05 meters. The observed mean base height in 2015 was 6.77 meters and the predicted mean base height was 5.41 meters. The RMSE between predicted and observed base height was 3.45 in 2005 and 3.62 in 2015. The R^2 was -0.11 in 2005 and 0.04 in 2015.

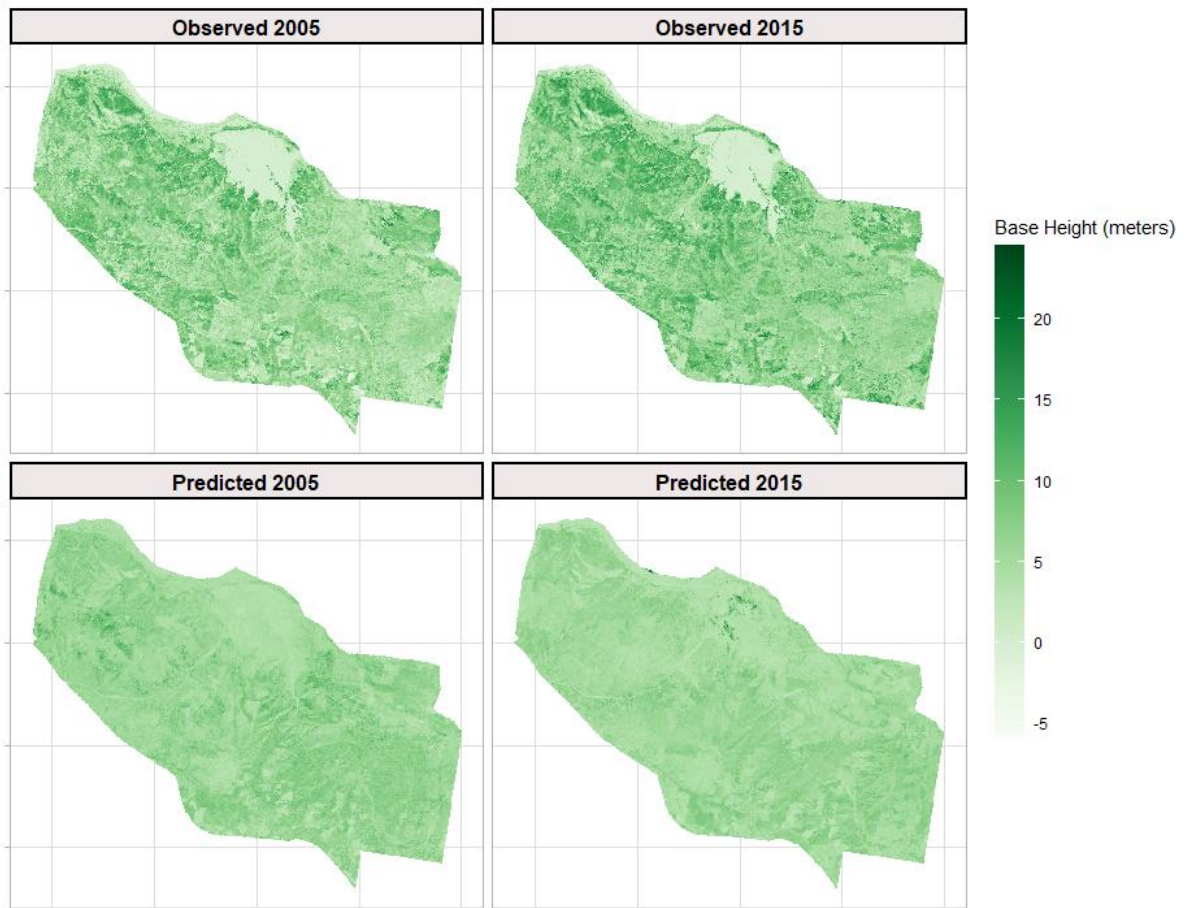


Figure 22: Observed (top) and predicted (bottom) base height at Lubrecht Experimental Forest in 2005 (left) and 2015 (right).

Residual Base Height
(predicted-observed)

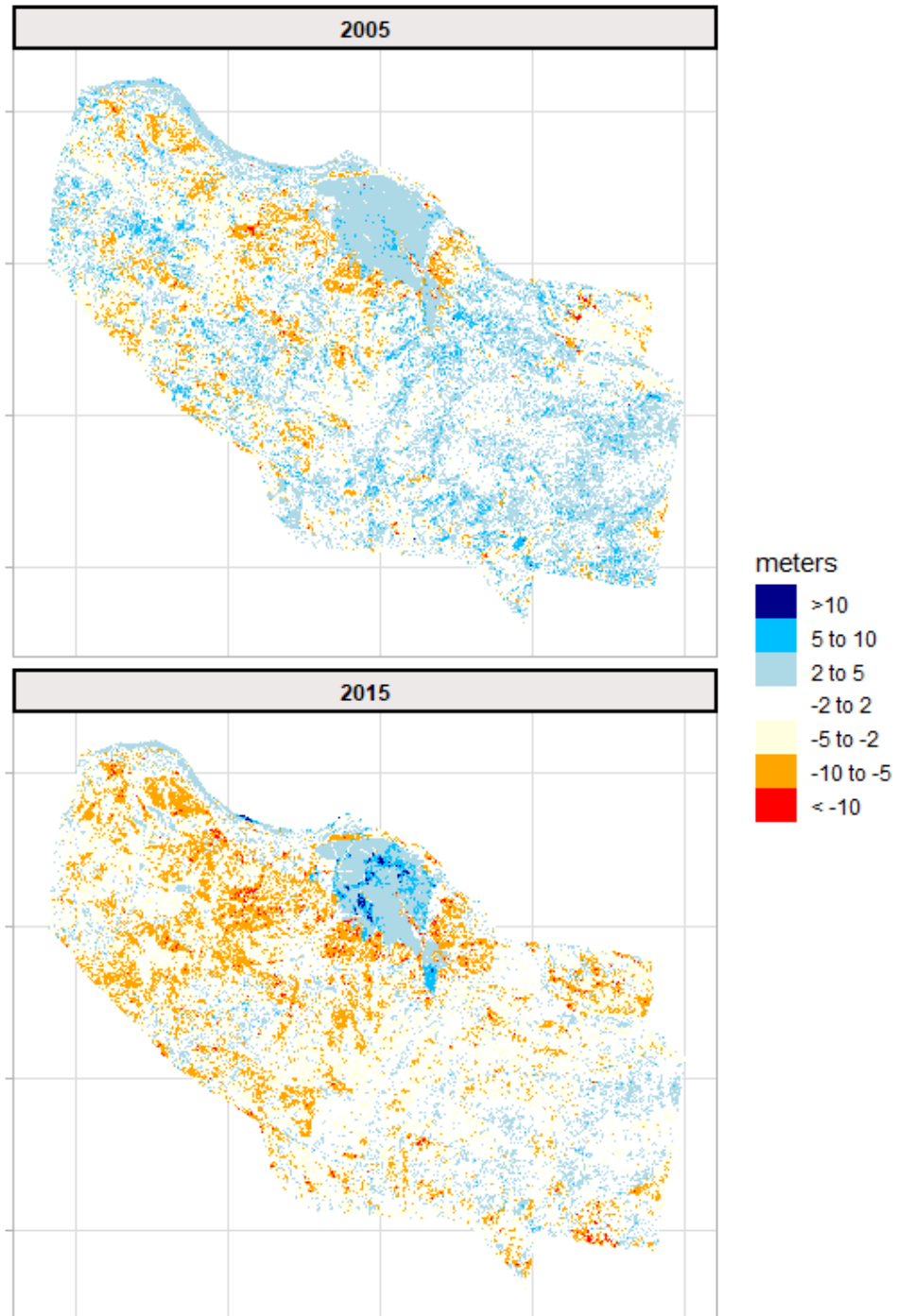


Figure 23: Residual (predicted-observed) base height at Lubrecht Experimental Forest in 2005 (top) and 2015 (bottom).

In 2005, the canopy cover predicted versus observed values were roughly linear with more underprediction. The model tended to overpredict height (especially in the mid-heights). Base height estimates did not correlate as well as the other predictions (Figure 24). The canopy cover predicted and observed values were linear in 2015, though the model tended to assign zero values to pixels with actual canopy covers up to 25%. The model overpredicted height more pronouncedly than in 2005. The model also tended to overpredict base heights on lower values. Only the height scatters were significantly different between 2015 and 2005 (Figure 24).

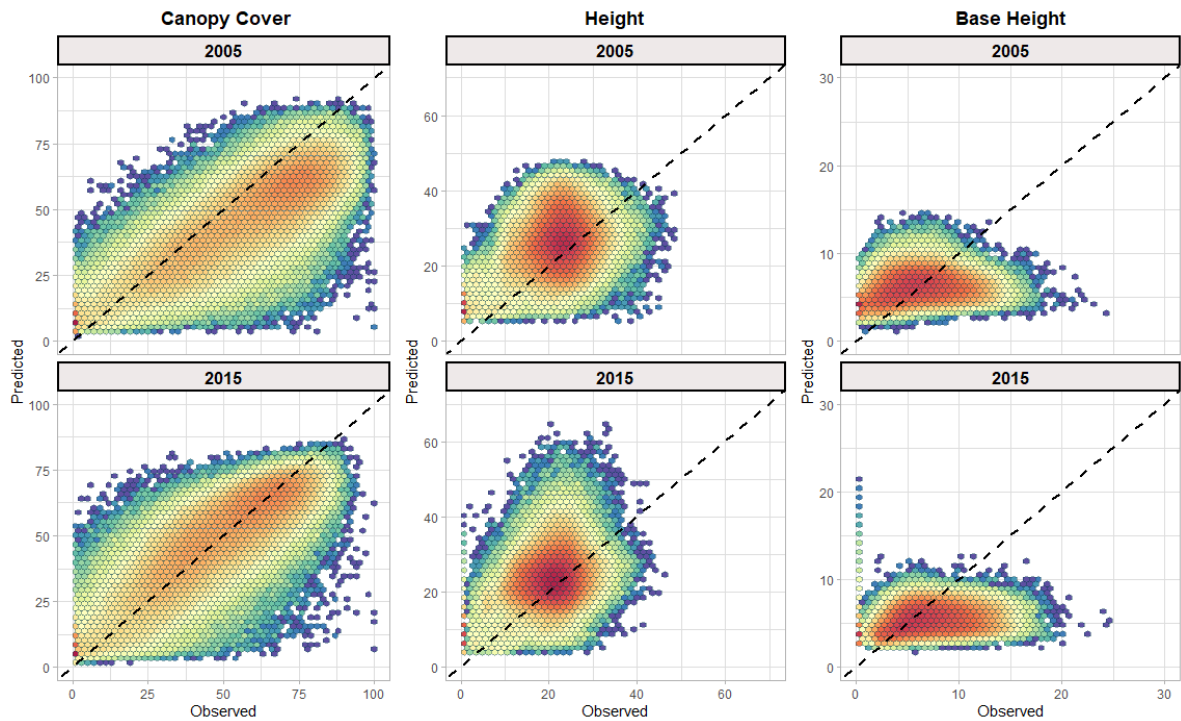


Figure 24: Predicted and observed canopy cover (left) height (middle) and base height (right) in 2005 (top) and 2015 (bottom)

LUBRECHT THROUGH TIME:

The canopy cover and height models at Lubrecht have a noticeable sensor effect where the underlying data changed from Landsat 5 to Landsat 8 in 2013 (Figure 25). In the canopy cover model, it is evident across the entire distribution of values in the later years, while the height model only reflects the sensor difference in the upper outliers.

The mean year to year change in canopy cover was 2.3%, as was seen at Powell.

The mean absolute annual change in height and base height were 0.75 and 0.22 meters respectively. The greatest single year increase in canopy cover was 7.89% and the greatest single year increases in height and base height were 2.31 and 0.95 meters respectively (Table 7).

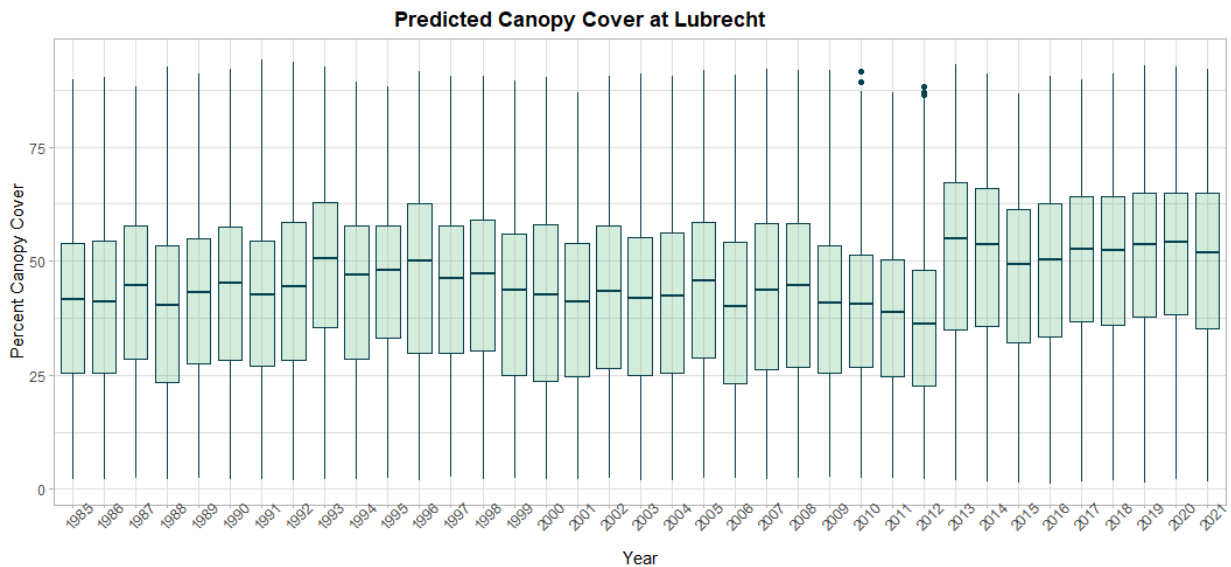


Figure 25: Predicted canopy cover from 1985 to 2021 at Lubrecht

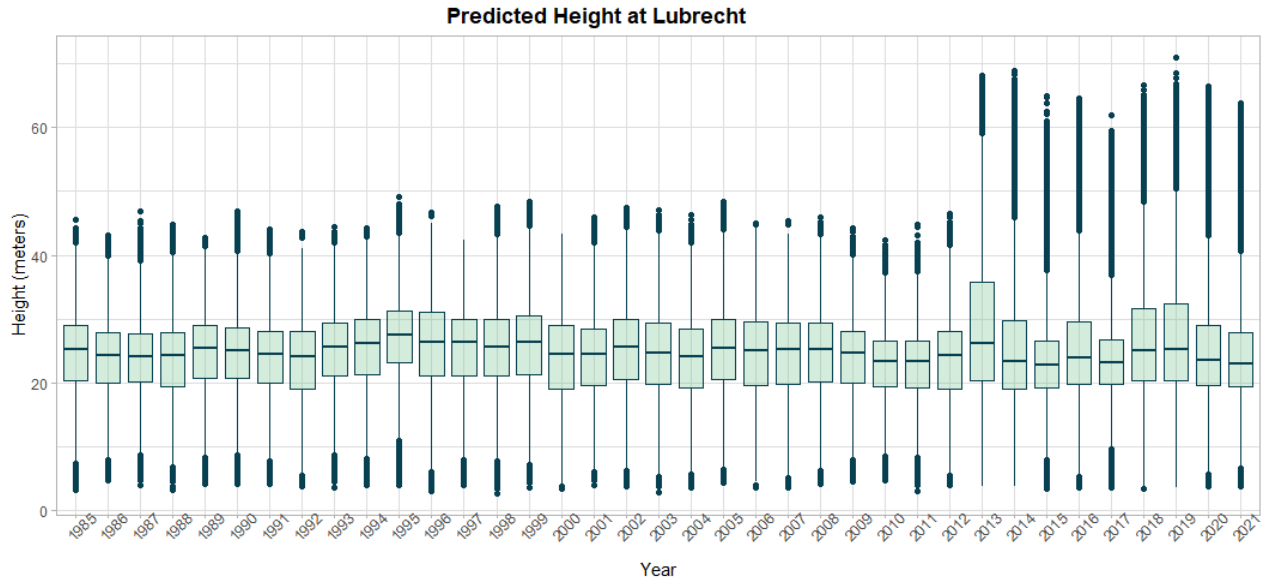


Figure 26: Predicted tree height from 1985 to 2021 at Lubrecht

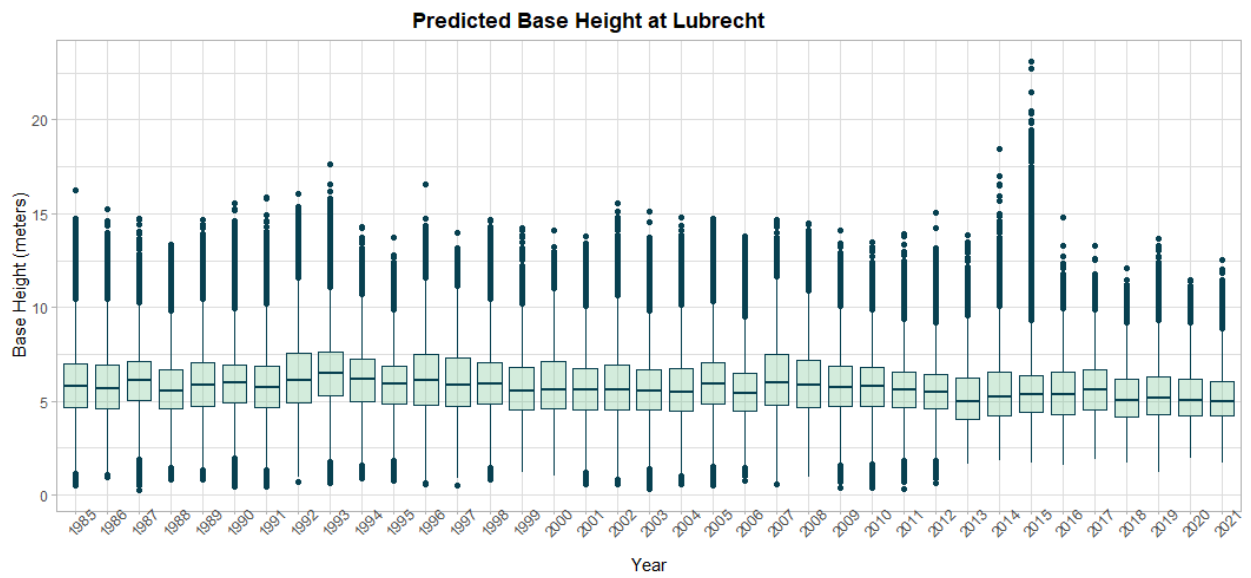


Figure 27: Predicted base height from 1985 to 2021 at Lubrecht

Year	Canopy Cover (%)				Height (m)				Base Height (m)			
	Median	Mean	Standard Dev.	Annual Change	Median	Mean	Standard Dev.	Annual Change	Median	Mean	Standard Dev.	Annual Change
2021	37.39	37.00	19.62	-0.90	23.11	22.88	7.18	-0.06	4.53	4.71	1.80	-0.09
2020	38.17	37.90	20.59	-2.29	22.57	22.94	7.11	-0.33	4.64	4.80	1.85	-0.16
2019	41.09	40.19	21.12	3.57	23.03	23.28	7.26	0.22	4.83	4.96	1.93	0.02
2018	36.27	36.62	19.59	-2.12	23.37	23.05	7.13	0.33	4.79	4.94	1.87	-0.02
2017	38.19	38.74	20.51	-1.57	23.09	22.72	7.02	-0.24	4.77	4.96	1.92	-0.22
2016	41.77	40.31	20.66	-1.10	22.95	22.97	6.88	0.65	5.09	5.18	1.83	-0.05
2015	43.03	41.42	21.17	0.07	22.15	22.31	6.86	-2.26	5.03	5.23	2.04	-0.14
2014	42.75	41.35	18.30	-1.56	25.54	24.57	7.04	0.33	5.30	5.36	1.99	0.22
2013	45.85	42.90	18.96	4.10	25.32	24.24	7.39	-0.24	5.12	5.15	1.99	-0.02
2012	39.97	38.81	16.71	-2.53	25.40	24.48	7.00	-0.23	5.23	5.16	1.82	-0.17
2011	42.03	41.34	18.92	-3.72	25.32	24.71	7.03	-1.41	5.33	5.33	1.91	-0.30
2010	49.16	45.05	19.52	1.40	26.92	26.12	7.12	0.92	5.69	5.63	1.95	-0.35
2009	47.21	43.66	21.43	-3.51	25.84	25.20	7.01	1.00	5.94	5.98	2.11	0.14
2008	50.16	47.16	22.01	2.64	23.99	24.20	7.33	0.34	5.78	5.84	2.20	-0.61
2007	47.67	44.52	22.11	1.47	25.36	23.87	7.18	-0.78	6.49	6.45	2.45	0.95
2006	46.74	43.05	19.93	-3.01	25.26	24.65	6.94	-0.31	5.50	5.51	1.93	-0.03
2005	49.66	46.06	19.34	0.89	25.03	24.96	7.09	1.11	5.61	5.54	1.90	0.32
2004	48.58	45.17	19.69	5.57	23.72	23.85	6.89	0.16	5.27	5.22	1.80	0.24
2003	41.31	39.60	19.18	-3.02	23.77	23.69	6.67	-1.11	4.88	4.98	1.69	-0.75
2002	46.34	42.61	20.00	-2.16	25.38	24.80	6.74	0.04	5.68	5.73	1.99	0.25
2001	48.50	44.77	18.63	2.36	25.70	24.77	7.02	1.02	5.50	5.48	1.98	0.05
2000	46.42	42.41	18.60	2.58	24.75	23.75	6.66	-1.35	5.41	5.44	2.02	0.82
1999	41.47	39.83	19.52	-4.16	24.64	25.09	7.14	-1.75	4.46	4.62	1.44	-0.21
1998	47.89	43.99	19.54	2.92	26.95	26.84	7.88	0.16	4.75	4.83	1.62	-0.02
1997	44.41	41.07	19.62	0.04	26.50	26.69	8.01	0.88	4.66	4.85	1.57	-0.05
1996	44.66	41.04	19.65	3.70	25.42	25.81	7.61	-0.10	4.72	4.90	1.64	0.20
1995	39.14	37.33	18.77	-3.11	26.04	25.91	7.55	-0.49	4.47	4.70	1.49	-0.21
1994	43.87	40.44	20.09	1.04	26.36	26.41	7.99	0.57	4.78	4.91	1.62	-0.19
1993	42.63	39.41	19.03	-2.90	25.54	25.83	7.24	-1.18	4.91	5.10	1.52	0.11
1992	45.71	42.31	19.37	2.09	27.10	27.02	7.85	2.03	4.83	5.00	1.60	0.28
1991	42.92	40.22	19.81	0.54	24.24	24.99	7.44	1.14	4.61	4.71	1.59	0.13
1990	41.18	39.68	20.27	-1.47	23.95	23.84	7.36	0.00	4.48	4.59	1.71	-0.47
1989	42.35	41.16	20.95	0.19	23.81	23.85	7.43	0.08	4.93	5.06	1.95	0.02
1988	42.59	40.97	20.09	7.84	23.40	23.77	7.19	2.31	4.99	5.03	1.76	0.16
1987	31.67	33.13	17.32	-1.95	20.97	21.46	6.60	0.64	4.55	4.87	1.84	0.17
1986	34.24	35.08	18.53	-1.28	20.15	20.81	6.61	-1.40	4.36	4.70	1.87	-0.03
1985	35.72	36.36	20.84		21.95	22.21	7.13		4.41	4.74	1.91	

Table 7: Annual change in canopy cover, height, and base height at Lubrecht Experimental Forest

CANOPY FUELS ON BURNED LANDSCAPES (OBJECTIVE 3):

The purpose of the fire analysis is to utilize GBM-derived predictions to explore the impact of fire to forest canopy and its recovery. 164 fires ultimately met the criteria of occurring in Montana, Idaho, or Wyoming between 1988 and 1994 with no subsequent reburns. Of these fires, 114 were predominately low severity, 30 were moderate severity, and 20 were high severity. Time series of cover, height, and base height by the severity class mode for each fire (Figures 28, 29, 30) are unremarkable. High severity fires tend to show sudden reductions in cover and height with gradual recoveries, but similar patterns are observable in the other severity classes. The disturbance signal is less clear in base height. For many fires, the disturbance signal did not appear until a few years after the disturbance. Many low and moderate severity fires have flat time series, perhaps reflecting the fact that they occur in rangeland environments with low canopy cover, or forested environments where only surface fire occurred. Rangeland fires are overwhelmingly classified as low severity and rangelands do not create as stark of a difference when they burn.

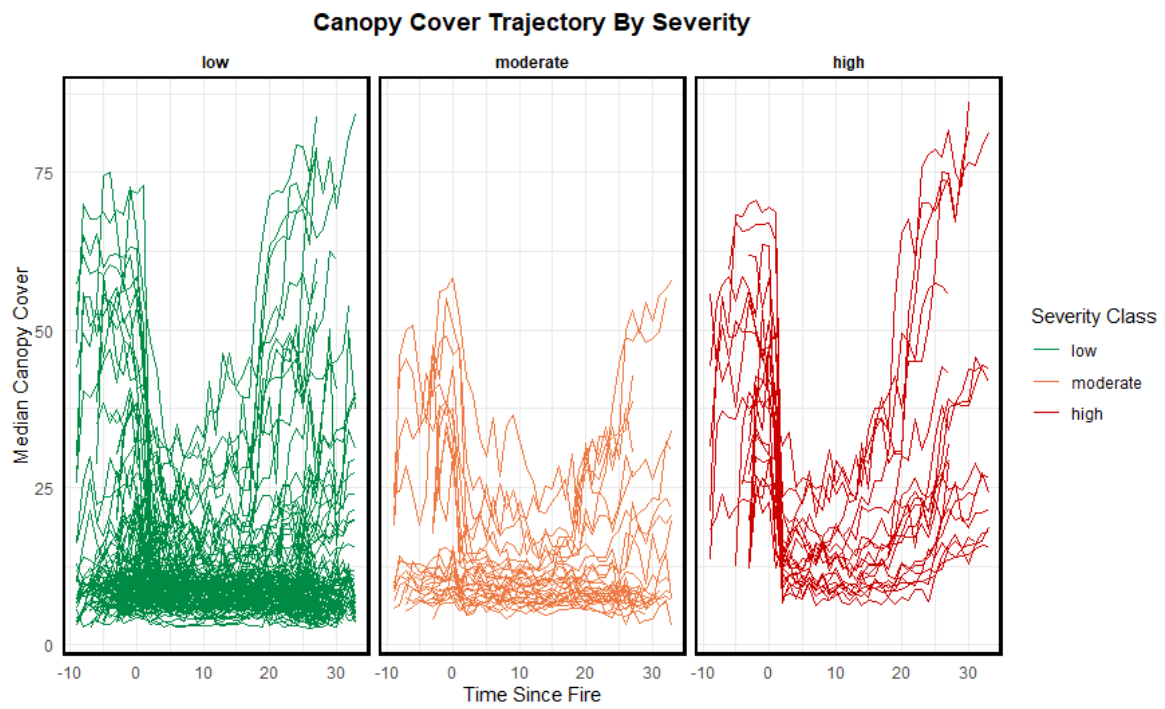


Figure 28: Canopy cover trajectory by severity.

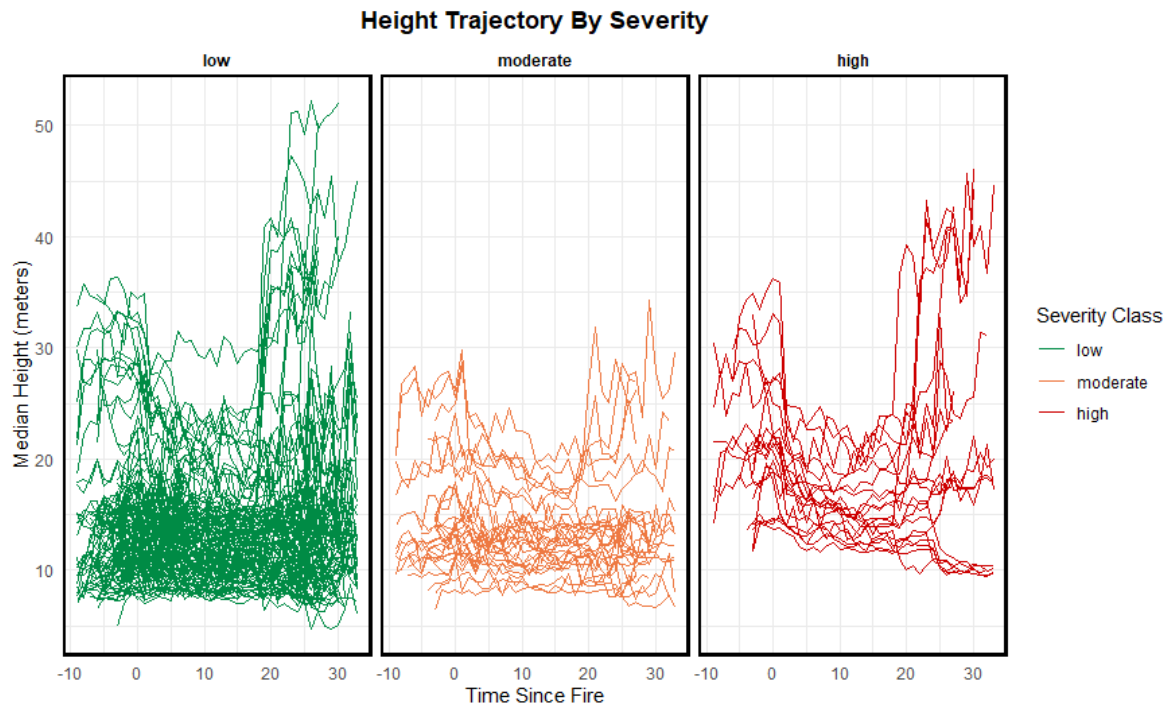


Figure 29: Height trajectory by severity.

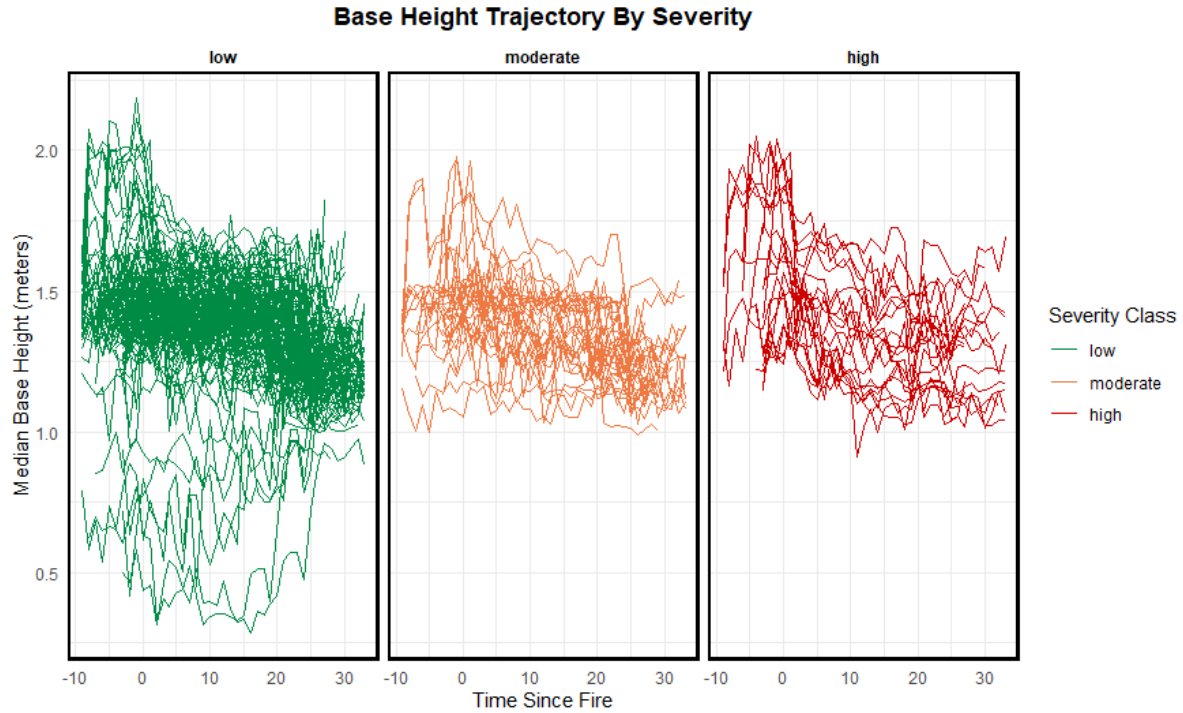


Figure 30: Base height trajectory by severity.

SHAPESELECTFOREST SPLINE CLASSIFICATION:

Each of the 164 fires was classified to the ShapeSelectForest spline it most closely resembled. Every possible shape had at least one fire associated with it (Figure 31). The highest severity fires tended to most closely resemble the V or double jump shape (Figure 32). Jumps are associated with many different kinds of disturbance, but V shaped trajectories are mostly associated with stress-related trajectories.

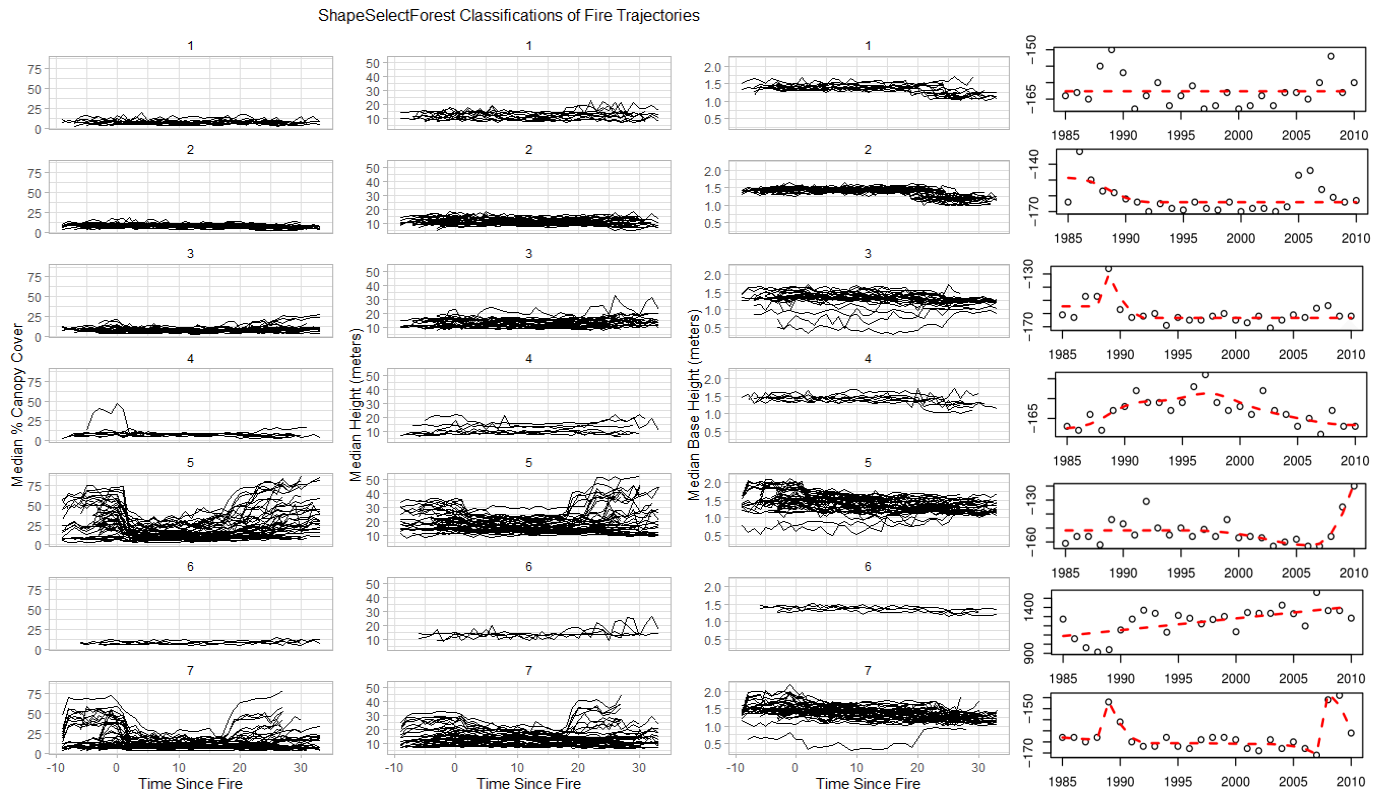


Figure 31: ShapeSelectForest splines from Moisen et al. 2016 (far right column) and the fire trajectories that resemble each spline. From left to right: canopy cover trajectories, height trajectories, and base height trajectories

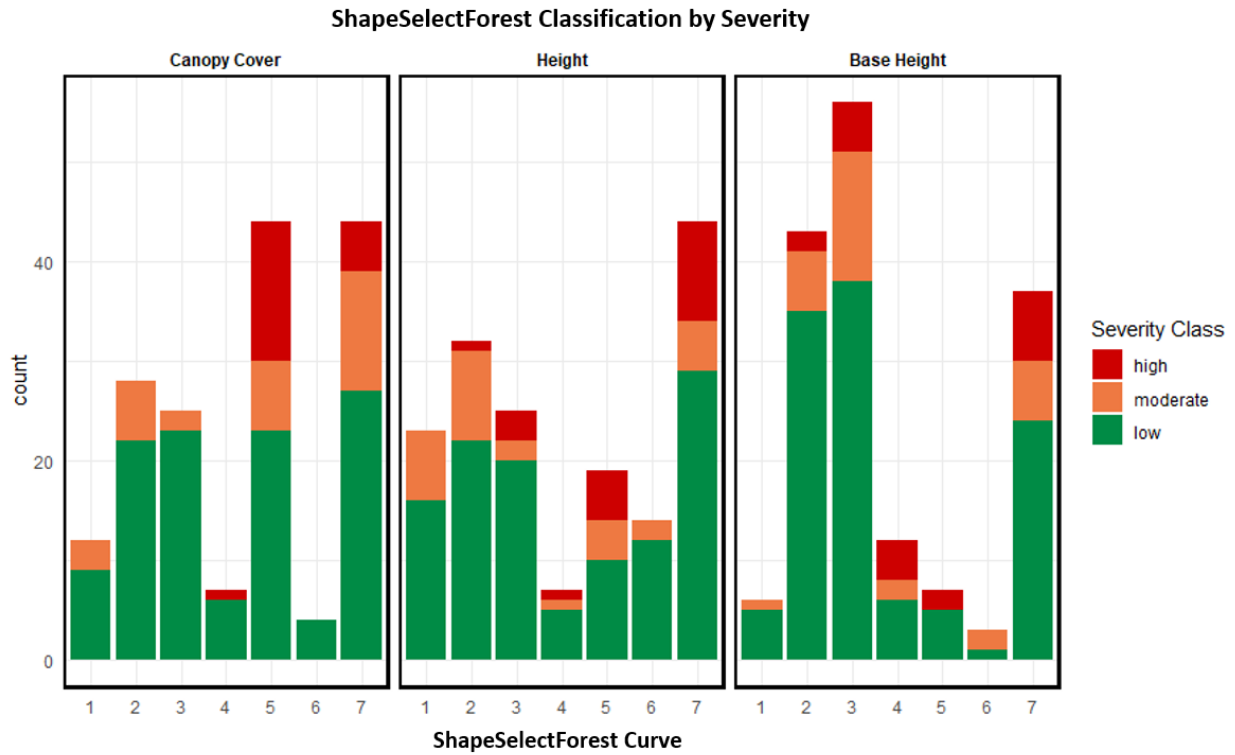


Figure 32: ShapeSelectForest classification by severity. See Figure 35 for classification splines

High severity fire was most associated with shapes 4, 5, and 7 for canopy cover. These shapes are inverted V, V, and double jump. There was no apparent correlation between severity and classification for height and base height curves (Table 8).

Canopy Cover			
SSF Class	Mean Pre-Fire Canopy Cover	Mean Canopy Cover Loss	Mean BIC
1	7.71	-0.14	163.12
2	9.00	0.61	137.05
3	9.01	0.31	152.22
4	11.23	3.20	155.62
5	32.69	10.10	228.21
6	7.79	-0.43	156.67
7	21.08	7.70	197.38
Height			
SSF Class	Mean Pre-Fire Height	Mean Height Loss	Mean BIC
1.00	11.82	0.04	128.50
2.00	13.25	1.03	117.55
3.00	15.61	0.67	132.74
4.00	13.33	0.52	156.71
5.00	18.48	1.77	140.41
6.00	12.53	-1.78	170.94
7.00	17.92	1.33	143.81
Base Height			
SSF Class	Mean Pre-Fire Base Ht.	Mean Base. Ht loss	Mean BIC
1	1.26	-0.04	-86.52
2	1.43	0.09	-71.66
3	1.49	0.12	-68.25
4	1.44	0.11	-58.73
5	1.15	0.07	-61.06
6	1.24	-0.07	-83.94
7	1.44	0.09	-75.41

Table 8: Canopy cover characteristics of fires in each ShapeSelectForest bin. See Figure 25 for the model splines each bin most closely resembles.

There was no significant difference in base height loss or pre-fire base height between groups, indicating that SSF is not effective for delineating different curves in base height response. Groups 5 and 7 (V shaped curves and double jump curves) had the greatest pre-fire height and canopy cover, and the greatest canopy losses (Table 8). So, the SSF classification system effectively parses out fires in forested environments with distinct canopy loss, but is not sensitive to other kinds of fire or sites.

SSF was also designed for monitoring Landsat images over time rather than GBM-derived outputs. The curves were built from a combination of raw spectral Landsat data, NDVI, and NBR. Often, GBM outputs have a non-positive and non-linear relationship with the underlying Landsat indices informing the predictions (Moran et al., 2020). Classification is important for defining kinds of recovery curves, but systems built for raw spectral data will likely be inaccurate for GBM-derived metrics.

CUSTOM CLASSIFICATION FOR GBM TIME SERIES:

There are four archetypical time series associated with canopy cover of the burned landscapes: Flat, U, V, and Wavy (Figures 33, 34, 35). U fires and V fires are associated with greater pre-fire canopy cover, height, and base height, and more dramatic losses in canopy. However, some V and U-shaped fires follow this trajectory without heavy initial fuel loading (Figure 33). Flat fires are associated with the least amount of canopy loss.

Each metric was classified separately and trajectories did not need to agree between metrics for the same fire. Canopy cover had more V fires and U fires than height or base height (Table 10). Site trajectories frequently did not agree between metrics (Tables 11, 12, 13).

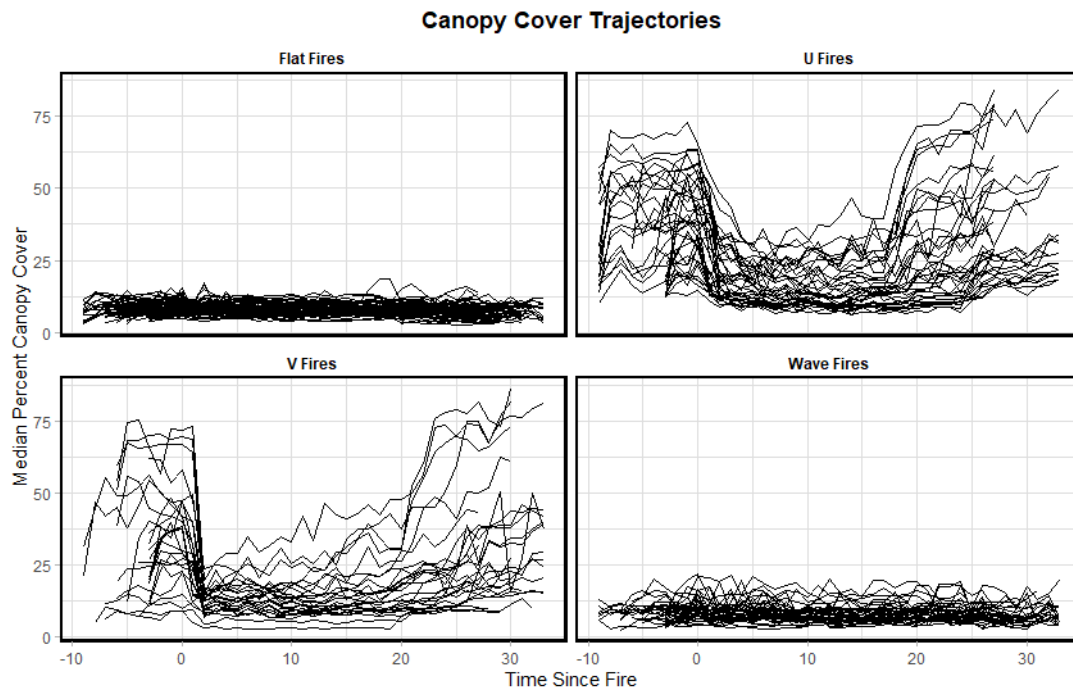


Figure 33: Canopy cover trajectories of burned sites over time. They are grouped by the fire shape they most closely resemble. Each line represents the trajectory of an individual fire. The fire occurred at year zero.

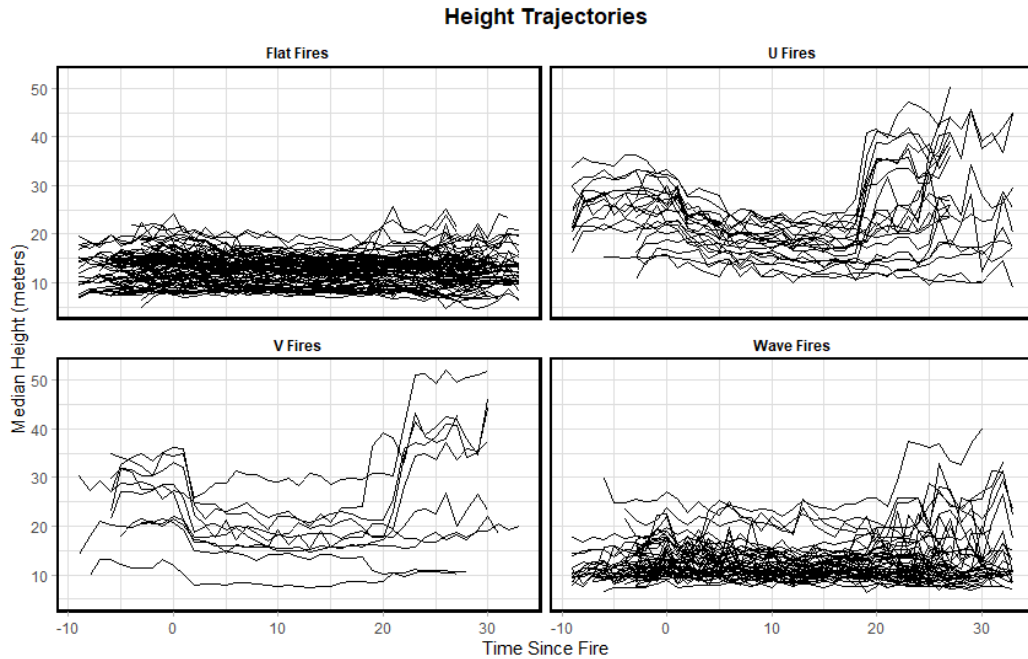


Figure 34: Height trajectories of burned sites over time. They are grouped by the fire shape they most closely resemble. Each line represents the trajectory of an individual fire. The fire occurred at year zero.

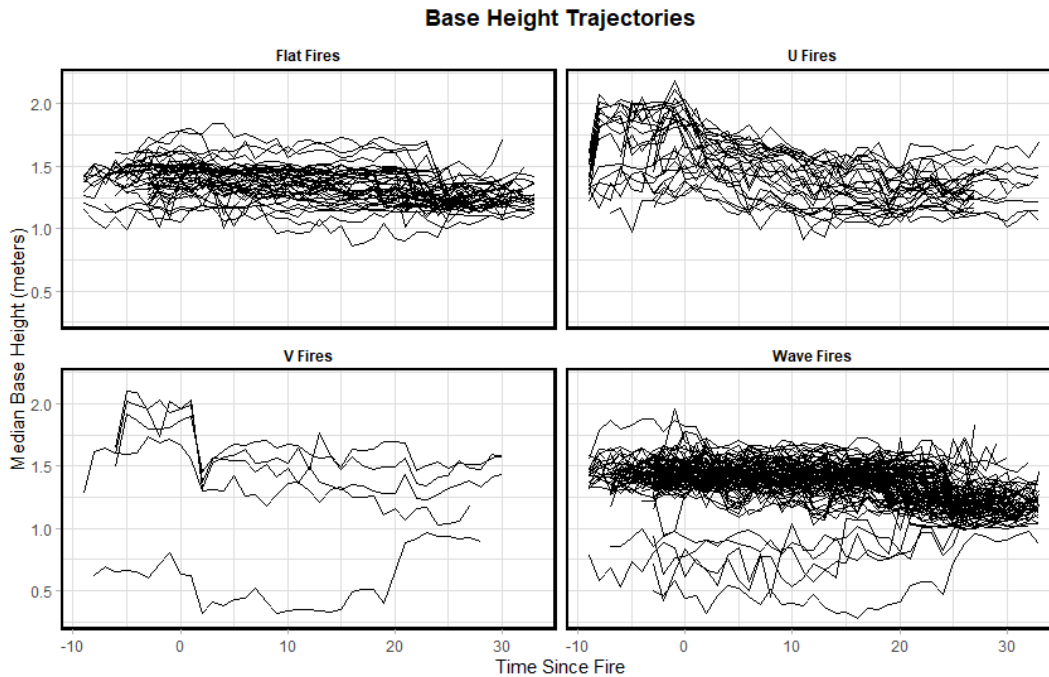


Figure 35: Base height trajectories of burned sites over time. They are grouped by the fire shape they most closely resemble. Each line represents the trajectory of an individual fire. The fire occurred at year zero.

Canopy Cover				Height				Base Height			
Group	Count	Pre-fire Mean	Loss	Group	Count	Pre-fire Mean	Loss	Group	Count	Pre-fire Mean	Loss
Flat fires	63	9.42	2.99	Flat fires	83	13.50	2.16	Flat fires	49	1.33	0.21
U fires	37	36.17	19.40	U fires	22	24.10	7.07	U fires	26	1.59	0.41
V fires	26	33.36	19.53	V fires	10	24.61	7.93	V fires	5	1.53	0.44
Wave fires	38	9.75	3.73	Wave fires	49	12.94	2.64	Wave fires	84	1.41	0.27

Table 9: Characteristics of flat fires, U fires, V fires, and Wave Fires. The count represents the number of fires that fall into each category. Loss is defined as the pre-fire mean minus the post fire minimum value. It represents the magnitude of disturbance.

		Height				Sum
		flat fires	U fires	V fires	Wave fires	
Canopy Cover	flat fires	47	0	0	16	63
	U fires	14	18	2	3	37
	V fires	9	3	8	6	26
	Wave fires	13	1	0	24	38
	Sum	83	22	10	49	

Table 10: Contingency Table of canopy cover and height classifications. Each metric was classified independently.

		Base Height				Sum
		flat fires	U fires	V fires	Wave fires	
Canopy Cover	flat fires	19	0	0	44	63
	U fires	11	19	0	7	37
	V fires	8	7	5	6	26
	Wave fires	11	0	0	27	38
	Sum	49	26	5	84	

Table 11: Contingency Table of canopy cover and base height classifications.

		Base Height				Sum
		flat fires	U fires	V fires	Wave fires	
Height	flat fires	40	5	0	38	83
	U fires	3	15	0	4	22
	V fires	1	4	5	0	10
	Wave fires	5	2	0	42	49
	Sum	49	26	5	84	

Table 12: Contingency Table of base height and height classifications.

FIRE RECOVERY:

This study defines recovery as the time it takes to meet or exceed pre-fire canopy conditions. Thirty-seven fires did not fully recover canopy cover within the 36-year time series. Four of those fires were high severity, five were moderate severity, and two were low severity. Two of those fires were flat, 5 were U shaped, 3 were V shaped, and 1 was wavy. Four fires did not yet fully recover pre-fire heights. One of those fires was high severity, one was moderate severity, and two were low severity. One was flat, one was U shaped, and two were V shaped. Thirteen fires have yet to recover base height. Four were high severity, 1 was moderate, and 8 were low severity. 1 was flat, 9 were U shaped, 1 was V shaped, and 2 were wavy.

Of the three metrics, canopy cover had the clearest relationship between shape classification and recovery time. All high severity fires were classified as U or V fires. These two classes were associated with slower recovery regardless of fire severity. U and V fires occurred

on a wide range of forest types, though wave and flat fires were associated with low cover forests (Figure 36). So, if two forests had similar pre-fire cover and both burned at low severity, the forest that recovered in a U or V shaped trajectory would take up to 40 years longer to recover than a forest that recovered in a flat or wavy shaped trajectory.

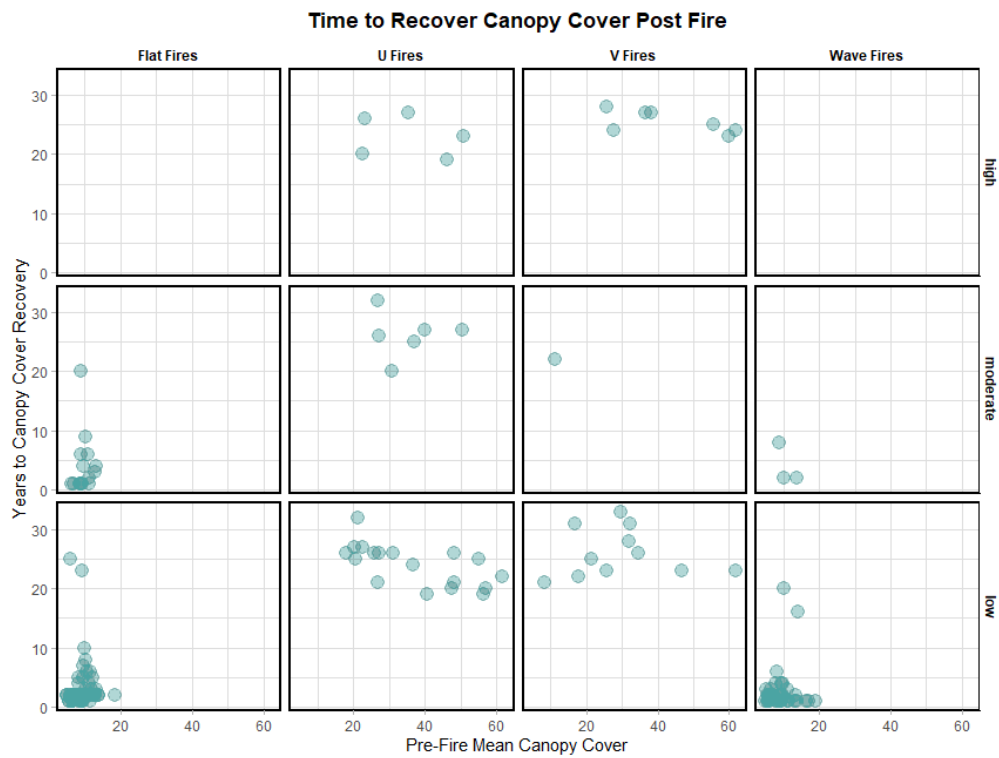


Figure 36: Time to recover canopy cover as a function of pre-fire mean canopy cover, trajectory shape, and severity. Recovery is defined as the year canopy cover met or exceeded pre-fire conditions

Height curves have a weaker relationship between severity and shape than canopy cover curves. However, fires tend to have slower recovery when following a V or U-shaped trajectory compared to other shapes of the same severity (Figure 37).

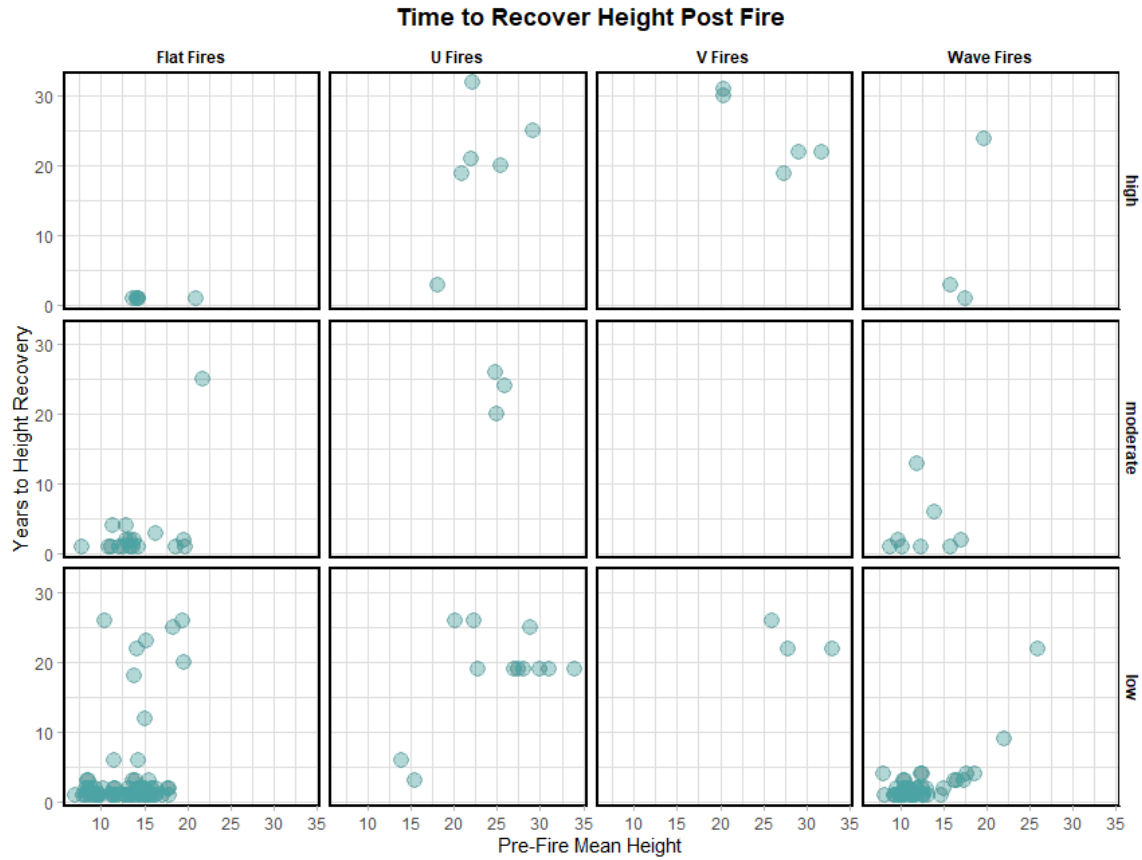


Figure 37: Time to recover height as a function of pre-fire mean canopy cover, trajectory shape, and severity. Recovery is defined as the year height met or exceeded pre-fire conditions

U and V shaped trajectories were much less common in base height curves. The disturbance events were also less visually obvious in these curves compared to canopy cover and height curves. Base heights recovered faster than canopy covers or heights, particularly on high severity fires (Figure 38).

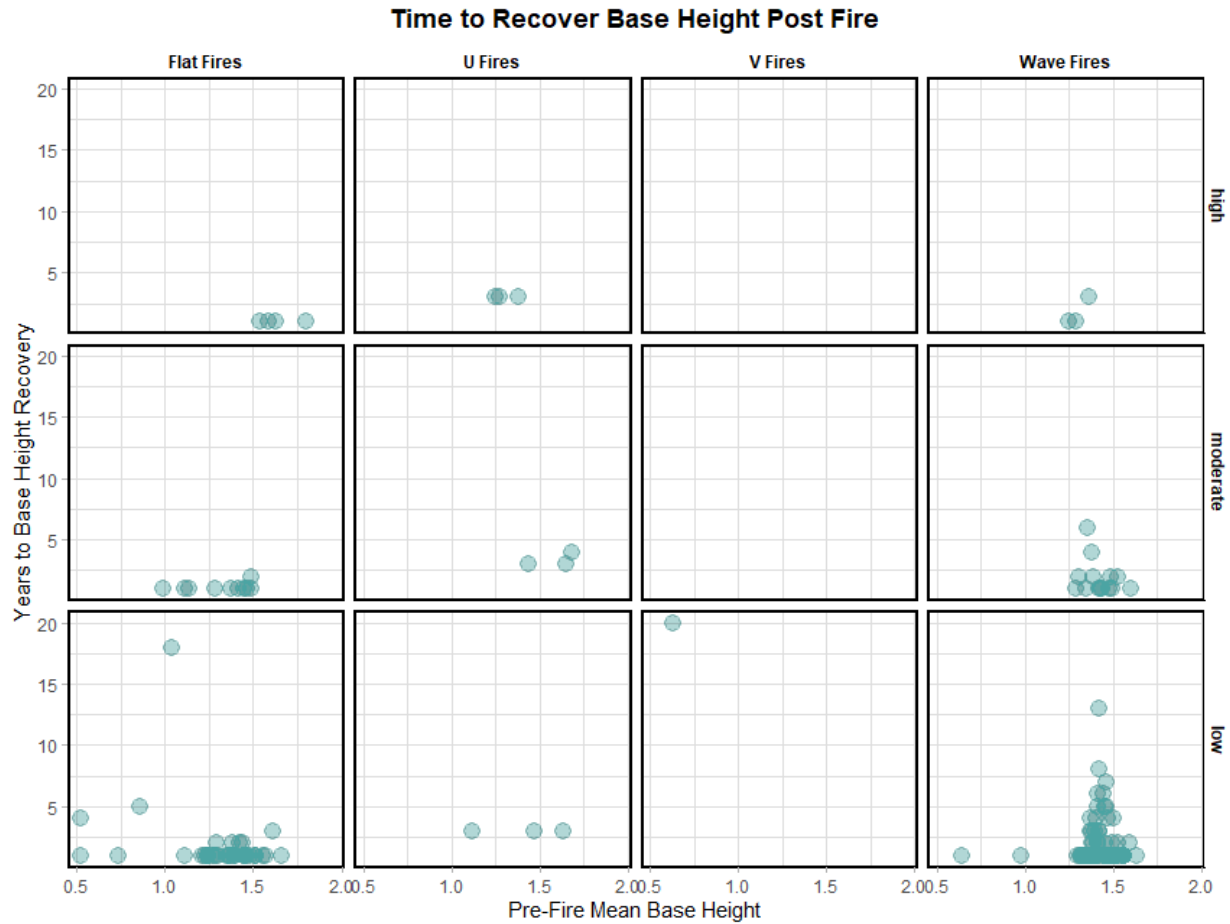


Figure 38: Time to recover base height as a function of pre-fire mean canopy cover, trajectory shape, and severity. Recovery is defined as the year base height met or exceeded pre-fire conditions

CASE STUDY: INTRA-FIRE HETEROGENEITY:

In order to classify fires into curve shapes, multi-pixel fires need to be summarized into a single trajectory. However, fires are not internally homogenous, and this method loses nuance in both internal severity and recovery dynamics. The purpose of a single fire case study is to evaluate the importance of pixel-level severity on recovery within the boundary of a single fire.

The Lost Fire occurred about 12 miles west of Buffalo, Wyoming in 1988. It covered 13,108 acres on the Bighorn National Forest and burned primarily at high severity between August 14 and

25. The bounds of the fire is still visible on the landscape today (Figure 39). It was chosen for analysis because I know the landscape, having worked on the Powder River Ranger District where the fire occurred.



Figure 39: Imagery of the Lost Fire in 2022.

The Monitoring Trends in Burn Severity (MTBS) system classifies most of the Lost Fire as high severity. There are scattered patches of low and moderate severity, and some islands that increased in greenness after the fire (Figure 40).

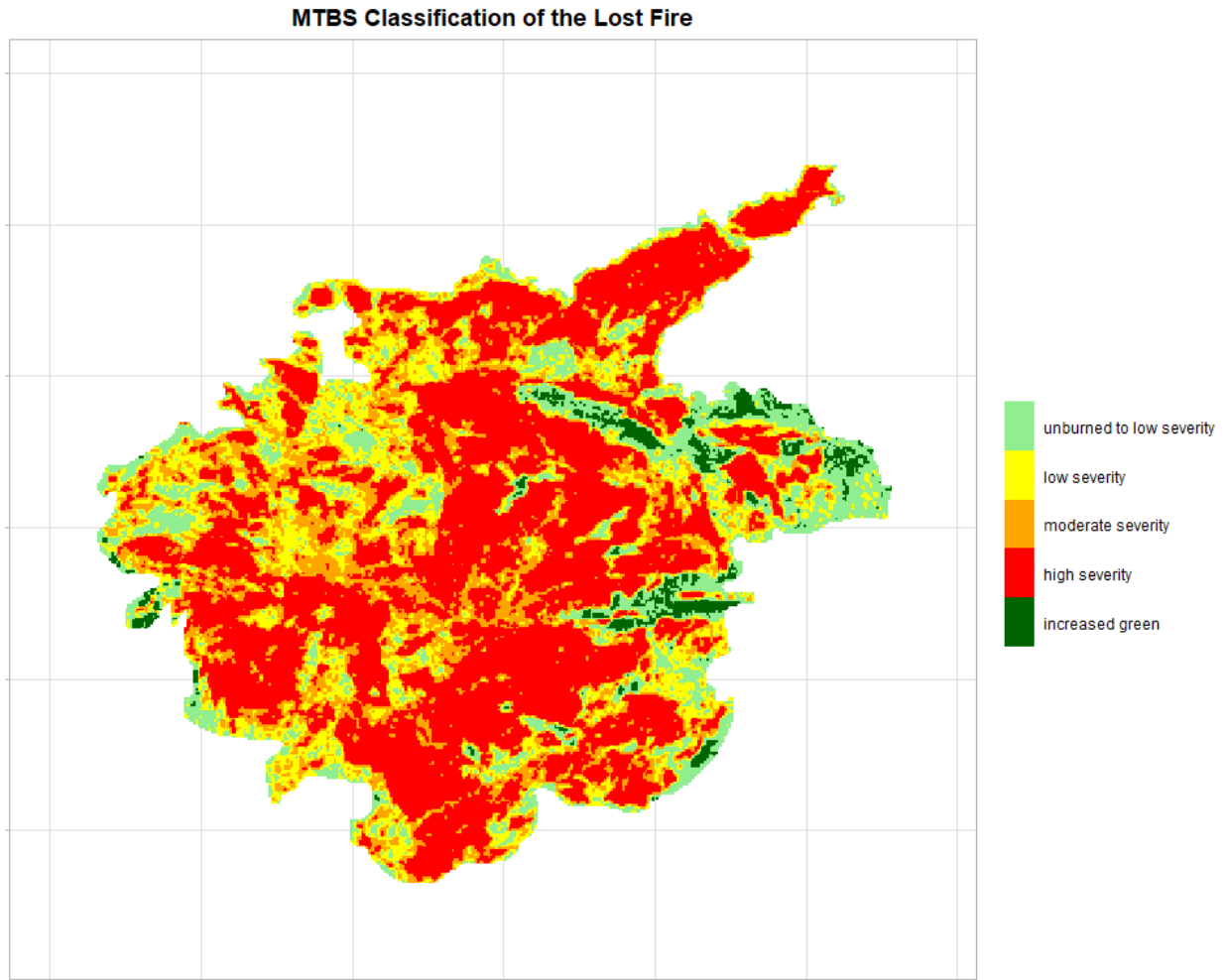


Figure 40: Monitoring Trends in Burn Severity (MTBS) severity classification for the Lost Fire

Lost Fire followed a V-shaped canopy cover trajectory. The pre-fire mean canopy cover was 27.75%. In 1989, the year following the fire, the mean canopy cover hovered at 26.6%. Not until 1990, two years following the incident, did the canopy cover drop to 10.8%. This site has not fully recovered its canopy cover to pre-fire levels, though it likely will in the next few years

if it follows its current recovery trajectory (Figure 41). The predicted mean canopy cover in 2021 was 23.1% and the median was 24.2%.

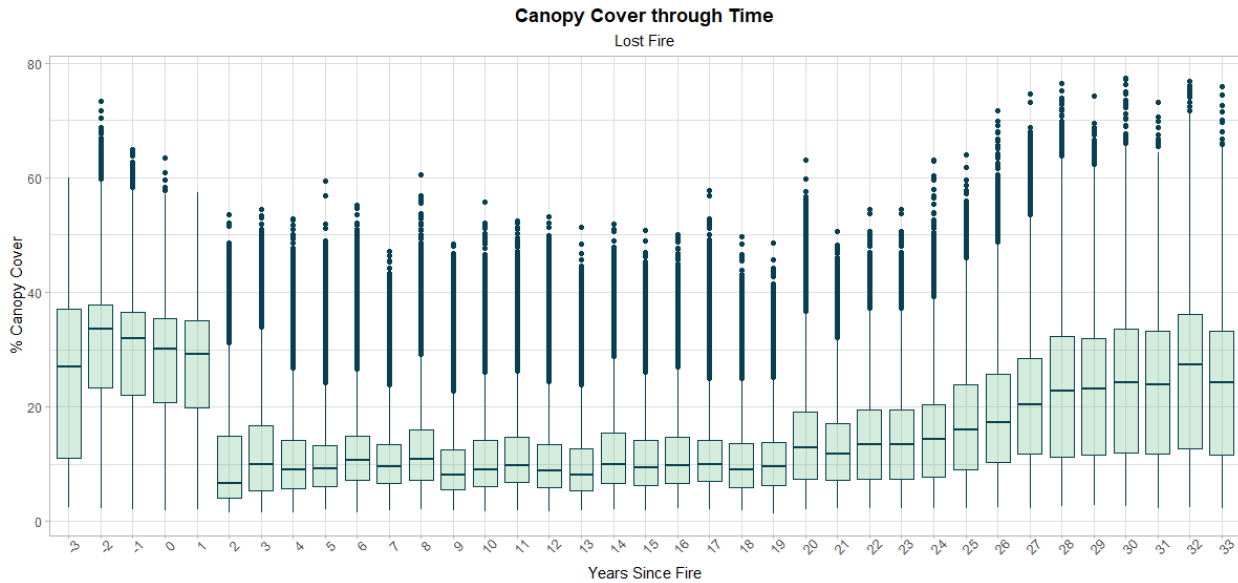


Figure 41: Canopy cover through time on the Lost Fire.

Predicted height on the Lost Fire was less sensitive to the disturbance event than canopy cover. The pre-fire mean height was 14.27 meters, and subsequent predictions ranged between 11 and 14 meters up until 2013. Predictions between 2013 and 2021 are consistently 1.5 to 2 meters lower than prior years, probably due to a sensor artifact associated with the transition from Landsat 5 to Landsat 8 (Figure 42).

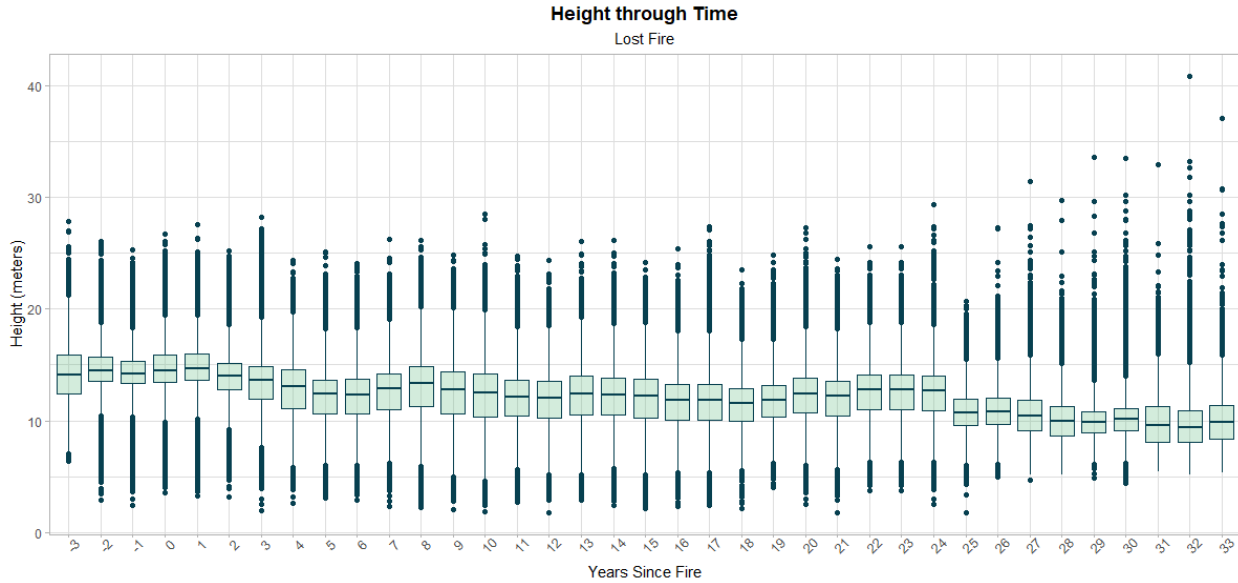


Figure 42: tree height through time on the Lost Fire

Lost Fire followed a wavy trajectory in recovering base height, with a local valley about four years post fire, and another one about 11 years post fire. The median base height trend was not significantly different than other fires, but Lost Fire had a notable number of low outliers across all years (Figure 43). The model was not trained on negative base height values but allowed to predict values outside the range of the training set to prevent overfitting.

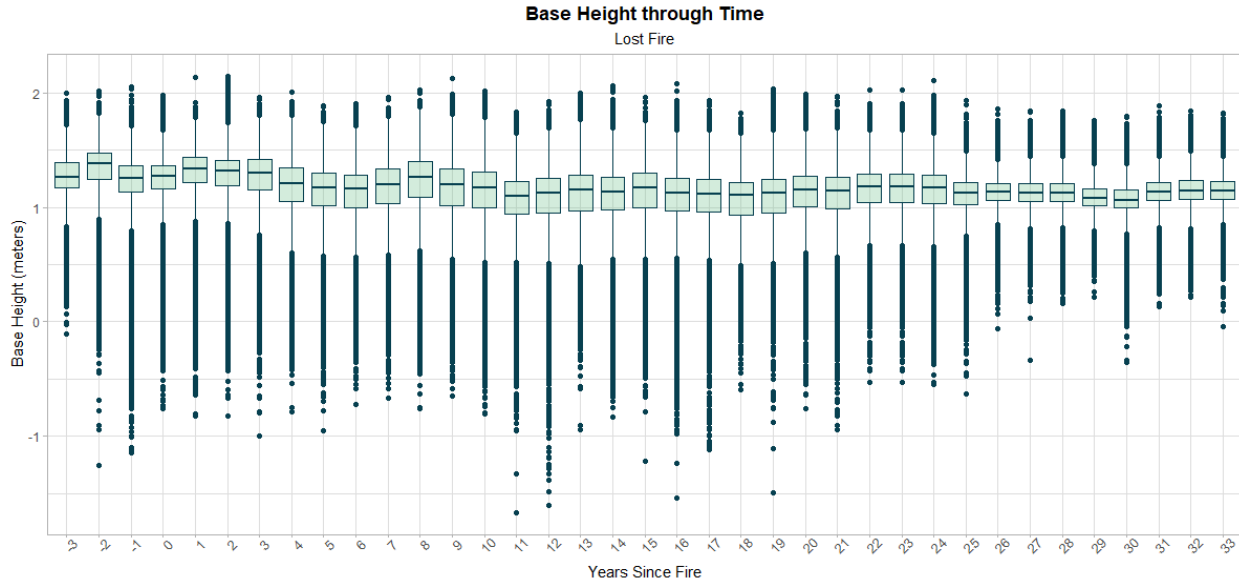


Figure 43: Base height through time on the Lost Fire

Two years post fire, the burn scar had islands of trees associated with the lower severity pixels, indicating agreement between the GBM model outputs and the MTBS severity classification system (Figures 40, 44). The site potentially experienced secondary mortality on the south and east sides between 1990 (two years post fire) and 2000 (12 years post fire), as evident by green pixels in 1990 with substantially lower canopy cover in 2000. By 2020, 32 years after the fire, the majority of the site had met or exceeded pre-fire canopy cover conditions. However, the southwest corner still had less than 25% of the pre-fire canopy cover (Figure 44), indicating a potential state change for this portion of the fire.

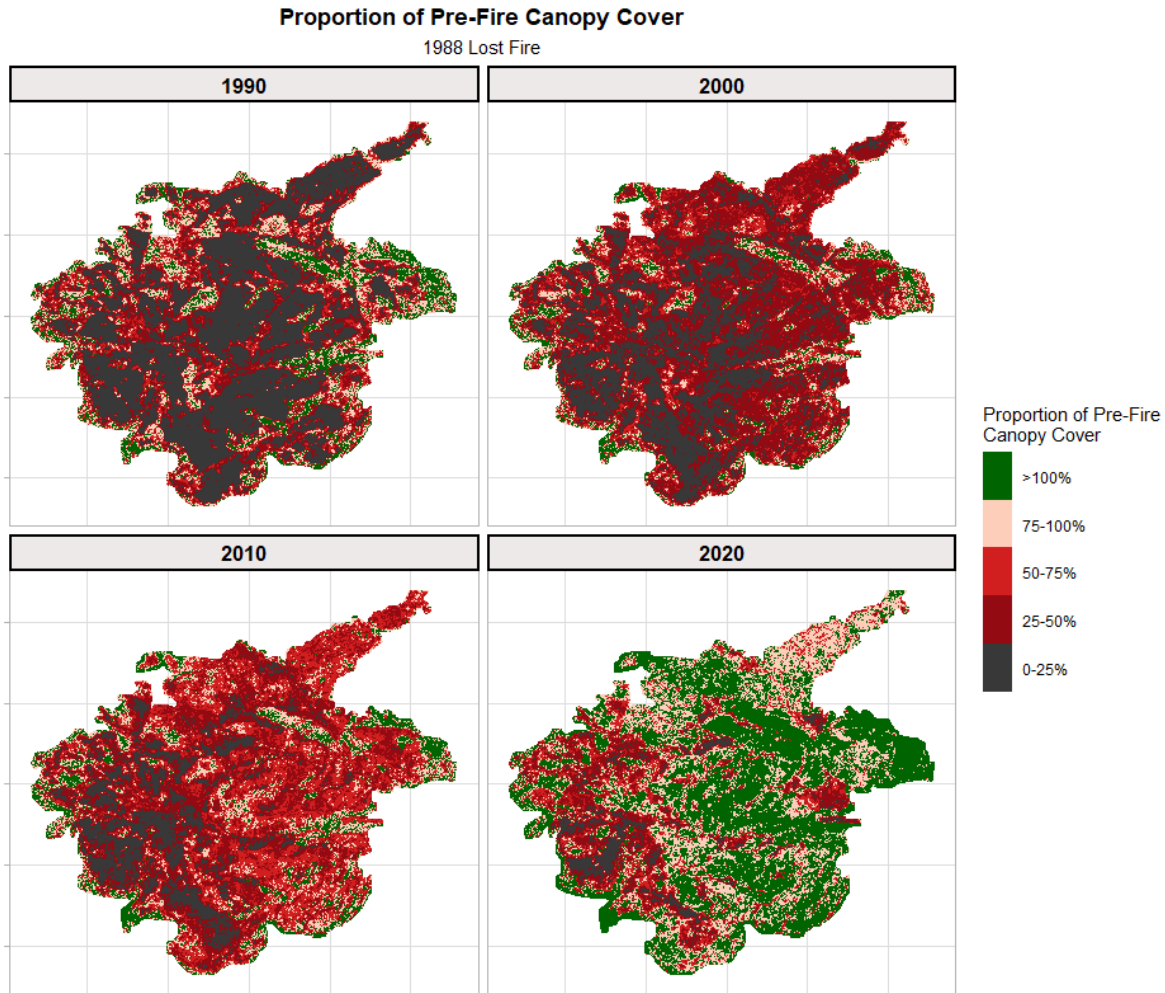


Figure 44: Proportion of pre-fire canopy cover on the Lost Fire 2 years post fire (top left) 12 years post fire (top right), 22 years post fire (bottom left), and 32 years post fire (bottom right)

Height loss was less dramatic in the years following the Lost Fire. Tree height on the burn scar trended slowly downward over the course of the 35-year time series (Figure 45). However, the height loss appeared in patches that are expanding over time. These patches might represent standing dead slowly being replaced by new growth, or conversion to meadows.

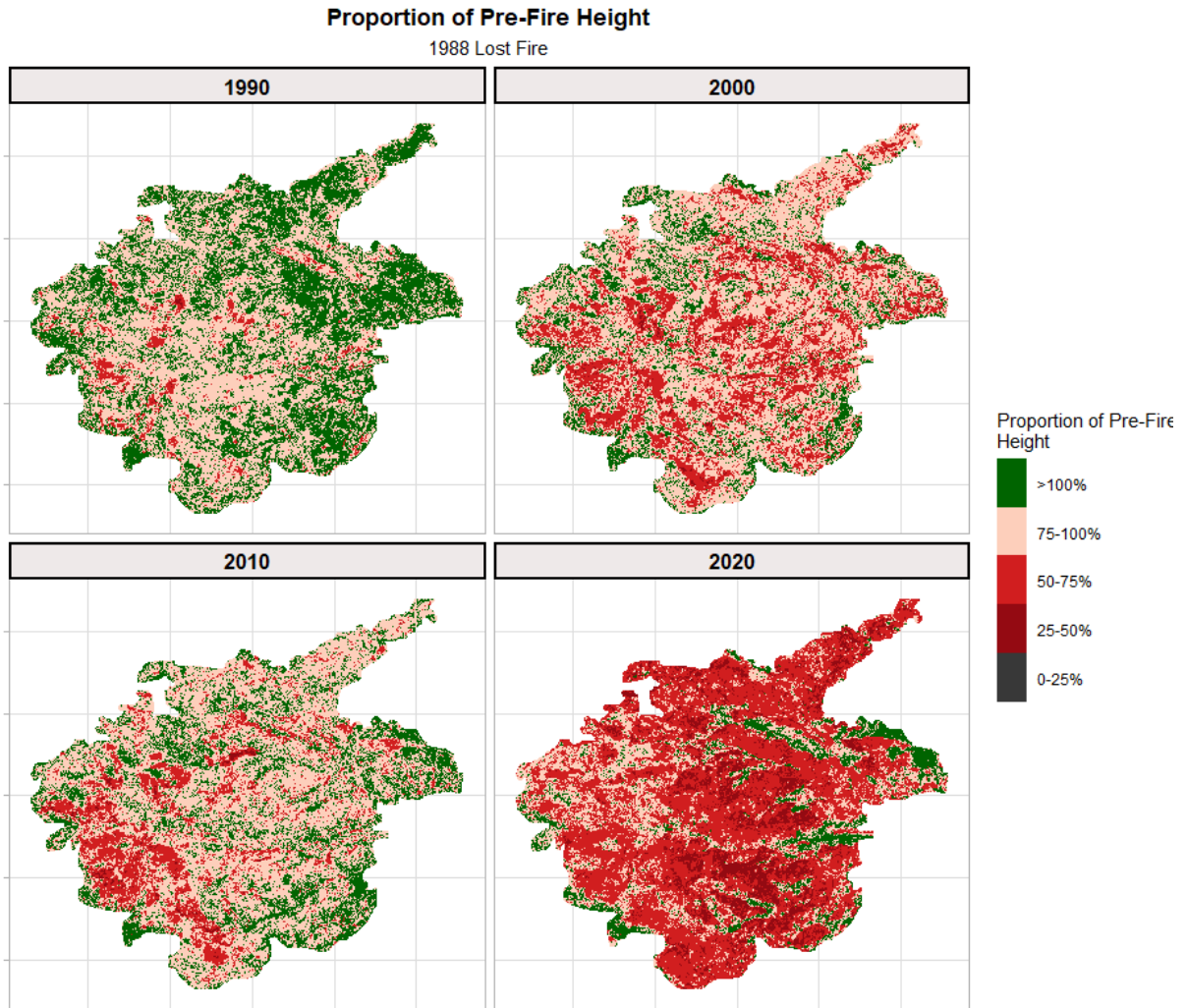


Figure 45: Proportion of pre-fire height on the Lost Fire 2 years post fire (top left) 12 years post fire (top right) 22 years post fire (bottom left) and 32 years post fire (bottom right)

Base height was steady through time (Figure 46). Spatially, the distribution of high and low base-height pixels is similar to that of height (Figure 45), though base height loss was dramatic than height loss compared to pre-fire conditions.

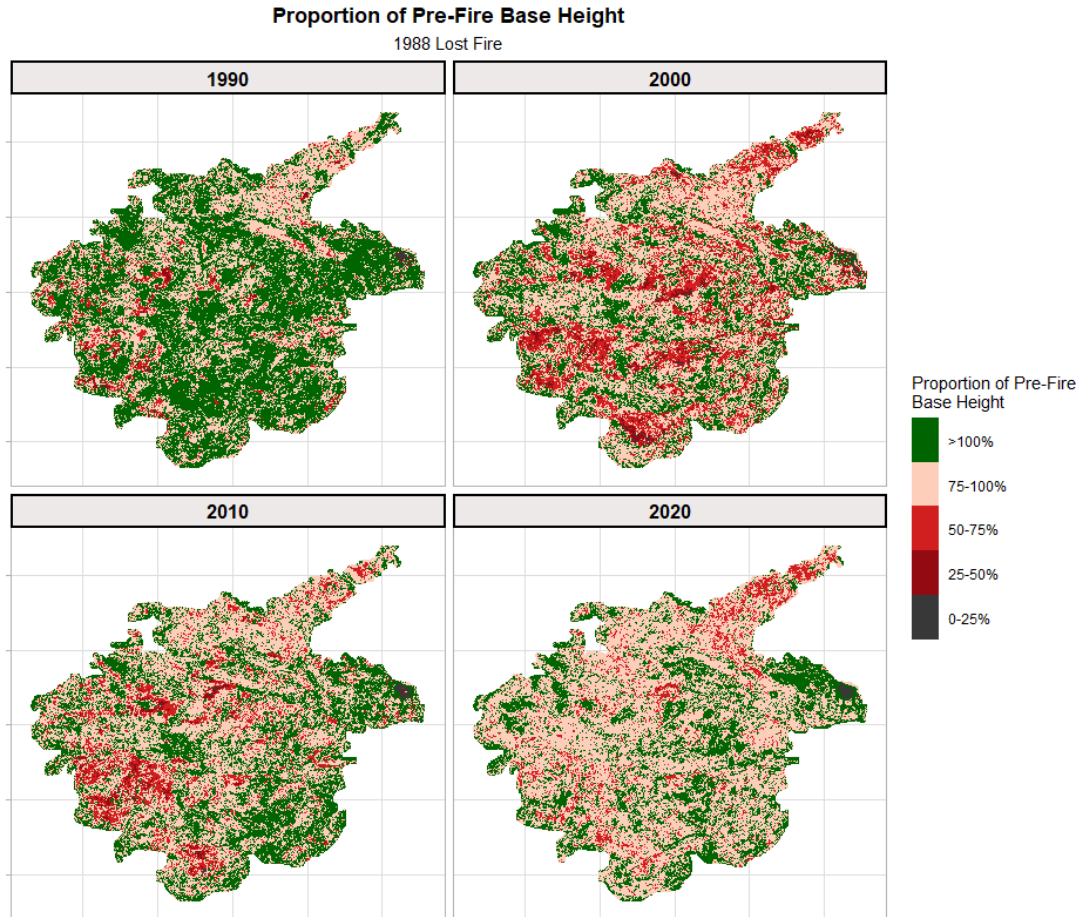


Figure 46: Proportion of pre-fire base height on the Lost Fire 2 years post fire (top left) 12 years post fire (top right) 22 years post fire (bottom left) and 32 years post fire (bottom right)

Predicted canopy cover was sensitive to disturbance across all severity classes. However, severity appears to impact the magnitude of disturbance. Unburned and low severity pixels tended to follow a U-shaped recovery trajectory, while moderate and high severity pixels followed a V-shaped trajectory. High severity pixels had a starker, more dramatic decrease than moderate severity pixels (Figure 47).

Height trajectories trended down over time. However, the magnitude of this downtrend depended on severity, with steeper declines associated with higher severity pixels. Base height also has a slight downward trajectory at moderate and high severities (Figure 47).

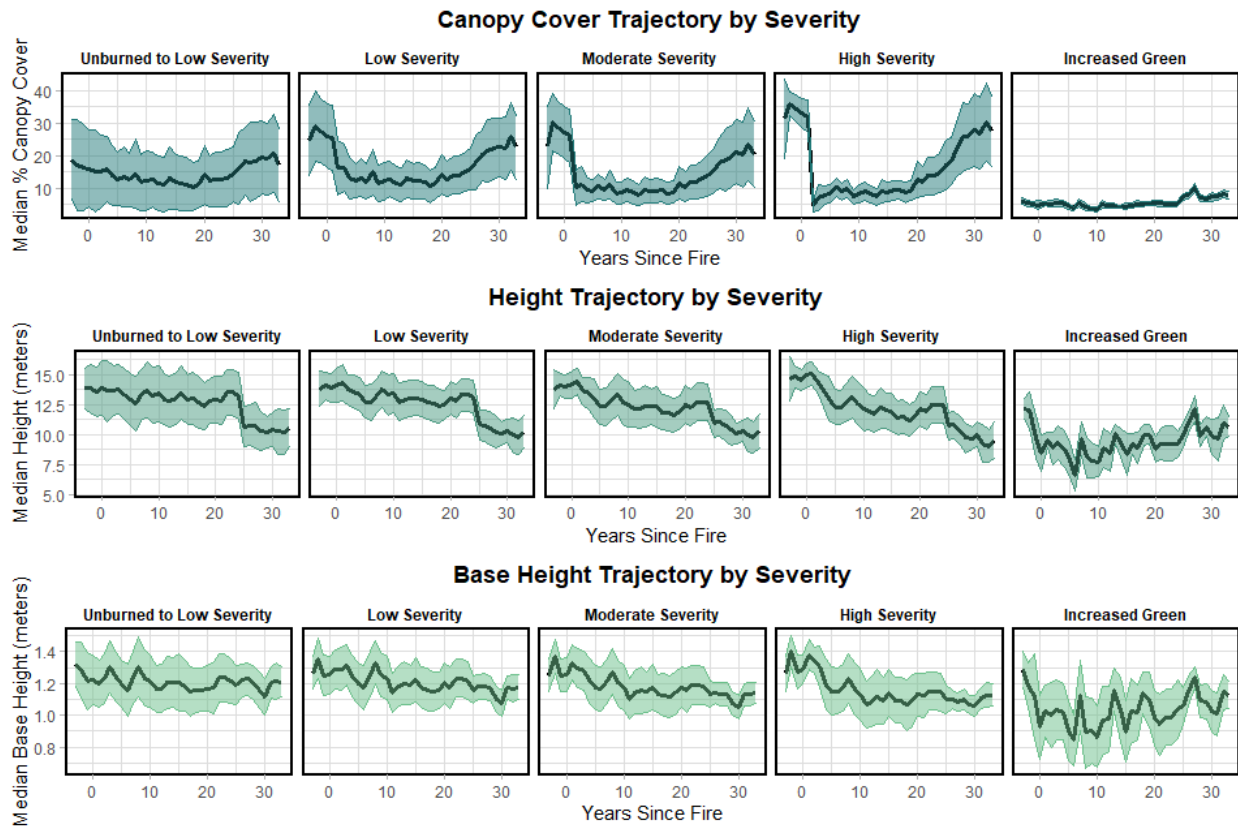


Figure 47: Canopy cover (top) height (middle) and base height (bottom) trajectory by severity. The lines represent median values and the ribbons the inter-quartile range

DISCUSSION

VARIABLE IMPORTANCE AND SENSOR EFFECT

The most important variables for predicting canopy cover were median wetness, median brightness, and median NBR. The most important variables for height and base height were median brightness, elevation, and median wetness (Figure 7). These variables were similar to past results from studies using LiDAR-Landsat covariance for predicting canopy characteristics. Moran et. al (2020) found median NBR and median brightness to be the most important variables across all three metrics, but in contrast to the findings of this study, did not find wetness to be particularly important.

Of the geophysical metrics, only elevation was important for predicting canopy structure. This might be because elevation delineates broader landscape trends, while slope and aspect are more site specific. Aspect and slope impact soil moisture gradients and available radiative energy. Variability in aspect and slope might already be captured by variability in NDVI, NBR, or the Tassled Cap indices, making the geophysical indices redundant.

Ranked variable importance provides insight into which variables the model drew upon most frequently and lead to the most improvement along the loss function. However, even less important variables can hold substantial sway on the final outputs of the model. The sensor variable is a binary variable which delineates whether a pixel came from the operational land imager (OLI) sensor on Landsat 8 or the enhanced thematic mapper (ETM+) sensor on Landsat 5. It is designed to allow the ML process to make small adjustments to account for the difference in the observed energy between the Landsat 5 and Landsat 8 satellites. Early model training did not include this variable because the sensor difference was already adjusted through linear transformation of the Landsat data prior to machine learning (Roy et al., 2016). However,

Landsat 8 has higher radiometric resolution and spectrally narrower bands, and these differences cannot be perfectly adjusted through linear transformation. Initial models tended to under-predict canopy structure metrics derived from Landsat 8 observations. So, the binary sensor variable was introduced to allow the model to adjust for sensor on a band by band basis. While some sensor effect is still evident at some sites and some metrics, it yields significantly more interoperable results than models that did not include a sensor variable.

Despite its obvious importance to final model outputs, ‘sensor’ is the least important variable across all three metrics. This might be a function of how the Gedeon method calculates variable importance. If sensor was an early split in most of the decision trees, it would only be used once. It also would not contribute much to improvement along the RMSE gradient, because sensor alone does not describe any variability in forest characteristics.

The models performed significantly better under these sensor adjustments than without, and created more ecologically sensible time series. However, some landscapes and metrics still show a noticeable difference at the sensor break, including Lubrecht. Interestingly, it is not reflected across all landscapes, and landscapes do not respond to the change in a uniform way, highlighting both the complexity of GBM models and the difficulty in interpreting their outputs. The model tends to overestimate height during Landsat 8 years, but a few individual fires had the opposite effect where the model underestimated height. The sensor effect is not necessarily site specific and can vary between metrics on the same site. Height is more impacted by the sensor effect than cover or base height, which can appear stable and ecologically sensible on sites where height predictions are nonsensical. Further work is needed to determine why the sensor effect is more pronounced for some sites and metrics, and to minimize its effect on the final time series.

STABILITY THROUGH TIME

Stability through time is important for detecting subtle, large scale forest trends. There are several sources of error that can lead to noisy, unstable predictions. Atmospheric effects, clouds, and cloud shadows can introduce error into the Landsat images, despite filtering and compositing to minimize the impact. The variability in the GBM can also be a source of noise in a time series. Machine learning approaches to predicting canopy cover have previously yielded root mean squared errors between 10 and 11% (Matasci et al., 2018; Moran et al., 2020). However, these models have yielded stable time series despite the inherent prediction uncertainties, albeit over very large geographic areas (Matasci et al., 2018).

This analysis indicates that smaller sites can also yield stable and ecologically sensible time series. The overall root means squared error for the canopy cover model was 9.4%, but the average year to year change at Powell and Lubrecht was 2.3%, indicating there is a bias that is consistent throughout time. Stark decreases in canopy cover, height, or base height could represent a disturbance like fire or harvest, but large single year increases do not make ecological sense. Powell and Lubrecht each had two years out of 36 where canopy cover increased more than 5% from the previous year. The three metrics also tended to oscillate together, despite their respective models being trained independently. This indicates they are responding to an underlying spectral signal rather than model noise.

The residuals in both North Powell and Lubrecht indicate a topographic or ecological influence on model errors. More work is required to determine the biophysical controls dictating where the model performs poorly.

SENSITIVITY TO DISTURBANCE

There is extensive evidence that GBM-derived time series are sensitive to both location and magnitude of disturbance at moderate and high severity. At North Powell, the model demonstrated the ability to pick out heterogeneity on the landscape caused by logging. The GBM predictions successfully recreated the checkerboard harvest pattern in the canopy, which is a difficult task for an ML since each pixel is predicted on independently. Additionally, model showed a clear response to disturbance on multiple fire sites, particularly in canopy cover. On the Lost Fire, canopy cover loss was associated with higher severity pixels, indicating agreement between the GBM outputs and MTBS severity predictions. Higher severity pixels were also associated with more dramatic losses in canopy cover and height.

However, it is unclear if the model is sensitive to subtle changes in canopy structure. Lubrecht Experiment Forest lost 7% of its canopy cover between 2005 and 2015, and yet the model predicted that canopy cover on the forest increased by 1%. The model correctly predicted the downward trend in forest height, but not the correct magnitude of the decrease. Mean observed height dropped 0.4 meters in the ten years between acquisition, while mean predicted height dropped by about 3 meters. Actual base height increased by 1.1 meters, while predicted base height decreased by 0.6 meters. Certainly, for canopy cover, these discrepancies can be explained by the relatively low quality of the 2005 LiDAR data. The large scan angle employed in that acquisition is known to inflate canopy cover by increasing the probability of canopy reflections in the relatively long paths obtained at oblique angles. This effect shouldn't impact canopy height (P99) significantly but it might increase mean height and thus affect predictions of base height. In the end, the 2005 results were left in the thesis to show how LiDAR data quality

could impact results, and to suggest that differences among acquisitions, if used in the modeling itself, might impact performance.

The canopy cover model produced in this thesis had an overall root mean squared error of 9.4%. The root means squared error was 13.6% at Powell, before introducing the spatial sources of error that occur when extrapolating the model beyond its training landscape. So, the intrinsic uncertainty within the predictions is greater than the actual forest change at Lubrecht. Lubrecht also spanned both Landsat sensors between 2005 and 2015, and the validation LiDAR was collected with slightly different return density standards in 2005 and 2015. It is unclear if the change at Lubrecht was too subtle to be detected by the model, or if it was an error associated with the LiDAR or Landsat observations. If the model is unable to detect small landscape changes, it is possible that some of the flat fires actually follow a U or V shaped trajectory that the model is unable to detect. Further work is required to determine if there is some minimum threshold below which the model is not sensitive to change.

There were several fires where the trajectories of canopy cover, height, and base height did not match, including the Lost Fire. Often, tree heights recover in very different ways than their corresponding canopy cover (Bolton et al., 2015, 2017; Matasci et al., 2018), which has been well documented in LiDAR based forest monitoring. Of the 63 fires that had a U or V shaped canopy cover trajectory, 32 had a flat or wavy height trajectory.

LiDAR observed 99th percentile height often detects residual structure and single surviving trees. Height trends can appear consistent as standing dead trees are gradually replaced by new growth (Matasci et al., 2018). However, standing dead vegetation is more spectrally similar to bare ground than to live trees (Liu et al., 2021). Standing dead could contribute to forest height in the LiDAR derived training data, but the GBM model predictions utilize purely

Landsat and geophysical information. So, it is unexpected that standing dead trees would still appear tall to the model.

Variable choice in the height model might also contribute to the shape of height trajectories. Elevation was also the third most important variable for predicting height. Elevation does not change year to year, so it might provide a stabilizing effect on model predictions. There are benefits and drawbacks to including a temporally static variable like elevation. It reduces year to year variability and creates more stable time series. Forest types tend to vary by elevation, so it is an effective strategy for parsing out forests into groups with similar heights. However, including height in a model might make it less sensitive to disturbance. If the GBM associates specific elevations with tall trees, then it requires a greater disturbance signal in the Landsat derived indices to overcome the effect of elevation on a prediction.

Base height was the least responsive variable to disturbance. Base height is important because it determines the amount of energy required to move a fire from the ground into the canopy (Wagner, 1977). Taller base heights require more energy to initiate crown fire. In this case, base height was defined as the mean Z value of all points greater than 2 meters, minus the standard deviation of all points greater than two meters. Directly measuring base heights is challenging because it requires the LiDAR sensor to penetrate layers of canopy to measure multiple points low in the vertical profile of a given tree (Stefanidou et al., 2020). However, under this definition, base height is highly related to variability within a pixel and somewhat difficult to interpret through time. Direct observation of base height is becoming increasingly more obtainable as LiDAR technology improves (Luo et al., 2018; Stefanidou et al., 2020) but will require enough acquisitions to form a body of training data before it can be integrated into LiDAR-Landsat covariance methods.

BURNED AREA CLASSIFICATION FRAMEWORK

Classifying forest trajectories is useful for monitoring carbon inventories, disturbance regimes, and forest conversion. The ShapeSelectForest approach is a preexisting classification scheme that has been widely applied in detecting change over time in Landsat imagery (Moisen et al., 2016; Schroeder et al., 2017). The framework is based on seven pre-existing splines, each representing a specific disturbance and recovery trajectory. Time series trajectories are sorted by the spline they most closely resemble (Moisen et al., 2016).

Initially, this analysis utilized the ShapeSelectForest (SSF) approach for classifying fire trajectories. The SSF algorithm primarily sorted fires into groups 5 and 7, which represent V-shaped and double jump shaped trajectories. The algorithm successfully parsed out the highest severity fires, but did little to describe the variability in less severe fires.

The original SSF approach was built for analyzing raw spectral data or indices like NDVI and NBR. GBM models often do not have a linear relationship with their underlying Landsat (Moran et al., 2020) and GBM derived canopy cover and height will likely have an inverse relationship with NBR, which SSF splines were designed to fit (Moisen et al., 2016).

Additionally, the SSF system assumes the long-term forest trend is stable. For example, a forest that is growing taller over decades, but experiences patches of stand replacing fire would not be well described by any SSF spline.

This analysis proposed an alternative method of classifying recovery trajectories using predicted canopy metrics rather than raw Landsat spectral data. The goal of the alternative classification system was to create a flexible classification that is more appropriate for GBM

derived time series of landscapes (burned areas) rather than pixels. Under this framework, fires were classified based on where the local minima occurred relative to the disturbance. V-shaped fires reached their minimum within two years of the disturbance. U shaped fires reached their minimum more than two years after the fire. Wavy fires had multiple peaks and valleys within the time series. Flat fires were stable without a distinct trend. These differences were observed in the time series and don't necessarily have a clear ecological basis. Each metric for each fire was classified independently, since height, canopy cover, and base height may not follow the same recovery trajectory post fire. For example, a stand that experiences crown scorch will potentially defoliate but not die (Varner et al., 2021), causing incongruent canopy cover and height recoveries. In the future, it may make more sense to classify the cover time series and let height and base height come with them (as opposed to classifying each metric separately) to aid in interpretation.

Flat fires were more likely to occur in grassland systems with low pre-fire canopy cover and height. Most forested fires followed a U or V shaped recovery trajectory, particularly those that burned at higher severity. However, U and V trajectories do not require heavy fuel loading, and included forests that initially had sparser canopy cover. Even though U shaped and V shaped fires occur on similar forests, their trajectories post-fire are likely ecologically different. U-shaped fires take longer to reach their local minimum than V-shaped fires. They likely represent fires with delayed secondary mortality and sites that were less supportive of new growth post fire. U-shaped fires were also less like to recovery fully in the 35-year time series than V fires.

There are few potential drivers for wavy recovery trajectories. The first mechanism might be intrinsic model error that creates an unstable time series. This is likely true of wavy fires with peaks and valleys that do not appear to correspond to a disturbance. Thinning and logging are

also potential drivers of wavy trajectories. Powell experienced patches of logging throughout the 36-year time series, and the canopy cover at Powell followed a wavy trajectory (Figure ten). U shaped fires often appear a bit wavy near the bottom of the U (Figure 28), before they reach their inflection point and begin recovery. This indicates that burned and early pioneer landscapes might have more on the ground variability as the vegetation returns in a patchy manner, causing a wavy trajectory.

Fires within the study area were mostly recovering. Of the 164 fires included in analysis, no burn scar experienced a notable state change, where it lost its canopy and did not begin re-growing it. The timeline of recovery predicted by the GBM models is consistent with expected recovery behavior. Most disturbed pixels recover 80% of their greenness and NBR within 10 years (Pickell et al., 2016) and past estimates suggest the Canadian boreal forest recovers 50% of its canopy cover in twenty years (Matasci et al., 2018).

Under anthropogenic climate change, more area is burning under higher severity (Parks & Abatzoglou, 2020) and the post-fire environment is becoming increasingly unfavorable for regeneration (Coop et al., 2020). However, none of the fires included in this analysis burned again after their initial disturbance between 1988 and 1994, which is a major driver of forest conversion (Coop et al., 2020).

CONCLUSION

This work encompassed three objectives. The first was to continue to refine the LiDAR-Landsat covariance methodology and to produce fuel metrics for Montana, Idaho, and Wyoming across a 36-year time series. The models developed for this work slightly outperformed earlier iterations of GBMs for predicting canopy fuel structure (Moran et al., 2020). The second

objective was to assess the quality of these fuel predictions and explore the spatial and temporal sources of variability in model predictions. Three distinct validations were used to assess model quality. First, the models were validated with randomly selected holdback pixels. Then, North Powell was used a spatially coherent validation site that is functionally identical to one of the training sites. Last, Lubrecht Experimental Forest was used to determine if the model could correctly prediction direction and magnitude of change. The last objective of this work was to evaluate recovery on burned sites from 1985 to 2021.

This work indicates that GBM derived canopy fuel time series are both stable through time and sensitive to episodic disturbance. However, Lubrecht Experimental Forest suggests that the model might not be sensitive to smaller, subtle change below a specific threshold. More work is needed to identify this threshold and continue to build the model's sensitivity to light disturbance and disturbance in more sparsely forested environments.

This analysis also indicated that fires that occurred in 1988 to 1994 have mostly recovered to pre-fire conditions by 2021. These fires have relatively simple trajectories because they did not reburn. The next steps of this work will include analyzing more complicated but more ecologically realistic sites with multiple reburns. This work used individual fires at the unit of analysis, but the Lost Fire indicated that there is significant heterogeneity within the bounds of a fire, and different areas recover in different ways. Pixel-based change-detection methods such as LandTrendr (Kennedy et al., 2010) could potentially be applied to GBM-derived fuels products to capture some of this intra-fire nuance. The ultimate goal of this line of research is to continue to develop LiDAR-Landsat covariance into a flexible, sensitive method for monitoring canopy fuels through time.

BIBLIOGRAPHY

- Abatzoglou, J. T., Battisti, D. S., Williams, A. P., Hansen, W. D., Harvey, B. J., & Kolden, C. A. (2021). Projected increases in western US forest fire despite growing fuel constraints. *Communications Earth & Environment*, 2(1), 227. <https://doi.org/10.1038/s43247-021-00299-0>
- Bolton, D. K., Coops, N. C., Hermosilla, T., Wulder, M. A., & White, J. C. (2017). Assessing variability in post-fire forest structure along gradients of productivity in the Canadian boreal using multi-source remote sensing. *Journal of Biogeography*, 44(6), 1294–1305. <https://doi.org/10.1111/jbi.12947>
- Bolton, D. K., Coops, N. C., & Wulder, M. A. (2015). Characterizing residual structure and forest recovery following high-severity fire in the western boreal of Canada using Landsat time-series and airborne lidar data. *Remote Sensing of Environment*, 163, 48–60. <https://doi.org/10.1016/j.rse.2015.03.004>
- Branco, P., Torgo, L., & Ribeiro, R. P. (2019). Pre-processing approaches for imbalanced distributions in regression. *Neurocomputing*, 343, 76–99. <https://doi.org/10.1016/J.NEUCOM.2018.11.100>
- Bright, B. C., Hudak, A. T., Kennedy, R. E., Braaten, J. D., & Henareh Khalyani, A. (2019). Examining post-fire vegetation recovery with Landsat time series analysis in three western North American forest types. *Fire Ecology*, 15(1), 8. <https://doi.org/10.1186/s42408-018-0021-9>
- Comer, P., Faber-Langendoen, D., Evans, R., Gawler, S., Josse, C., Kittel, G., Menard, S., Pyne, M., Reid, M., Schultz, K., Snow, K., & Teague, J. (2003). *Ecological Systems of the United States: A Working Classification of U.S. Terrestrial Systems*. NatureServe.
- Coop, J. D., Parks, S. A., Stevens-Rumann, C. S., Crausbay, S. D., Higuera, P. E., Hurteau, M. D., Tepley, A., Whitman, E., Assal, T., Collins, B. M., Davis, K. T., Dobrowski, S., Falk, D. A., Fornwalt, P. J., Fulé, P. Z., Harvey, B. J., Kane, V. R., Littlefield, C. E., Margolis, E. Q., ... Rodman, K. C. (2020). Wildfire-Driven Forest Conversion in Western North American Landscapes. *BioScience*, 70(8), 659–673. <https://doi.org/10.1093/biosci/biaa061>
- Coops, N. C., Tompalski, P., Goodbody, T. R. H., Queinnec, M., Luther, J. E., Bolton, D. K., White, J. C., Wulder, M. A., van Lier, O. R., & Hermosilla, T. (2021). Modelling lidar-derived estimates of forest attributes over space and time: A review of approaches and future trends. *Remote Sensing of Environment*, 260, 112477. <https://doi.org/10.1016/j.rse.2021.112477>
- Davis, K. T., Dobrowski, S. Z., Holden, Z. A., Higuera, P. E., & Abatzoglou, J. T. (2019). Microclimatic buffering in forests of the future: the role of local water balance. *Ecography*, 42(1), 1–11. <https://doi.org/10.1111/ecog.03836>
- D'Este, M., Elia, M., Giannico, V., Spano, G., Laforteza, R., & Sanesi, G. (2021). Machine Learning Techniques for Fine Dead Fuel Load Estimation Using Multi-Source Remote Sensing Data. *Remote Sensing*, 13(9), 1658. <https://doi.org/10.3390/rs13091658>

- Eidenshink, J., Schwind, B., Brewer, K., Zhu, Z.-L., Quayle, B., & Howard, S. (2007). A Project for Monitoring Trends in Burn Severity. *Fire Ecology*, 3(1), 3–21. <https://doi.org/10.4996/fireecology.0301003>
- Garcia Leiva, R., Fernandez Anta, A., Mancuso, V., & Casari, P. (2019). A Novel Hyperparameter-Free Approach to Decision Tree Construction That Avoids Overfitting by Design. *IEEE Access*, 7, 99978–99987. <https://doi.org/10.1109/ACCESS.2019.2930235>
- Gedeon, T. D. (1997). Data Mining of Inputs: Analysing Magnitude and Functional Measures. *International Journal of Neural Systems*, 08(02), 209–218. <https://doi.org/10.1142/S0129065797000227>
- Guo, Q., Su, Y., Hu, T., Guan, H., Jin, S., Zhang, J., Zhao, X., Xu, K., Wei, D., Kelly, M., & Coops, N. C. (2021). Lidar Boosts 3D Ecological Observations and Modelings: A Review and Perspective. *IEEE Geoscience and Remote Sensing Magazine*, 9(1), 232–257. <https://doi.org/10.1109/MGRS.2020.3032713>
- Hagmann, R. K., Hessburg, P. F., Prichard, S. J., Povak, N. A., Brown, P. M., Fulé, P. Z., Keane, R. E., Knapp, E. E., Lydersen, J. M., Metlen, K. L., Reilly, M. J., Sánchez Meador, A. J., Stephens, S. L., Stevens, J. T., Taylor, A. H., Yocom, L. L., Battaglia, M. A., Churchill, D. J., Daniels, L. D., ... Waltz, A. E. M. (2021a). Evidence for widespread changes in the structure, composition, and fire regimes of western North American forests. *Ecological Applications*, 31(8). <https://doi.org/10.1002/eap.2431>
- Hagmann, R. K., Hessburg, P. F., Prichard, S. J., Povak, N. A., Brown, P. M., Fulé, P. Z., Keane, R. E., Knapp, E. E., Lydersen, J. M., Metlen, K. L., Reilly, M. J., Sánchez Meador, A. J., Stephens, S. L., Stevens, J. T., Taylor, A. H., Yocom, L. L., Battaglia, M. A., Churchill, D. J., Daniels, L. D., ... Waltz, A. E. M. (2021b). Evidence for widespread changes in the structure, composition, and fire regimes of western North American forests. *Ecological Applications*, 31(8). <https://doi.org/10.1002/eap.2431>
- Hanan, E. J., Ren, J., Tague, C. L., Kolden, C. A., Abatzoglou, J. T., Bart, R. R., Kennedy, M. C., Liu, M., & Adam, J. C. (2021). How climate change and fire exclusion drive wildfire regimes at actionable scales. *Environmental Research Letters*, 16(2), 024051. <https://doi.org/10.1088/1748-9326/abd78e>
- Hudak, A. T., Lefsky, M. A., Cohen, W. B., & Berterretche, M. (2002). Integration of lidar and Landsat ETM+ data for estimating and mapping forest canopy height. *Remote Sensing of Environment*, 82(2–3), 397–416. [https://doi.org/10.1016/S0034-4257\(02\)00056-1](https://doi.org/10.1016/S0034-4257(02)00056-1)
- Hyde, P., Dubayah, R., Walker, W., Blair, J. B., Hofton, M., & Hunsaker, C. (2006). Mapping forest structure for wildlife habitat analysis using multi-sensor (LiDAR, SAR/InSAR, ETM+, Quickbird) synergy. *Remote Sensing of Environment*, 102(1–2), 63–73. <https://doi.org/10.1016/j.rse.2006.01.021>
- Kennedy, R. E., Yang, Z., & Cohen, W. B. (2010). Detecting trends in forest disturbance and recovery using yearly Landsat time series: 1. LandTrendr — Temporal segmentation algorithms. *Remote Sensing of Environment*, 114(12), 2897–2910. <https://doi.org/10.1016/j.rse.2010.07.008>
- Liu, X., Frey, J., Denter, M., Zielewska-Büttner, K., Still, N., & Koch, B. (2021). Mapping standing dead trees in temperate montane forests using a pixel- and object-based image fusion method and stereo

- WorldView-3 imagery. *Ecological Indicators*, 133, 108438.
<https://doi.org/10.1016/j.ecolind.2021.108438>
- Luo, L., Zhai, Q., Su, Y., Ma, Q., Kelly, M., & Guo, Q. (2018). Simple method for direct crown base height estimation of individual conifer trees using airborne LiDAR data. *Optics Express*, 26(10), A562. <https://doi.org/10.1364/OE.26.00A562>
- Malohlava, M., & Candel, A. (2021). *Gradient Boosting Machine with H2O* (A. Bartz, Ed.; 7th ed.).
- Matasci, G., Hermosilla, T., Wulder, M. A., White, J. C., Coops, N. C., Hobart, G. W., & Zald, H. S. J. (2018). Large-area mapping of Canadian boreal forest cover, height, biomass and other structural attributes using Landsat composites and lidar plots. *Remote Sensing of Environment*, 209, 90–106. <https://doi.org/10.1016/J.RSE.2017.12.020>
- McGranahan, D., & Wonkka, C. (2018). Wildland Fire Science Literacy: Education, Creation, and Application. *Fire*, 1(3), 52. <https://doi.org/10.3390/fire1030052>
- Moisen, G. G., Meyer, M. C., Schroeder, T. A., Liao, X., Schleeweis, K. G., Freeman, E. A., & Toney, C. (2016). Shape selection in Landsat time series: a tool for monitoring forest dynamics. *Global Change Biology*, 22(10), 3518–3528. <https://doi.org/10.1111/gcb.13358>
- Moran, C. J., Kane, V. R., & Seielstad, C. A. (2020). Mapping forest canopy Fuels in the Western United States with LiDAR-Landsat Covariance. *Remote Sensing*, 12(5).
- Noonan-Wright, E. K., Opperman, T. S., Finney, M. A., Zimmerman, G. T., Seli, R. C., Elenz, L. M., Calkin, D. E., & Fiedler, J. R. (2011). Developing the US Wildland Fire Decision Support System. *Journal of Combustion*, 2011, 1–14. <https://doi.org/10.1155/2011/168473>
- Parks, S. A., & Abatzoglou, J. T. (2020). Warmer and Drier Fire Seasons Contribute to Increases in Area Burned at High Severity in Western US Forests From 1985 to 2017. *Geophysical Research Letters*, 47(22). <https://doi.org/10.1029/2020GL089858>
- Pascual, C., García-Abril, A., Cohen, W. B., & Martín-Fernández, S. (2010). Relationship between LiDAR-derived forest canopy height and Landsat images. *International Journal of Remote Sensing*, 31(5), 1261–1280. <https://doi.org/10.1080/01431160903380656>
- Peterson, B., Nelson, K. J., Seielstad, C., Stoker, J., Jolly, W. M., & Parsons, R. (2015). Automated integration of lidar into the LANDFIRE product suite. *Remote Sensing Letters*, 6(3), 247–256. <https://doi.org/10.1080/2150704X.2015.1029086>
- Pflugmacher, D., Cohen, W. B., Kennedy, R. E., & Yang, Z. (2014). Using Landsat-derived disturbance and recovery history and lidar to map forest biomass dynamics. *Remote Sensing of Environment*, 151, 124–137. <https://doi.org/10.1016/J.RSE.2013.05.033>
- Pickell, P. D., Hermosilla, T., Frazier, R. J., Coops, N. C., & Wulder, M. A. (2016). Forest recovery trends derived from Landsat time series for North American boreal forests. *International Journal of Remote Sensing*, 37(1), 138–149. <https://doi.org/10.1080/2150704X.2015.1126375>
- Reeves, M. C., Kost, J. R., & Ryan, K. C. (2006). Fuels Products of the LANDFIRE Project. *USDA Forest Service Proceedings RMRS-P-41*, 239–252.
- Roy, D. P., Zhang, H. K., Ju, J., Gomez-Dans, J. L., Lewis, P. E., Schaaf, C. B., Sun, Q., Li, J., Huang, H., & Kovalskyy, V. (2016). A general method to normalize Landsat reflectance data to nadir BRDF

- adjusted reflectance. *Remote Sensing of Environment*, 176, 255–271.
<https://doi.org/10.1016/J.RSE.2016.01.023>
- Schroeder, T. A., Schleeweis, K. G., Moisen, G. G., Toney, C., Cohen, W. B., Freeman, E. A., Yang, Z., & Huang, C. (2017). Testing a Landsat-based approach for mapping disturbance causality in U.S. forests. *Remote Sensing of Environment*, 195, 230–243. <https://doi.org/10.1016/j.rse.2017.03.033>
- Skowronski, N. S., Gallagher, M. R., & Warner, T. A. (2020). Decomposing the Interactions between Fire Severity and Canopy Fuel Structure Using Multi-Temporal, Active, and Passive Remote Sensing Approaches. *Fire*, 3(1), 7. <https://doi.org/10.3390/fire3010007>
- Stefanidou, A., Gitas, I., Korhonen, L., Stavrakoudis, D., & Georgopoulos, N. (2020). LiDAR-Based Estimates of Canopy Base Height for a Dense Uneven-Aged Structured Forest. *Remote Sensing*, 12(10), 1565. <https://doi.org/10.3390/rs12101565>
- USDA Forest Service, & US Geological Survey. (2017). MTBS Data Access: Fire Level Geospatial Data . In *mtbs.gov*.
- US Department of Agriculture. (2021). Timber Harvests. In *FSGeodata Clearinghouse*.
- U.S. Department of Interior, G. S., & U.S. Department of Agriculture. (2022). LANDFIRE: Aspect, Elevation, and Slope. In *landfire.cr.usgs.gov*.
- US Geological Survey, & US Department of Agriculture. (n.d.). Existing Vegetation Type Layer, LANDFIRE . In *landfire.gov*.
- Varner, J. M., Hood, S. M., Aubrey, Doug. P., Yedinak, K., Hiers, J. K., Jolly, W. M., Shearman, T. M., McDaniel, J. K., O'Brien, J. J., & Rowell, E. M. (2021). Tree crown injury from wildland fires: causes, measurement and ecological and physiological consequences. *New Phytologist*, 231(5), 1676–1685. <https://doi.org/10.1111/nph.17539>
- Wagner, C. E. van. (1977). Conditions for the start and spread of crown fire. *Canadian Journal of Forest Research*, 7(1), 23–34. <https://doi.org/10.1139/x77-004>
- Wilkes, P., Jones, S., Suarez, L., Mellor, A., Woodgate, W., Soto-Berelev, M., Haywood, A., & Skidmore, A. (2015). Mapping Forest Canopy Height Across Large Areas by Upscaling ALS Estimates with Freely Available Satellite Data. *Remote Sensing*, 7(9), 12563–12587. <https://doi.org/10.3390/rs70912563>